Toward Crowdsensing-based Monitoring of Bridges Using Smartphones

by

Nima Shirzad Ghaleroudkhani

A thesis submitted in partial fulfillment of the requirements for the degree of

Doctor of Philosophy

in

Structural Engineering

Department of Civil and Environmental Engineering

University of Alberta

ABSTRACT

The sustainability of urban cities is contingent upon the adequate performance of their infrastructure. The transportation system is one of the crucial components of the city infrastructure and the sustainability and the economic development of a city depend on its proper operation. Monitoring bridge structures, as key components of the transportation infrastructure, is a popular topic among researchers. While most conventional bridge monitoring methods focus on using fixed sensors, including accelerometers and strain gauges, to collect data, indirect bridge monitoring methods focus on using a moving sensor inside a vehicle as the data collector. As such, one mobile sensor can collect data from many bridges with no fixed instrumentation required, leading to a more efficient and cost-effective bridge monitoring. However, drive-by collected vibrations are significantly dominated by operational factors, including the vehicle and road features.

Recent technology developments have provided invaluable tools for monitoring urban infrastructure. Smartphones, currently the most popular smart devices, are equipped with many sensors, which data could be used for monitoring urban infrastructure through a crowdsensed framework. In this regard, this thesis aims at proposing a crowdsensing-based indirect bridge monitoring method considering operational effects. A novel inverse filtering method is proposed to eliminate operational effects from drive-by vibrations and enhance bridge feature extraction. The off-bridge vibrations, i.e., when the vehicle is not on the bridge and is moving on the ground, is employed to create a filter capable of eliminating operational effects. Later, this filter is applied to the on-bridge vibrations to magnify bridge dynamic features.

In the initial chapters of this thesis, the focus is on the frequency identification of bridges. Later, a more complex damage detection method using Mel-frequency cepstral analysis is applied

in conjunction with inverse filtering. At each stage of this study, a series of controlled laboratory experiments and real-life tests are conducted to investigate the performance of the proposed method. The proposed approach is proved successful in eliminating operational effects from drive-by collected vibrations, addressing one of the major challenges facing indirect bridge monitoring. In addition, the data acquisition devices in the proposed method are passengers' smartphones, which demonstrates the potential of implementing the proposed method in crowdsensed frameworks for future smart cities.

PREFACE

This thesis includes original research conducted by Nima Shirzad Ghaleroudkhani. Four journal papers have been published/submitted for publication on the basis of this thesis. The details of each chapter are summarized below:

Chapter 1 presents modified and reorganized versions of the literature review parts of all four papers related to this thesis.

A version of Chapter 2 has been published as ***Shirzad-Ghaleroudkhani, N., Mei, Q., and Gül, M. (2020) "Frequency Identification of Bridges Using Smartphones on Vehicles with Variable Features." Journal of Bridge Engineering. 25(7): 04020041.*** For the consistency and coherence of this thesis, contents have been modified, removed, or added from the published paper. Nima Shirzad-Ghaleroudkhani was responsible for conceptualization, methodology development, conducting experiments, analysis implementation, and paper composition. Mustafa Gül was in charge of conceptualization, supervision, funding acquisition, and paper editing. Qipei Mei was involved in experiments and paper composition.

A version of Chapter 3 has been published as ***Shirzad-Ghaleroudkhani, N., and Gül, M. (2020) "Inverse Filtering for Frequency Identification of Bridges Using Smartphones in Passing Vehicles: Fundamental Developments and Laboratory Verifications," Sensors, 20(4), 1190.*** For the consistency and coherence of this thesis, contents have been modified, removed, or added from the published paper. Nima Shirzad-Ghaleroudkhani was responsible for conceptualization, methodology development, conducting experiments, analysis implementation, and paper composition. Mustafa Gül was in charge of conceptualization, supervision, funding acquisition, and paper editing.

A version of Chapter 4 has been published as ***Shirzad-Ghaleroudkhani, N., and Gül, M. (2021). "An Enhanced Inverse Filtering Methodology for Drive-By Frequency Identification of Bridges Using Smartphones in Real-Life Conditions." Smart Cities, 4(2), 499-513.*** For the consistency and coherence of this thesis, contents have been modified, removed, or added from the published paper. Nima Shirzad-Ghaleroudkhani was responsible for conceptualization, methodology development, conducting experiments, analysis implementation, and paper composition. Mustafa Gül was in charge of conceptualization, supervision, funding acquisition, and paper editing.

A version of Chapter 5 is under review for publication as ***Shirzad-Ghaleroudkhani, N., and Gül, M. (2022). "A Crowdsensing-based Framework for Indirect Bridge Monitoring Using Mel-frequency Cepstral Analysis Considering Elimination of Operational Effects." Journal of Structural Engineering.*** For the consistency and coherence of this thesis, contents have been modified, removed, or added from the published paper. Nima Shirzad-Ghaleroudkhani was responsible for conceptualization, methodology development, conducting experiments, analysis implementation, and paper composition. Mustafa Gül was in charge of conceptualization, supervision, funding acquisition, and paper editing.

DEDICATION

To my wife, Shaghayegh

And to my parents

ACKNOWLEDGEMENTS

Foremost, I would like to express my sincere gratitude to my supervisor, Dr. Mustafa Gül, for his continuous support and encouragement in my Ph.D. studies at the University of Alberta. His novel ideas and deep knowledge guided me through my research path. He trained me to be an independent researcher and this thesis would never come to fruition without his support and mentorship.

Besides my supervisor, I would like to thank my supervisory committee members, Dr. Yong Li and Dr. Karim El-Basyouny, for their constructive feedback toward my research. I would also like to thank my Ph.D. defense examiners and chair, Dr. Hae Young Noh, Dr. Ioanis Nikolaidis, and Dr. Ali Imanpour.

I also like to thank my coursework instructors, Dr. Robert Driver, Dr. Samer Adeeb, Dr. Yong Li, and Dr. Carlos Cruz Noguez, for teaching me the knowledge to conduct this research. My deepest gratitude goes to Dr. Albert Vette for his proficient teaching skills in the field of signal processing, which led me toward major innovations in my Ph.D. research.

I thank my fellow structural health monitoring research group members, Qipei Mei, Md Riasat Azim, Haiyang Zhang, and Ngoan Do, for their valuable feedback and assistance during my Ph.D. studies. Also, I would like to thank my friends, Massoud, Mahyar, Ali, Parnian, Nikoo, and Reyhaneh, for their support, patience, and encouragement during this chapter of my life.

And last but not the least, I want to thank my family, my parents, my sister, and especially my wife, for all their love and support in the most difficult times during my journey.

TABLE OF CONTENTS

LIST OF TABLES

LIST OF FIGURES

Chapter 1. INTRODUCTION

1.1. MOTIVATION

Urban population growth in recent decades has created complications in the management of major urban cities [1]. The sustainability of these urban cities is contingent upon the adequate performance of their infrastructure [2], [3]. Meanwhile, recent technology developments have provided reliable and efficient means for monitoring the city infrastructure through smart sensing, computing, and communication technologies, defining the new term of Smart City [4]–[6].

Transportation system is at the core of the city infrastructure and the sustainability and economic development of a city rely on its proper operation [7], [8]. However, in many developed countries, most of the transportation infrastructure has reached its life cycle and is in need of monitoring and maintenance. For instance, a recent report [9] concludes that almost 40 percent of roads and bridges in Canada are in fair, poor, or very poor condition, with roughly 80 percent older than 20 years. Hence, Structural Health Monitoring (SHM) techniques have been proposed as a critical component of viable transportation networks [10].

Monitoring bridge structures, as key components of transportation infrastructure, is a popular topic among researchers. Traditionally, most of the proposed SHM methods require bridge instrumentation with fixed sensors installed on the bridge; see Catbas et al. [11], Guan et al. [12], Gül and Catbas [13], Hoult et al. [14], Hsieh et al. [15], Ko and Ni [16], and Wong [17] among others. The functionality and accuracy of these methods have been demonstrated in those studies. Although these methods were proved to be effective, direct data collection from bridge structures could be challenging. The complexity of the installation of the devices as well as the necessity for power and data storage networks are major concerns when dealing with a population of bridges.

Moreover, during the course of the project, the serviceability of the bridges is frequently constrained by lane closures [18], which may negatively impact the capacity of the transportation system.

1.2. LITERATURE REVIEW

1.2.1. Drive-By Bridge Health Monitoring

Researchers have recently become interested in an alternate monitoring strategy that uses an instrumented vehicle to collect vibrational data. Initially studied by Yang et al. [19], [20], drive-by approaches offer low-cost and efficient opportunities for indirectly monitoring bridges without the need for direct equipment installation, albeit introducing new challenges compared to direct methods. Mixed vibrations recorded on the vehicle are highly dominated by vehicle vibrations, including engine, suspension system, tire effects, and the effect of road roughness. Extracting bridge dynamic features from those mixed vibrations was the main concern of indirect bridge monitoring studies in recent years [21]–[23].

Extracting bridge frequencies was the focus of a plethora of studies, including the ground-breaking study by Yang et al. [20]. They performed dynamic analysis of vehicle-bridge interaction for a simple 2D beam model representing the bridge and a moving mass-spring system representing the vehicle. It was shown that the frequency of the bridge can be extracted from the vibration of the vehicle. Later, many studies aimed at addressing the challenge of detecting bridge frequencies in the spectrum of mixed drive-by recorded vibrations [24]. Lin and Yang [19] investigated the potential of using a tractor-trailer system for detecting the fundamental frequency of a bridge in real-life conditions. They concluded that lower speeds of the vehicle provide higher resolution spectra, which are more suitable for frequency detection, while reduction of excitation level leads to less bridge presence in the recorded mixed vibrations. On the other hand, higher

speeds result in the dominance of road roughness in the vibrations, which too fades bridge presence in the spectrum. Keenahan et al. [25] provided a solution for that issue by proposing the subtraction of the vibrations recorded on the two axles of the vehicle. They showed that the road roughness effect could be substantially reduced using their proposed method. Later, other studies employed novel approaches for detecting bridge frequencies, including Empirical Mode Decomposition (EMD) [26], Generalized Pattern Search Algorithm (GPSA) [27], and Frequency Domain Decomposition (FDD) [28]. All these studies arrive at the same conclusion that the presence of the bridge in drive-by vibrations is not significant and the effect of vehicle and road roughness factors needs to be considered.

Another group of studies took the next step toward detecting bridge mode shapes. Mode shapes could be decisive in bridge monitoring as any discontinuity in the mode shape could reveal both the intensity and location of the damage [29], [30]. Among the first studies in this field, Zhang et al. [31] employed a shaker-equipped vehicle model to approximate the mode shape of the bridge. Although the level of accuracy of their method was obtained for low vehicle speeds of less than 18 km/hr, it was a remarkable study that showed the potential of extracting bridge mode shapes using indirect methods. Afterwards, researchers employed different methodologies to increase the accuracy of indirect bridge mode shape detection, using Hilbert Transform (HT) [32], Singular Value Decomposition (SVD) [33], Short-time Frequency Domain Decomposition (STFDD) [34], and matrix completion methods [35]. Most of these studies conducted low-speed vehicle passages over the bridge to reduce the effect of noise and operational effects.

Detection of damage on the bridge is not limited to the identification of modal parameters. For instance, O'Brien et al. [36] utilized Moving Force Identification (MFI), a method based on finding the time history of forces applied to the bridge, to detect damage on the bridge. Zhang et

al. [37] employed Operating Deflection Shape Curvature (ODSC) method. Yin and Tang [38] used Proper Orthogonal Decomposition (POD) to calculate the difference between the displacement responses of a vehicle passing damaged and healthy bridges. In addition, multiple studies [39]–[41] focused on the application of wavelet transform for bridge damage detection. Another group of studies [24], [42]–[44] focused on using machine-learning methods for indirect bridge monitoring. Recently, a novel damage detection approach based on Mel-frequency cepstral analysis has been proposed in the authors' research group [45].

1.2.2.   Crowdsensing-based Transportation Infrastructure Monitoring

Many studies have investigated applications of modern technologies for monitoring transportation systems [46], [47]. These studies demonstrated that modern technologies significantly improve the efficiency of transportation management. With the rapid technology development, there are more data sources available through crowdsourcing methods, which can be employed for monitoring and management of the cities [48]–[50].

Nowadays, smartphones are the most popular personal smart devices in the world. These devices are not only means of communication but also contain a variety of sensors, including an accelerometer, gyroscope, GPS, etc. These sensors provide data that could be employed on a local and global level to increase the efficiency of the management and decision-making in a smart city through crowdsensed frameworks. Regarding transportation networks, smartphones have been previously proved as an effective tool to estimate traffic incidents, like congestions or accidents [51]–[53]. Although they have been employed for SHM purposes in different studies [54]–[59], their application to indirect bridge monitoring had not been investigated until recent studies show that smartphones can be used as reliable sensors to collect acceleration data and apply them into indirect health monitoring techniques to assess bridge conditions.

Mei and Gül [60] proposed an indirect damage detection method based on Mel-frequency cepstral coefficients and used a smartphone to detect multiple damage states on a lab-scale bridge model. They showed for the first time in the literature that the damage in the bridge model can be identified using the smartphone on a car model even if the speed, weight, and suspension of the car vary between experiments. In another study, Matarazzo et al. [61] performed a real-life experiment to investigate the possibility of capturing bridge frequencies using smartphones. These studies arrive at the same conclusion that the recorded vibration of the vehicle is highly dominated by vehicle features, such as suspension, mass, speed, etc., as well as road roughness

1.3. PROBLEM STATEMENT

The main challenge facing indirect bridge monitoring, as mentioned before, is the presence of operational factors, primarily vehicle and road properties, as presented in Figure 1-1. Physical properties of the vehicle, including the mass, suspension, engine vibrations, and tire effects, are almost constant along the travel. However, the speed of the vehicle and road roughness effects are varying continuously. All previous studies focused on capturing bridge properties from on-bridge vibrational signals which are dominated by operational effects through a variety of methods. However, no approach was proposed specifically for the elimination of these operational factors from drive-by vibrations. Such a method needs to be robust against vehicle and road roughness features.

From a crowdsensing point of view, limited studies were dedicated to the use of smart cars or smartphones for drive-by monitoring of bridges. Most of those studies, especially the ones conducted under real-life conditions, were studied under lower speeds of the vehicle, where bridge presence among operational factors is stronger compared to higher speeds of the vehicle. However,

future crowdsensing-based drive-by bridge monitoring platforms need to be robust against vehicle speeds, including higher speeds on major roadways and highways.
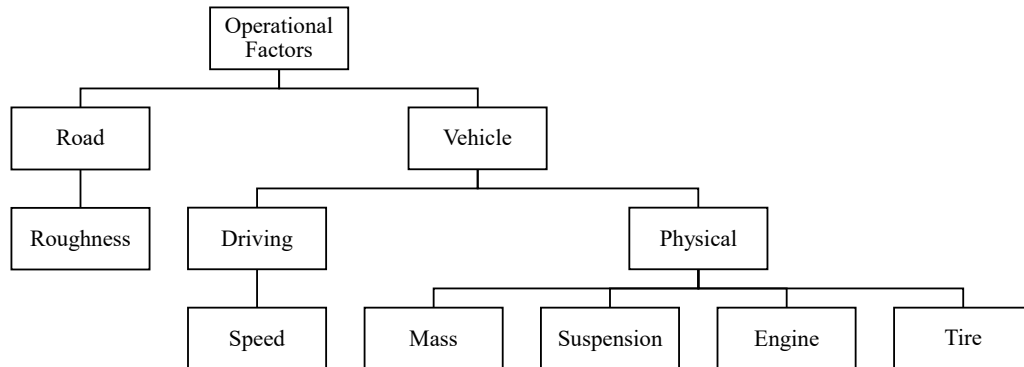
Figure 1-1: Variety of factors affecting drive-by collected vibrations

1.4. OBJECTIVES AND SCOPE

This thesis aims at addressing issues presented in the previous section through developing a novel methodology for analyzing drive-by vibrations. The method not only eliminates operational effects presented in Figure 1-1 but also employs smartphones as data acquisition devices, paving the path toward implementing the methodology in crowdsensing-based monitoring of transportation infrastructure in future smart cities.

In addition to the development phase, such a method needs to be assessed in practice. Hence, two phases of assessment need to be performed. First, a controlled laboratory experiment will be designed to limit the effective operational parameters and focus on the initial development of the methodology. Later, the enhanced version of the methodology will be assessed under real-life conditions, i.e., using full-scale vehicles and monitoring full-scale bridges.
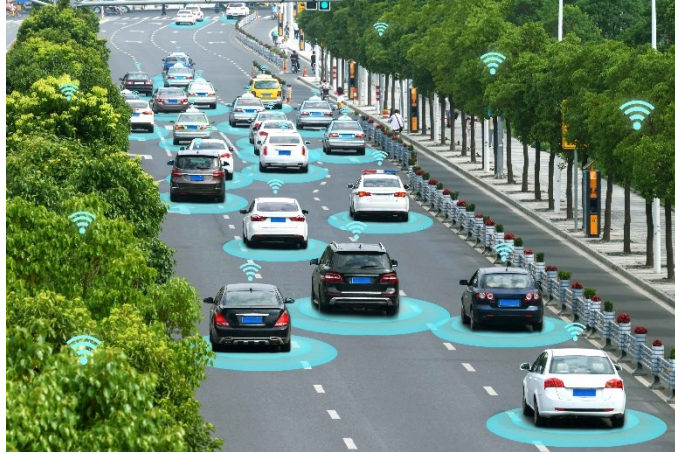
Figure 1-2: Crowdsensing-based monitoring of transportation infrastructure in future smart cities [62]

1.5. ORGANIZATION OF THE THESIS

The organization of this thesis is as follows:

Chapter 2 presents a problem investigation for the potential of using smartphones for the means of drive-by bridge monitoring. A controlled laboratory experiment is designed and employed with the focus of detecting the fundamental frequency of the bridge. The setup includes a robot car capable of modeling different suspensions and speed values to account for different vehicle types. The bridge was modeled using steel plates resting on different boundary conditions.

Chapter 3 presents the development of a novel methodology for the elimination of operational effects from drive-by bridge monitoring. Inverse filtering is introduced which employs off-bridge vibrations to design a filter for suppressing operational effects. The proposed method is then assessed for detecting the fundamental frequency of the bridge through a series of controlled laboratory experiments.

Chapter 4 presents the enhanced inverse filtering methodology, capable of addressing road roughness and speed changes of the vehicle. A database of vehicle vibrations per different speeds and roughness levels is proposed in this chapter. The performance of the enhanced inverse

filtering method is investigated for fundamental frequency detection of two full-scale bridges located in the city of Edmonton under real-life conditions.

Chapter 5 presents an application of the proposed inverse filtering method for damage detection of bridges. Unlike previous chapters which focused on bridge frequency detection, the method proposed in this chapter employs Mel-frequency cepstral analysis to detect patterns in the inverse filtered spectrum, introducing an abnormality index to detect changes in bridge state. The performance of the proposed method in eliminating operational effects is assessed both in controlled laboratory and real-life conditions. The damage detection capability of the method is studied through modeling a series of damage levels at different locations in laboratory experiments.

Chapter 6 presents the summary and conclusions of this thesis. Recommendations and possible future research topics are also included.

Chapter 2.   PROBLEM INVESTIGATION

2.1.   OVERVIEW

In this chapter, the potential of using smartphones for indirect frequency identification of bridges is investigated. First, the theoretical development of the methodology is discussed. Since there are a variety of vehicles with different features traveling over the bridge at different speeds, it is critical to investigate the robustness of indirect monitoring methods against vehicle features. Hence, an experimental study has been performed, including two lab-scale bridges with different boundary conditions and a robot car capable of maintaining a variety of speeds and suspension systems. The proposed framework focuses on the identification of frequencies of the bridge using acceleration signals recorded on the car. It is demonstrated that through a large set of passing cars with different features, the fundamental frequency of the bridge can be captured. Successful identification of the deviation of fundamental frequencies between two bridges with relatively close frequency values proves that the framework is capable of detecting damage-induced frequency changes in the bridge.

Several laboratory experiments are conducted in this chapter using two experimental bridge models with different support conditions, and also a robot car model capable of changing suspension springs and traveling speeds. In total, three spring types and three speeds were applied to the car, resulting in 9 combinations. The experiment consists of three stages. First, vibration analysis of the bridge is conducted to extract the natural frequencies of the bridge. Next, robot car vibration is analyzed to study the frequency spectrum of the car while moving on a rigid non-vibrating surface. Finally, the vibration of the car while moving on the bridge is studied. Comparing the results of these three stages provides the possibility of investigating the robustness of using smartphones to capture bridge frequencies against vehicle features.

2.2. VEHICLE-BRIDGE INTERACTION

Vehicle-bridge interaction (VBI) is the main concept in indirect bridge monitoring. Due to the dynamic interaction, vibrations of the vehicle and bridge are coupled to each other. In other words, the vibration of a vehicle moving over a bridge consists of both the vehicle and the bridge vibration. One of the first studies to investigate this notion was performed by Yang and Yau [63]. In that study, a simple 2D beam model was used to model a bridge and a moving spring-mass system was considered as the vehicle. The coupled equation on the vehicle bridge interaction was presented as follows [64]:

$$\begin{cases} \bar{m}(x)\ddot{u}_b(x,t) + E(x)I(x)u_b''''(x,t) = c(x,t) \\ m_v\ddot{u}_v(t) + k_v\left[u_v(t) - u_b(x,t)\right] = 0 \end{cases} \tag{2-1}$$

where x is the distance to the bridge end, t is the time, v is the speed of the vehicle, $\bar{m}(x)$ is the distributed mass of the bridge per unit length, $E(x)$ and $I(x)$ are the elastic modulus and moment of inertia of the bridge section, respectively, m_v and k_v are the mass and stiffness of the vehicle, and $c(x, t)$ is the contact force. Furthermore, u_b and u_v are the vertical displacements of the bridge and the vehicle relative to the equilibrium position, respectively. Note that the dot refers to the derivation with respect to time, while the prime denotes derivation with respect to x. The first equation is the governing dynamic equilibrium of the bridge, and the second one is of the vehicle. As seen in Eq. (2-1), the dynamic response of the vehicle includes dynamic characteristics of the bridge which means using an appropriate signal processing technique, it would be possible to extract bridge dynamic features, e.g., frequencies, from the vibration of the vehicle. Although this model is simple and it does not account for many challenges such as complicated vehicle model, road roughness, and environmental effects, the fact that the dynamic features of the bridge exist in the vibration of the vehicle still governs.

2.3. FREQUENCY-DOMAIN ANALYSIS

In this research, the frequency content of the acceleration signal is calculated through an averaging method proposed by Welch [65], here called Averaged Discrete Fourier Transform (ADFT), by averaging Fourier Transforms of the main signal over small windows. Eq. (2-2) describes Discrete Fourier Transform (DFT) as follows:

$$X[k] = \sum_{n=0}^{N-1} u_v''[n] e^{-j\frac{2\pi}{N}kn} \tag{2-2}$$

In this equation, u_v'' shows the acceleration signal recorded on the vehicle as previously defined in Eq. (2-1), N is the number of data points in the signal, and X denotes the vector of DFTs, which is a complex vector containing amplitude and phase values. Moreover, k is an index representing step frequencies through the following equation:

$$f = \frac{k}{N} f_s \qquad \text{for } 0 \leq k \leq N-1 \tag{2-3}$$

where f_s is the sampling frequency. Applying Eq. (2-2) to the whole acceleration signal results in a highly fluctuated spectrum, which is not suitable for peak analysis. However, if the signal is divided into multiple segments and each segment is considered as a separate signal in the DFT process, followed by averaging all the spectrums, the resulting spectrum will be smoother and more convenient for peak analysis. Among a variety of window functions proposed for selecting sub-signals [66], the hamming window is considered in this study. In addition, selected windows are not mutually exclusive to account for the effect of the transition, and a percentage of the window length is considered as an overlap. Therefore, the ADFT of the signal is calculated through the following equation:

$$\bar{X}[k] = \frac{1}{M} \sum_{m=1}^{M} \sum_{n=0}^{N-1} w_m[n] u_v''[n] e^{-j\frac{2\pi}{N}kn} \tag{2-4}$$

11

In Eq. (2-4), w_m is the function for the mth window and M is the total number of windows calculated by

$$M = 1 + \frac{N - N_w}{(1-p) \cdot N_w} \tag{2-5}$$

in which p is the overlap percentage of the windows. In this thesis, since the lengths of most acceleration signals are between 6 to 12 seconds, 5 seconds hamming window and 75% overlap are considered. Note that this window length is selected in order to balance between the smoothness and the resolution of the resulting spectrum. Shorter window length results in a smoother spectrum, whilst leading to the loss of most frequency contents due to the lower resolution. To increase the frequency resolution of the ADFT spectrum, all windows are zero-padded to 10 seconds, resulting in a 0.1 Hz resolution. Figure 2-1 illustrates the resulting FFT and ADFT spectra of an acceleration signal recorded on the robot car. As seen, the ADFT spectrum is smoother and more appropriate for filter design and peak analysis. Furthermore, the acceleration signals from the smartphone are resampled by interpolation before being converted to the frequency domain. The reason is that the sampling intervals of smartphones may not be perfectly consistent and deviate from the pre-set value. Although the Android application developed in the author's research group [60] significantly improves the stability of sampling frequency, resampling of the signal still increases the accuracy of the calculation.
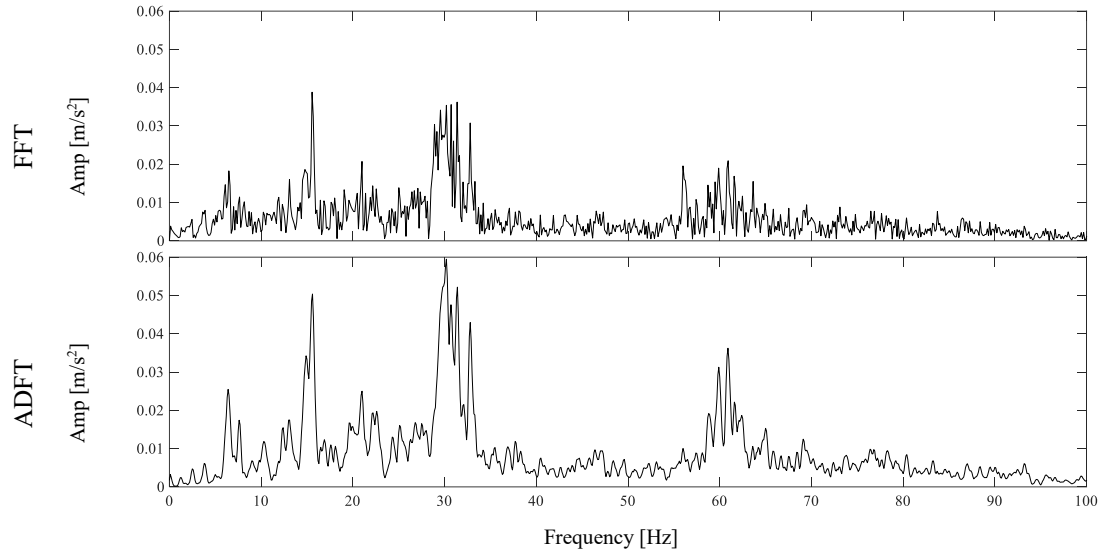
Figure 2-1: FFT vs. ADFT spectra.

In order to identify the most significant frequencies in each spectrum, a peak picking technique based on amplitude and prominence has been employed using MATLAB function *findpeaks* [67]. The prominence of a peak, shown in Figure 2-2, represents how the peak stands out due to its intrinsic height and location with respect to other adjacent peaks. A low but isolated peak can be more prominent than another one that is higher but is among a range of tall peaks. On the other hand, two equally prominent peaks with a substantial difference in amplitude are not equally significant in a spectrum. Hence, both the prominence and amplitude are considered as the criteria in this study. To this end, the amplitude and prominence values for all peaks in a spectrum are scaled to 100, and the peak score is defined as the average of its amplitude and prominence scores. This averaged score is then used as a criterion to quantify the significance of the peaks in the spectrum.
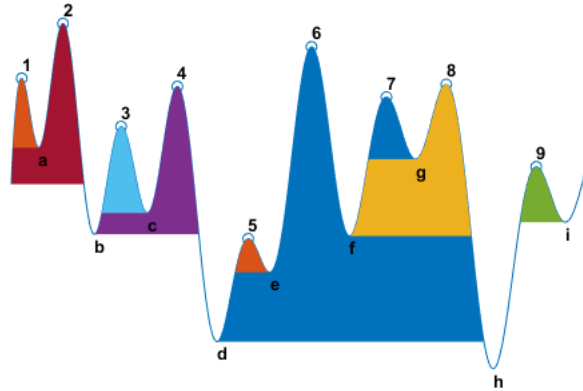
Figure 2-2: A sample spectrum showing the prominence of different peaks [67].

2.4. EXPERIMENTAL SETUP

This section illustrates the material and devices used in this experiment. First, two bridge models are described. Subsequently, the features of the robot car are explained. Finally, the instruments utilized to collect data during the experiment are presented.

2.4.1. Bridge

In this study, two types of bridges, one pin-roller and one fixed-fixed support, are considered. For both bridges, hot rolled steel plates of W44, which has a modulus of elasticity of 200 GPa, yield strength of 250 MPa, and ultimate strength of 310 MPa, are used. These plates are 2 m long and 330 mm wide. The thickness of the plates in the two bridge types are different: a 12.7 mm thick plate is used for the pin-roller bridge setup whereas a 6.35 mm thick plate is used for the fixed-fixed bridge setup. The reason for this selection is that using the low thickness plate for the pin-roller support bridge results in a significant sag in the middle of the bridge, which prevents the speed of the robot car to be constant while traveling over the bridge. On the other hand, using a thick plate for the fixed-fixed support bridge will intensively increase the stiffness and frequency of the bridge, which not only makes the bridge vibration negligible with respect to the car but also makes the experiment unrealistic.

Figure 2-3 shows the setup for the pin-roller bridge. Here, one pin support and one roller support are employed to carry the 12.7 mm thick plate. In Figure 2-4, the pin-roller support structure is illustrated. Both supports have the same structure, except that the pin is prevented from moving horizontally while the roller is free to move. As seen, an approaching span is also considered for the first few seconds that the car accelerates and reaches the constant target speed. Furthermore, another plate is used at the end of the bridge so that the car completely leaves the bridge and then stops. An additional small thick plate is employed between the main span plate and the supports so that the approaching and end spans do not have any contact with the supports and hence do not affect their free rotation.

Figure 2-3: Pin-roller bridge setup.
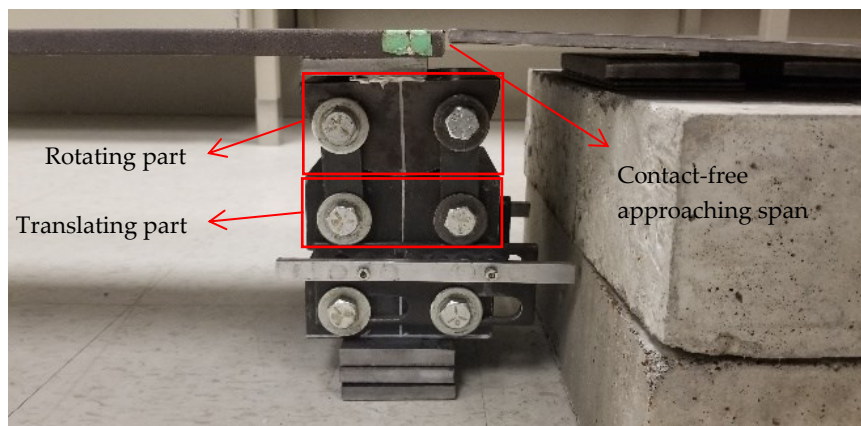
Figure 2-4: Pin/roller support.

Figure 2-5 demonstrates the setup for the fixed-fixed bridge. In this bridge, both supports are assumed to be completely fixed. In order to reach full fixity, two 25 cm long W10×54 steel

profile beams are used as the supports, which are connected to the main span plate of 6.35 mm thick through four bolts on both sides, as seen in Figure 2-6. In addition, to prevent the supports from moving horizontally, nine reinforced concrete blocks are used at both ends. Similar to the pin-roller bridge, two plates are used as the approaching and end spans.

Figure 2-5: Fixed-fixed bridge setup.

Figure 2-6: Fixed support.

2.4.2. Vehicle

In this study, a robot car was designed and built as shown in Figure 2-7 and Figure 2-8. This car consists of two identical rectangular aluminum plates of 350 mm by 125 mm with a thickness of 3.1 mm. The motor and the wheels are connected to the bottom plate. Four aluminum rods with a radius of 4 mm and length of 15 cm surrounded by four springs are used to connect the bottom plate to the top plate, where the acceleration data will be collected. Four linear bearings are connected to the top plate to ensure a smooth vertical movement on the springs.

The robot car in this experiment is capable of maintaining constant speeds between 0.2 and 0.4 m/s over flat surfaces or gentle slopes. Thus, three speed cases of 0.2, 0.3, and 0.4 m/s are considered here. In addition, in order to model three different suspension systems, three springs with stiffness values of 425, 615, and 726 N/m are employed. These springs are herein referred to as A, B, and C, respectively. The total mass of the top plate, including the smartphone and the sensor, is kept constant at 1.2 kg in all cases to make a better comparison of the effect of the suspension system on the spectrum of the passing car.
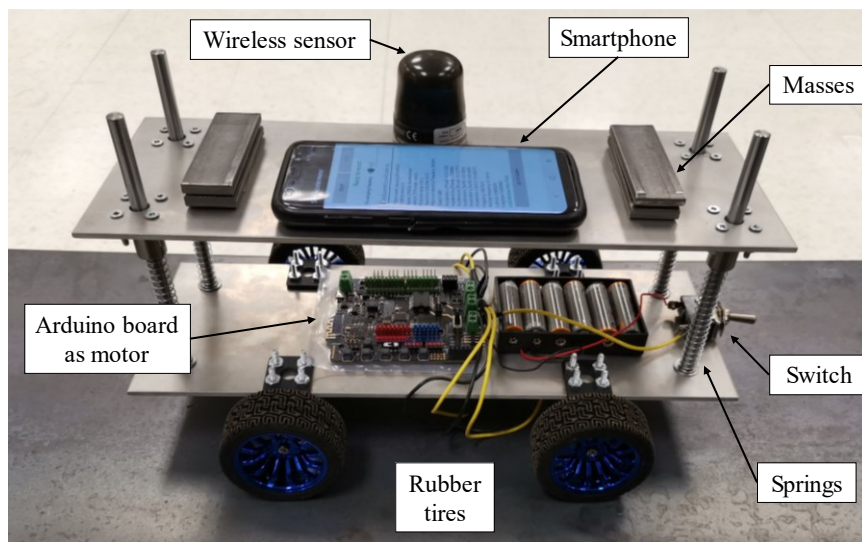
Figure 2-7: The custom-designed and -built robot car.
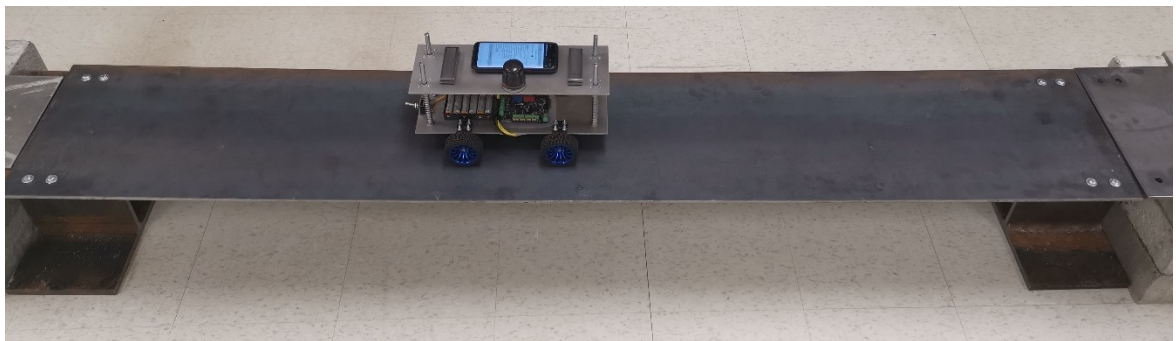
Figure 2-8: Robot car on the fixed-fixed bridge.

2.4.3. Instruments

To collect the acceleration from the car, one smartphone, the Samsung Galaxy S8, with a sampling frequency of 400 Hz is used. Recording acceleration data from the smartphone is performed using an Android app previously developed and used in [60], which provides the global vertical acceleration by using the gyroscope and magnetometer in combination with the accelerometer. This app also applies sampling frequency correction to the recorded data. In addition to the smartphone and in order to have a benchmark for comparison, one G-Link©-200 wireless accelerometer with the sampling frequency of 512 Hz is placed on the car, as seen in Figure 2-7.

As a verification, the acceleration data are collected from the bridge using three G-Link©-200 wireless accelerometers with a sampling frequency of 512 Hz. To detect as many modes as possible, these sensors are mounted at the mid-span, quarter-span, and 3/8th-span of both bridges, shown previously in Figure 2-3, which guarantees capturing the vibration of at least the first four modes, based on the approximate mode shapes of the pin-roller and fixed-fixed beams.

2.5. RESULTS

In this section, the results are discussed in three parts, including the bridge alone, the vehicle alone, and the vehicle while moving over the bridge. Through comparison of these results, it would be possible to investigate the potential of detecting bridge frequency using vehicle recorded vibrations.

2.5.1. Frequency Analysis of the Bridge

This section provides an overview of the natural frequencies of two bridges considered in this study. First, a free vibration test is performed on each bridge by applying an initial deflection at 40% span length. Applying initial deflection to this point not only creates a relatively larger amplitude vibration but also excites at least the first four modes of both bridges. Figure 2-9

illustrates the ADFT spectrum of the acceleration signals. The three columns in this figure represent three sensors located on the bridge, and two rows represent two considered bridges. The fundamental frequency of the pin-roller and fixed-fixed bridges are identified as 7.6 and 9 Hz, respectively. As expected, the amplitudes of the 1st and 3rd modes are significant in the mid-span sensor spectrum, while the 2nd and 4th have a relatively major presence in the quarter-span sensor spectrum, especially in the fixed-fixed bridge. The other observation is that the first mode always has the largest amplitude in the free vibration test.

To identify higher mode frequencies with higher accuracy and larger amplitudes, another test was conducted through multiple tapping over different points along the bridge, to mimic ambient vibration tests. This way, higher modes of the bridge are excited and higher peaks appear due to those modes, as seen in Figure 2-10, which has a similar organization to Figure 2-9. Considering the frequency range of 0~100 Hz, 2nd and 3rd modes of the pin-roller bridge are 29.9 and 65.7 Hz, and 2nd to 5th modes of the fixed-fixed bridge are 26, 34.1, 50.3, and 69.8 Hz, respectively.
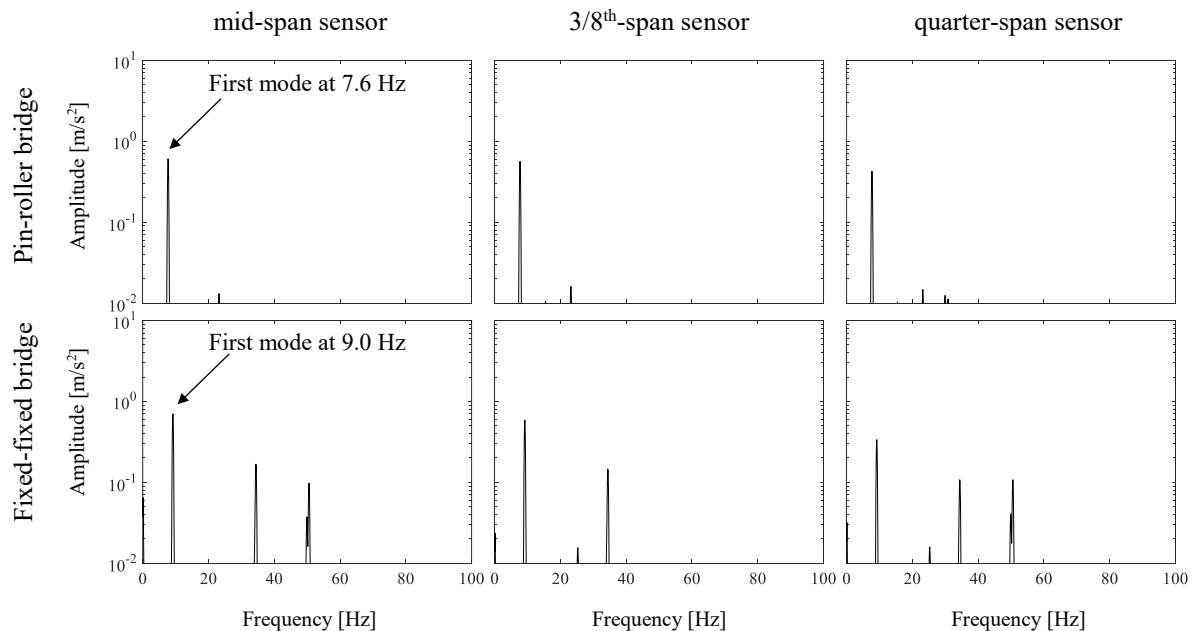
Figure 2-9: ADFT Spectrum of bridge sensors under free vibration of the bridge.
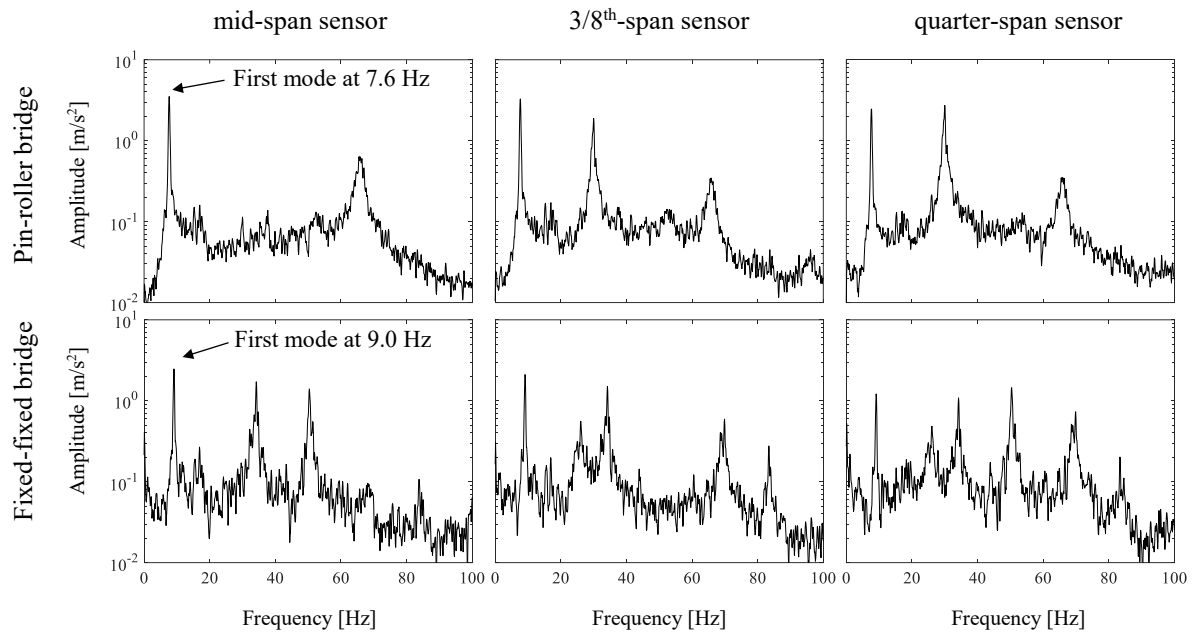
Figure 2-10: ADFT Spectrum of bridge sensors under tapping-forced vibration of the bridge.

2.5.2. Frequency Analysis of the Vehicle

This section aims to experimentally investigate the frequency content of the vibration of the robot car considering three different suspension systems. First, the suspension system of the car is studied through a free vibration test, which is performed by applying an initial deflection to the top plate of the car when the car is at a stationary position. Since the damping of the suspension system in this model is very large due to imperfections, the length of the free vibration signal is very short, i.e. around two seconds. Thus, the ADFT analysis was conducted using smaller windows, resulting in a very smooth spectrum in Figure 2-11. This figure has three rows representing three spring types used in this study, and each graph contains two curves related to the sensor and the smartphone mounted on the car. As seen, the frequency of the suspension system is clearly visible in all three graphs and is equal to 3.9, 5, and 5.4 Hz, for three springs of A, B, and C, respectively. As expected, the frequency of the suspension system increases with the stiffness of the springs. Another important observation in this figure is that the spectrum of the

sensor and the smartphone agree in capturing the peak, but with different amplitudes. Since the main focus of this study is to find the significant frequencies in the spectrum, it means that smartphones can be considered a reliable tool for this purpose.
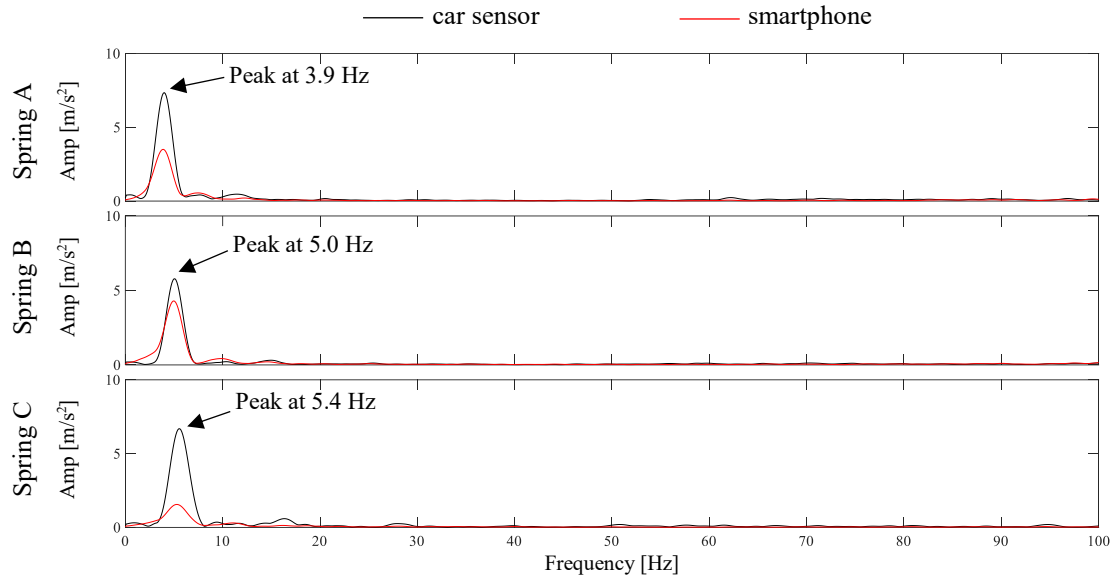
Figure 2-11: ADFT Spectrum of the car sensor and smartphone under suspension test using three different springs.

After analyzing the suspension system, the vibration analysis of the car while moving on a rigid surface, i.e. off-bridge test, is conducted. Such a test could be suitable for comparing the vibration of the same car moving on the bridge, in order to investigate the effect of the bridge on the car vibration. Figure 2-12 demonstrates the spectrum of the sensor and the smartphone mounted on the car in different conditions. Three columns in this figure illustrate the speed values of the car, while three rows represent different springs and hence different suspension systems. As seen, there are three major peak ranges visible in these graphs. Considering v=0.2 m/s, there are multiple peaks at around 14, 30, and 54 Hz. However, these peaks change to 18.5, 34, and 67.5 in v=0.3 m/s, and 22, 43, and 85 in v=0.4 m/s, respectively. On the other hand, the columns of Figure 2-12 prove that these peaks do not change with the suspension system of the car. In fact, based on the results from Figure 2-11, the frequencies of the suspension system are all below 10 Hz, which are not significantly excited in this experiment in Figure 2-12. The reason could be the fact that unless

there is a huge surface disruption, like potholes, the suspension frequency will be noticeably less excited with respect to other sources of vibration, like motor vibration or the moving frequency of the vehicle. In addition, similar to Figure 2-11, this experiment corroborates the potential application of smartphones to detect the frequency content of the car.
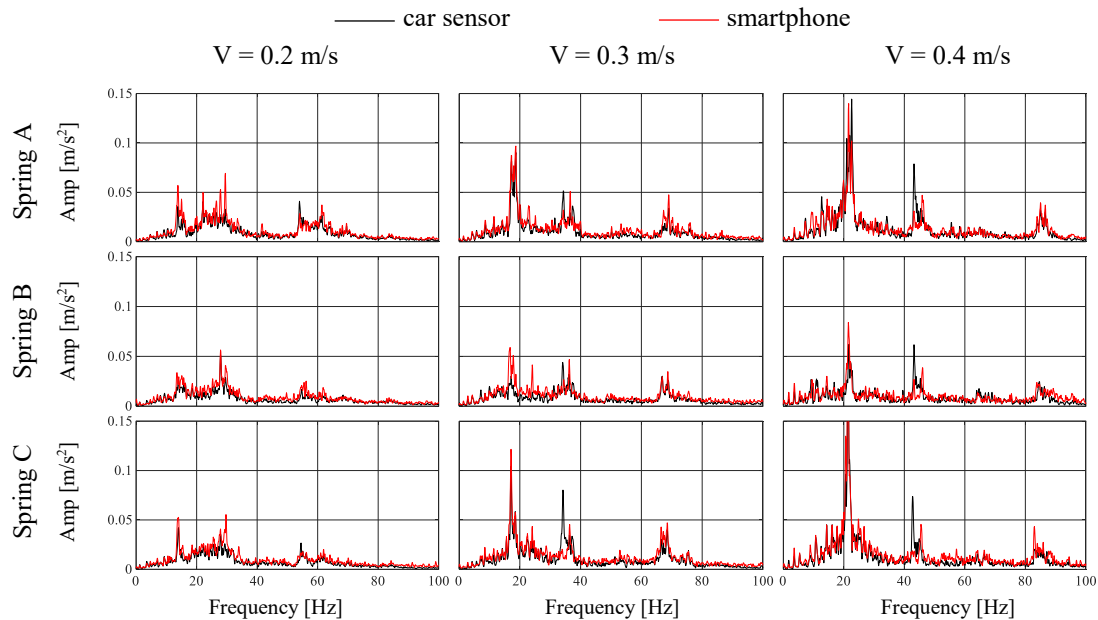
Figure 2-12: ADFT Spectrum of the car sensor and smartphone under off-bridge test using three different springs at three different speeds.

2.5.3. Frequency Analysis of the Vehicle Moving On the Bridge

In this section, the vibration recorded on the car while moving on the bridge is studied. Similar to the previous section of Frequency Analysis of the Bridge, first the condition of the moving car as the only source of vibration, i.e. with no external force acting on the bridge, is considered. Afterward, along with the car moving, multiple tapping on different points on the bridge is applied to account for larger vibrations of the bridge due to other forces, such as other cars or wind loads. Comparing the frequency contents of this section with those of the off-bridge experiment in the previous section of Frequency Analysis of the Vehicle makes it possible to identify the effect of bridge vibration on the recorded acceleration of the car.

Figure 2-13 and Figure 2-14 show the spectra of the car moving over pin-roller and fixed-fixed bridges, respectively, while no external forces are acting on the bridge. The organizations of both figures are similar to Figure 2-12 except that there are vertical dashed lines added to the graphs showing the first three frequencies of each bridge identified through the bridge experiments. Both Figure 2-13 and Figure 2-14 almost show the same pattern seen in the off-bridge analysis, Figure 2-12, with the only difference that there is one extra relatively sharp peak below 10 Hz, close to the fundamental frequency of the bridge. In Figure 2-13, the first peak in the first column, i.e. when v=0.2m/s, is equal to 7.3 Hz, while this peak changes to 7.2 and 7 Hz for v=0.3m/s and v=0.4m/s, respectively. This deviation from the exact bridge frequency, 7.6 Hz, verifies the previously shown phenomena of shifted frequency [20] of the bridge in the vibration of the car, which increases with the speed of the vehicle. Likewise, in Figure 2-14, the identified frequencies of the bridge are 8.7, 8.6, and 8.4 for v=0.2m/s, v=0.3m/s, and v=0.4m/s, respectively, compared to the exact fundamental frequency of 9 Hz.
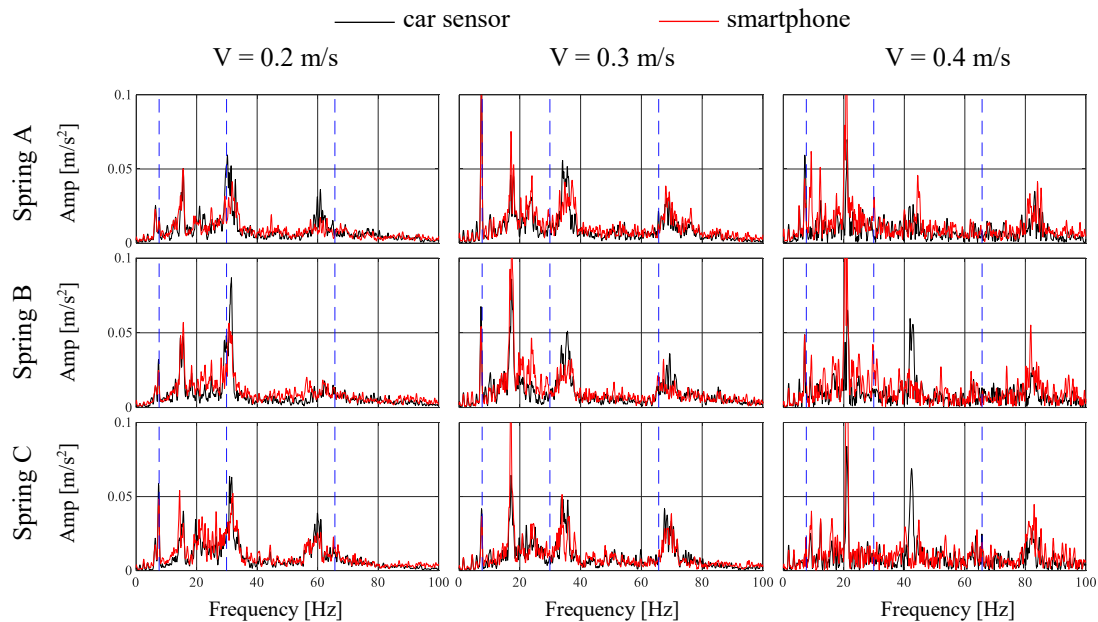
Figure 2-13: ADFT Spectrum of the car sensor and smartphone under free on-bridge test on the pin-roller bridge using three different springs at three different speeds.
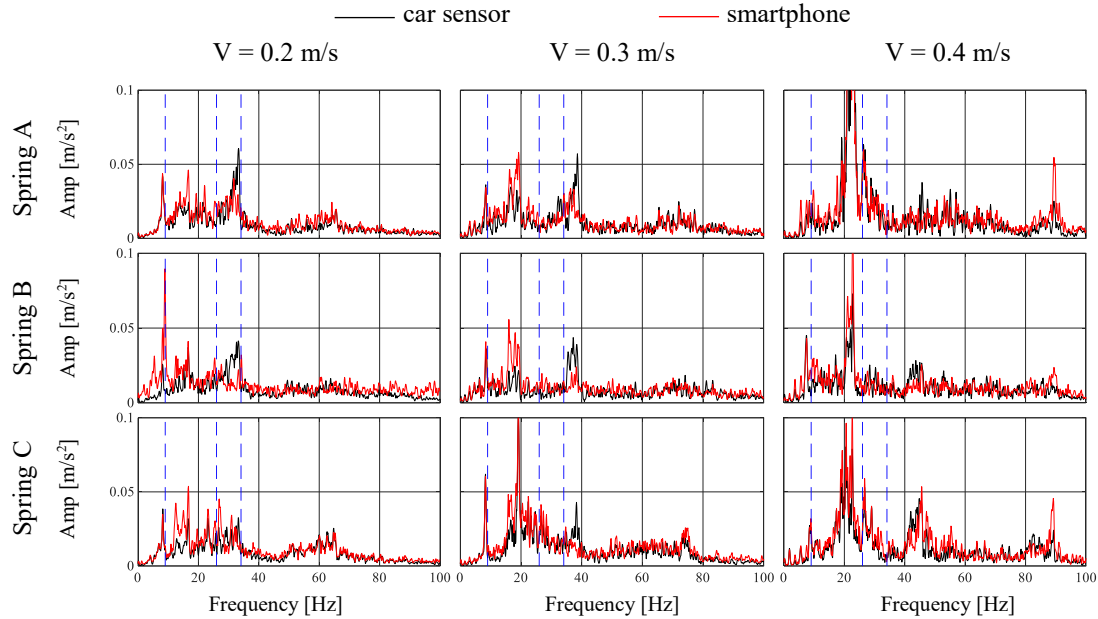
Figure 2-14: ADFT Spectrum of the car sensor and smartphone under free on-bridge test on the fixed-fixed bridge using three different springs at three different speeds.

As seen in both Figure 2-13 and Figure 2-14, it seems that higher modes are either not excited or their amplitude is very low when there is no other source of excitation except the moving car. In fact, in this experiment, the higher modes of the bridge, excited with relatively lower amplitudes, lie within the peaks of the car spectrum, excited with significantly larger amplitudes, preventing those modes to be visible in the combined vibration spectrum. However, the fundamental frequency of the bridge is below 10 Hz, where there are no significant peaks visible in the off-bridge spectrum in Figure 2-12.

In real-life situations, there are many sources of excitation acting simultaneously on the bridge, e.g. many cars moving in multiple lanes in similar or opposite directions, effects of winds, etc., which results in larger vibration of the bridge and hence stronger presence of its frequencies in the car spectrum. Therefore, another set of experiments was conducted by tapping multiple points along the bridge while the car moves over the bridge. Figure 2-15 and Figure 2-16 illustrate the spectrum of the car vibration during this experiment for pin-roller and fixed-fixed bridges, respectively. As expected, the presence of tapping-forced excitation that mimics other real-life

sources of excitation increases the bridge vibration, resulting in a clear significant peak close to the fundamental frequency of the bridge. In addition, in some cases for the pin-roller bridge and nearly all cases in the fixed-fixed bridge, the second mode of the bridge is also clearly present in the car spectrum.

The important conclusion from this section is that if there is a substantial difference between the frequencies of the bridge and different cars passing over the bridge, it is possible to detect the shifted fundamental frequency of the bridge using the acceleration signal of the car recorded on the smartphone. In addition, with sufficient vibration of the bridge, there is a potential that the second mode of the bridge could be captured as well. Moreover, it should be noted that, in future studies, the speed of the car while crossing the bridge can be easily obtained using the built-in GPS of a smartphone and this information can be used to eliminate the effects of the speed on the identified frequencies.
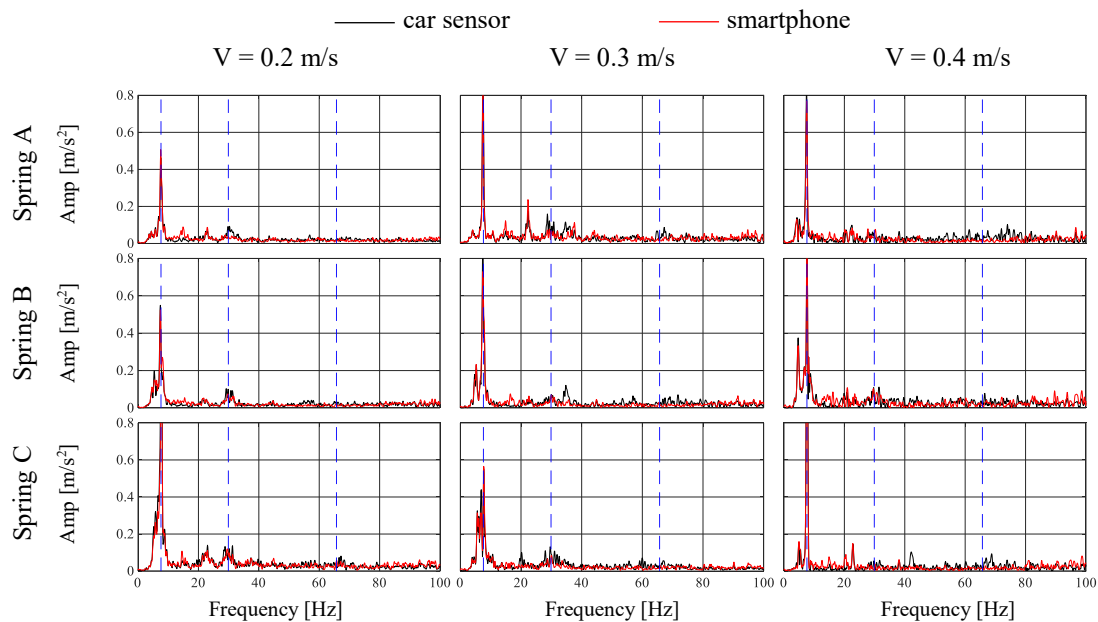
Figure 2-15: ADFT Spectrum of the car sensor (black line) and smartphone (red line) under tapping-forced on-bridge test on the pin-roller bridge using three different springs at three different speeds.
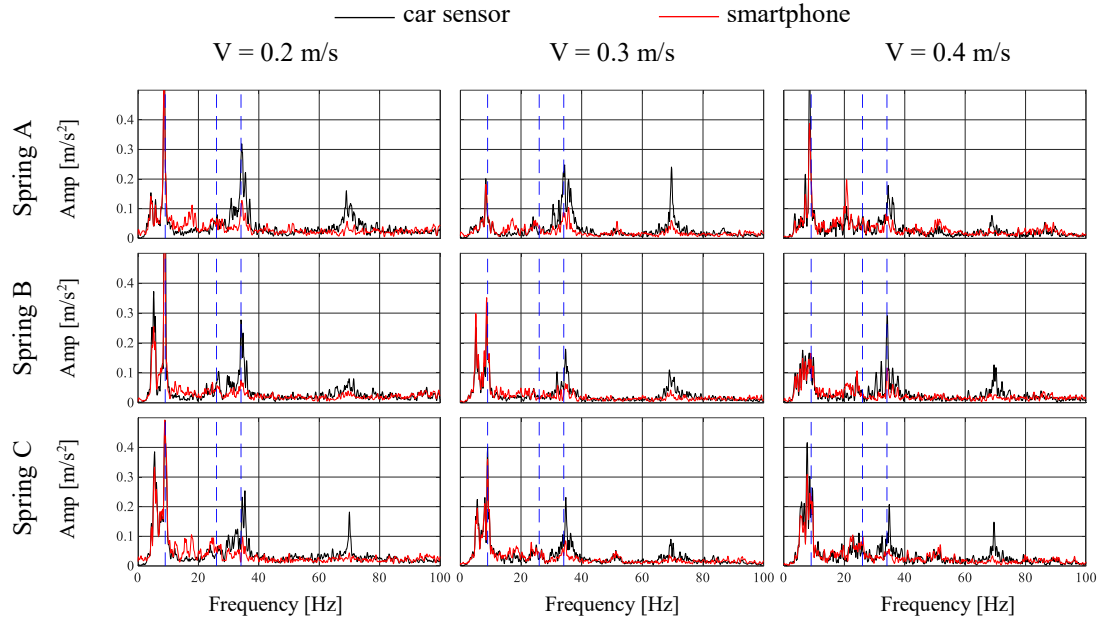
Figure 2-16: ADFT Spectrum of the car sensor and smartphone under tapping-forced on-bridge test on the fixed-fixed bridge using three different springs at three different speeds.

2.6. APPLICATION TO BRIDGE STATE DETECTION

This section focuses on the application of the proposed frequency analysis of smartphone data for assessing the changes in the structural condition of the bridge. Consider a large number of smartphones, as sources of data, located on many cars with different systems traveling over a bridge at different speeds. It is shown in this study that it is possible to capture at least the first shifted frequency of the bridge through frequency analysis of the acceleration signals recorded on smartphones. At this point, the main challenge is the damage detection capability of such signals.

To investigate the potential of the framework presented in this study for damage detection of bridges, analysis results presented in the previous sections are compared in Figure 2-17. The organization of this figure is similar to previous figures containing all cases of different suspension systems at different speeds. However, each graph contains three curves: off-bridge spectrum with a black solid line, on-bridge spectrum over the pin-roller bridge with a red solid line, and on-bridge spectrum over the fixed-fixed bridge with a blue solid line, all using recorded signals with the

smartphone. In addition, exact values of the fundamental frequencies of both bridges are shown using dashed lines, i.e. red line for the pin-pin bridge and blue line for the fixed-fixed bridge. Note that a narrow range of 0~20 Hz has been selected to concentrate on the fundamental frequency of the bridge in the spectra.
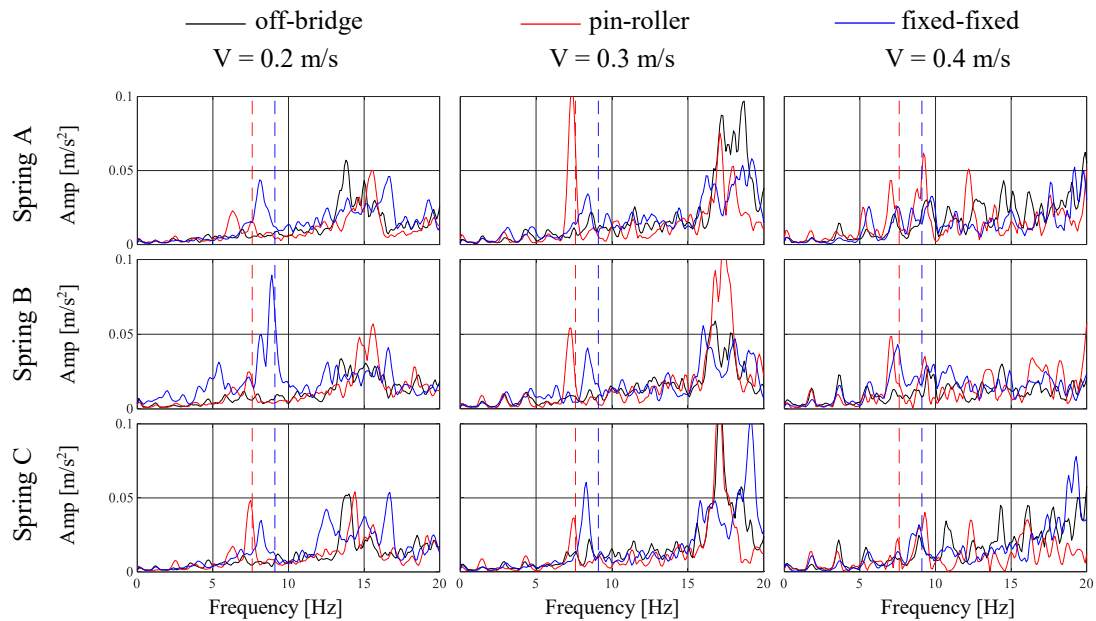
Figure 2-17: ADFT Spectrum of the smartphone under the off-bridge test, on-bridge test over the pin-roller bridge, and on-bridge test over the fixed-fixed bridge using three different springs at three different speeds.

Figure 2-17 illustrates that if there are many different vehicles moving over a bridge, it is possible to identify changes in the frequency of the bridge in most cases, although this deviation is not clearly captured in some cases, especially at higher speeds. The off-bridge spectrum provides a reliable tool to distinguish between car-related and bridge-related peaks. Although the source and amount of the shift in the frequency of the bridge are still unknown and a subject of contention in the literature, these experiments demonstrate that it is possible to use smartphone data to detect changes in the bridge state, such as boundary conditions. The relatively large mass ratio of the robot car to the bridge in the experiments plays a major role in increasing the shift of the identified frequency since the mass distribution of the system changes as the car passes over the bridge and

the frequency tends to be smaller due to larger total weight. It is expected that in real-life practice with a lower car-to-bridge mass ratio, the amount of the shift would be smaller.

In order to investigate the capability of detecting bridge frequency, the peak picking technique described in the Methodology section is applied to the data in Figure 2-17. The resulting peak scores are then used to find the most probable range for the frequency of both pin-pin and fixed-fixed bridges. For this purpose, successive 0.5 Hz-wide windows are considered in each spectrum and the score of all peaks in those windows are averaged. This averaged score represents the significance of the peaks in each frequency range of that spectrum. Comparing averaged peak scores for each frequency range among two different passes, i.e. off-bridge, pin-pin, or fixed-fixed bridge, makes it possible to detect the frequency range with the largest score change, which represents the frequency range of the corresponding bridge.

This process is conducted on all different combinations of suspension and speed shown in Figure 2-17 and the results are illustrated in Figure 2-18 through Figure 2-20. The red and blue dashed lines in these figures show the fundamental frequency of pin-pin and fixed-fixed bridges, respectively. Figure 2-18 demonstrates the change in the averaged peak score of the pin-pin bridge with respect to the off-bridge condition. As seen, the largest increase in the averaged peak score is in the 7~8 Hz range, which is close to the exact frequency of 7.6 Hz. It is expected that most of the bridge-related peaks are smaller than 7.6 since the shifted frequency is expected to be smaller. Similarly, Figure 2-19 which represents the change in the averaged peak score of the fixed-fixed bridge with respect to the off-bridge shows the most changes in 7.5~9 Hz, close to 9 Hz of the fixed-fixed bridge fundamental frequency.
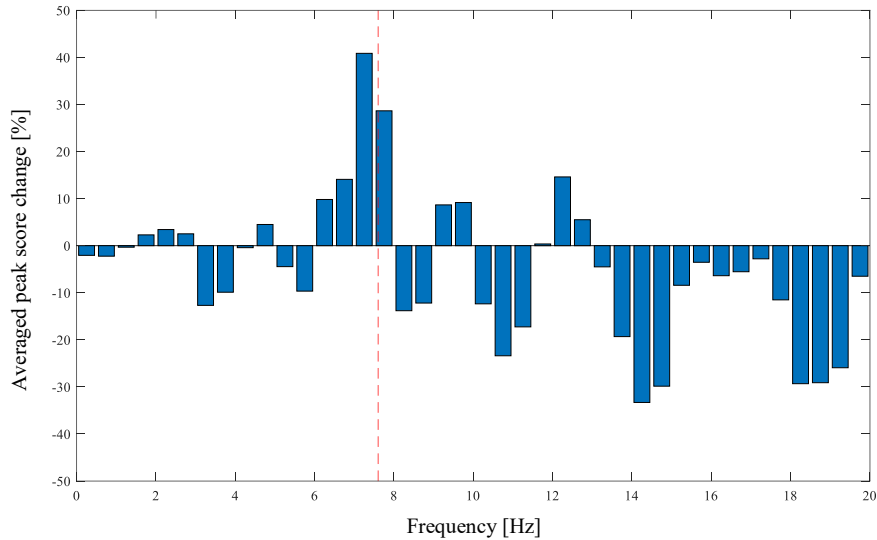
Figure 2-18: Averaged peak score change of all passes on pin-pin bridge vs. off-bridge.
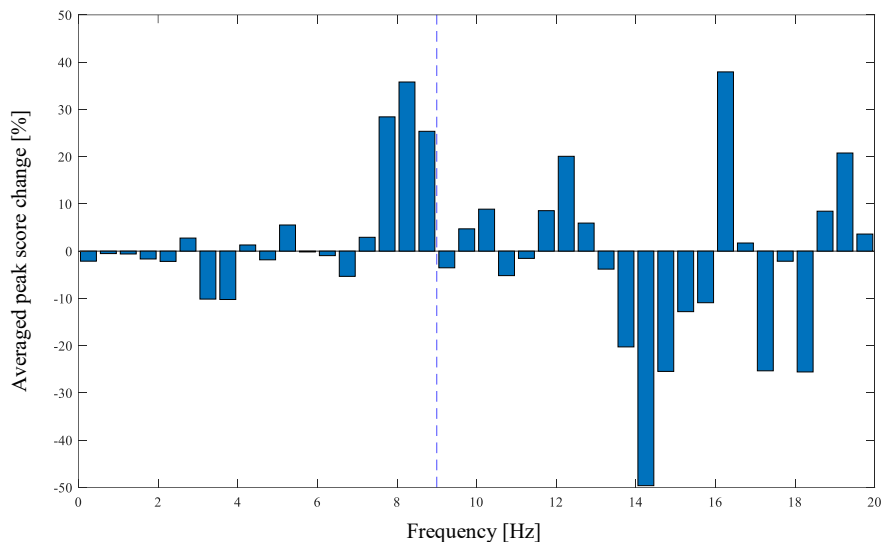
Figure 2-19: Averaged peak score change of all passes on fixed-fixed bridge vs. off-bridge.

More insights are provided by comparing the passes over pin-pin and fixed-fixed bridges. Figure 2-20 illustrates the same score change described in Figure 2-18 and Figure 2-19 considering the fixed-fixed bridge as the baseline. As seen, there is a large drop in the averaged peak score of the frequencies near the fixed-fixed bridge, while there is a large increase close to that of the pin-pin bridge. This plot represents the main output of this section, which is bridge state detection. Using the vibration data from different cars with different speeds passing over two different bridge states, this methodology would be able to detect the change in the frequency of those bridges

29

without prior knowledge of their frequency. It is noteworthy that the resolution and accuracy of the identified frequencies are expected to increase with the use of future smartphones as the quality and performance of the built-in sensors in smartphones increase considerably in time. For example, the maximum sampling frequency for a Samsung Galaxy S5 is 200Hz whereas it is 400Hz for the Samsung Galaxy S8 used for the experiments presented in this study. Such developments in technology will further increase the benefits of the framework presented in this study.
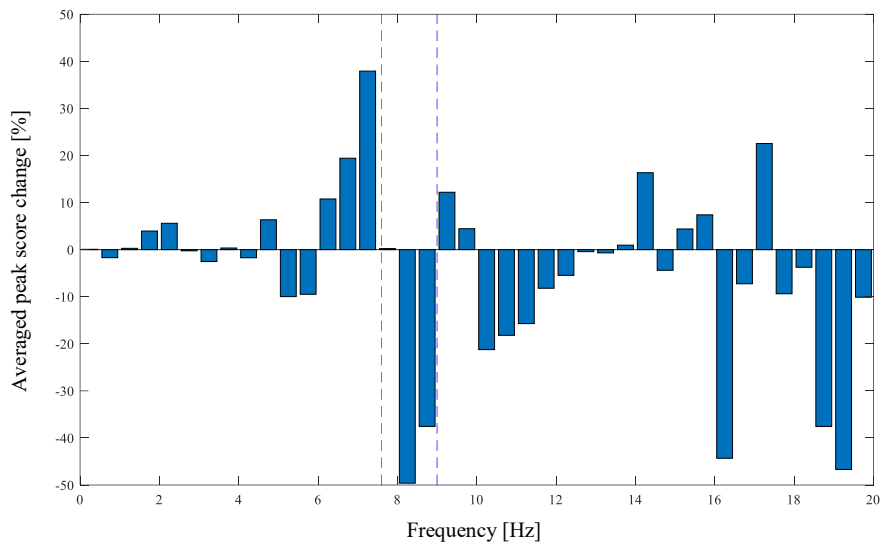
Figure 2-20: Averaged peak score change of all passes on pin-pin bridge vs. fixed-fixed bridge.

2.7. CHAPTER CONCLUSION

The study presented in this chapter demonstrates the potential of using smartphones as the means of detecting bridge frequency through a controlled laboratory experiment. Different combinations of the suspension springs and speeds for the vehicle as well as considering two bridges with different support systems provide strong evidence for the robustness of the method against vehicle and bridge properties. In addition, since any severe damage to the bridge will have a significant impact on its fundamental frequency, this study proves that there is a possibility that such damage could be identified through an appropriate crowdsensing framework that gathers data from a large population of smartphones on different cars passing over a bridge.

It should be noted that the results in this chapter demonstrated that the frequency detection of the bridge using a smartphone is prone to major challenges, especially vehicle features. In fact, vehicle features seem to dominate the frequency content of the recorded acceleration signals and detecting bridge frequency may be challenging in some cases, particularly at high speeds. In addition, the controlled laboratory experiments were performed in nearly ideal conditions, where the speed of the vehicle was kept constant while traveling over the bridge, and also the surface roughness variations were not included in the analyses. Such challenges are to be addressed in the next steps of the methodology development in order to be applicable in real-life practice.

Chapter 3. METHODOLOGY DEVELOPMENT

3.1. OVERVIEW

As mentioned in the previous chapter, the drive-by vibrations are significantly dominated by operational factors, such as vehicle and road roughness. This chapter aims at developing a methodology for eliminating such effects from drive-by vibrations through creating a filtering process.

Signal processing and filtering methods have been widely used in SHM and bridge engineering. For instance, Ding et al. [68] employed an adaptive finite impulse response filter to study temperature effects on bridges. In addition, using the Kalman filter for bridge health monitoring was a subject of many studies [69], [70]. However, employing an appropriate filtering method in indirect bridge monitoring is a challenge since every signal is recorded on a different device located on a different vehicle. Thus, any effective filter resulting in bridge features when applied to the vibration data of the moving vehicle needs to be unique to the vehicle and the device.

One common element of all previous studies on detecting bridge features from mixed vibrations recorded on the vehicle was the focus on the on-bridge signal alone. Looking from a different point of view, this chapter proposes a filtering method by employing off-bridge signals, i.e., those recorded while the vehicle was not on the bridge and was moving on the ground. Hence, this chapter proposes the inverse filtering method to eliminate operational effects from drive-by vibrations.

In general, inverse filters are designed to extract a specific feature from a noisy signal. In other words, the signals in noisy conditions are used to create a filter which then can be applied to the new signals to remove the effect of the noise. Some of the first applications of inverse filtering were in voice processing [71], [72]. Later, it was used in other fields such as image processing in

medical sciences [73] and geophysics [74]. This study proposes an inverse filtering method for indirect monitoring of bridges, which utilizes the vibration data recorded on the vehicle while moving off-bridge, i.e., moving on the ground, to filter out car features from the vibration of the vehicle while moving on-bridge. Therefore, each device on each vehicle will have a unique filter that is compatible with the features of the device and the vehicle, and makes it possible to be applied to a population of devices to monitor bridges.

The effectiveness of the proposed methodology is evaluated with experiments using a robot car as the vehicle moving over a lab-scale simply supported bridge, similar experimental setup to that of the previous chapter. Nine combinations of speed and suspension stiffness of the car have been considered to investigate the robustness of the proposed methodology against car features. The results demonstrate that the inverse filtering method offers significant promise for identifying the fundamental frequency of the bridge. Since this approach considers each data source separately and designs a unique filter for each data collection device within each car, it is robust against device and car features. It should be noted that for simplicity, the proposed methodology considers similar conditions for off- and on-bridge tests, including the surface roughness, mass and speed of the vehicle, orientation of the smartphone, etc. The variations of these factors and their effect on the drive-by vibrations will be addressed in the next chapter.

In the following, first, the methodology of the proposed signal processing and inverse filtering is explained. Later, the performance of the method is assessed through a series of laboratory experiments which are provided in the following sections.

3.2. INVERSE FILTERING METHODOLOGY

In this chapter, a novel method of filtering is proposed based on the comparison of off-bridge and on-bridge acceleration signals. In fact, most of the frequency content of the recorded signals is

dominated by moving car features, like speed, suspension, weight, engine vibrations, etc. These effects are present in both off-bridge and on-bridge data. However, bridge frequency is only expected to appear in the on-bridge data. Hence, if a filter is designed to remove major frequency content of the off-bridge data, and then applied to the on-bridge data, it is expected that the filtered on-bridge data will contain mostly frequencies related to the bridge dynamics. For more clarity, consider the hypothetical spectrum of the off-bridge and on-bridge signals as illustrated in Figure 3-1 using black and red curves, respectively. These curves are created using cubic polynomials. It is expected that the major peaks of the off-bridge spectrum will be present in the on-bridge one. However, if the frequency of the bridge is not close to the major frequencies of the car, there will be an unexpected change in the amplitude of the spectrum at a specific frequency, as seen in Figure 3-1. This relatively small change may not be considered as a peak in the on-bridge spectrum; while after applying the inverse filtering, this peak will become more visible.
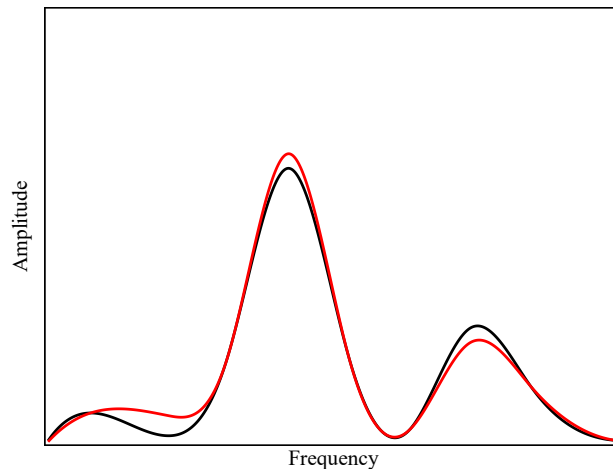
Figure 3-1: Hypothetical spectrum of off-bridge (black) and on-bridge (red) acceleration signals.

In order to design the filter shape, the off-bridge spectrum is considered. As discussed in the previous section, ADFT is used to convert the time-domain off-bridge signal to the frequency domain. The proposed windowing and averaging technique ensures that a sudden external factor, such as a sharp road defect, which drastically alters the shape of the spectrum of a single window,

does not affect the total shape of the resulting averaged spectrum. Afterward, the spectrum is inverted to form the filter shape prototype using the equation below:

$$\tilde{F}[k] = \frac{1}{X[k]} \tag{3-1}$$

where X denotes the ADFT spectrum of the off-bridge signal and represents the filter shape prototype. In Figure 3-2, the black curve shows the hypothetical ADFT of the off-bridge signal, and the blue curve represents its inverse, which would be the prototype for the inverse filter. As expected, the filter shape amplifies the frequencies with low amplitude in the off-bridge spectrum and suppresses those with higher amplitudes, i.e. peaks, in the off-bridge spectrum.
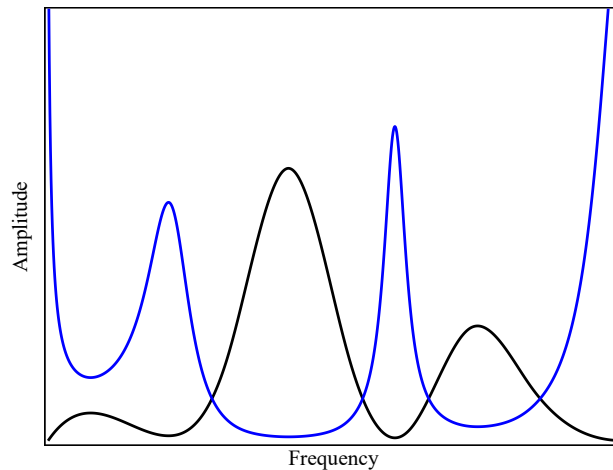
Figure 3-2: Hypothetical spectrum of the off-bridge signal (black) and corresponding filter shape prototype (blue).

To apply the inverse filter to the on-bridge spectrum, the filter shape prototype needs to be scaled. Since the filter prototype was designed based on the pure inverse function, it will scale all amplitudes to one, which is not a meaningful scale for acceleration amplitudes. Furthermore, the amplitude level of the on-bridge signal may be different than that of the off-bridge because of external factors, like surface roughness or road defects. Here, the mean value of the spectrum as a measure of the energy level within the signal is considered for scaling, which is calculated by

$$\bar{X} = \frac{\displaystyle\sum_{0}^{N-1} X[k]}{N} \tag{3-2}$$

where $\bar{X}$ denotes the mean value of the off-bridge spectrum. Therefore, the inverse filter shape will follow this equation:

$$F[k] = (\bar{X})\tilde{F}[k] = \frac{(\bar{X})}{X[k]} \tag{3-3}$$

The filter in Eq. (3-3) can be applied to the on-bridge spectrum to form the filtered spectrum:

$$Y_f[k] = F[k]Y[k] = \frac{(\bar{X})}{X[k]} Y[k] \tag{3-4}$$

In Eq. (3-4), $Y[k]$ and $Y_f[k]$ represent unfiltered and inverse filtered on-bridge spectra, respectively. Figure 3-3 demonstrates the application of this procedure to the hypothetical spectra in Figure 3-1 and Figure 3-2, where the red curve represents the unfiltered on-bridge spectrum and the blue curve shows the filtered spectrum. As seen, the resulting filtered spectrum has one major peak at the frequency of the deviation in amplitudes of off- and on-bridge spectra. Although there might be some fluctuations at other frequencies, the major peak with significantly higher amplitude and prominence expresses the desired frequency of the target. The flowchart of the proposed method is presented in Figure 3-4.
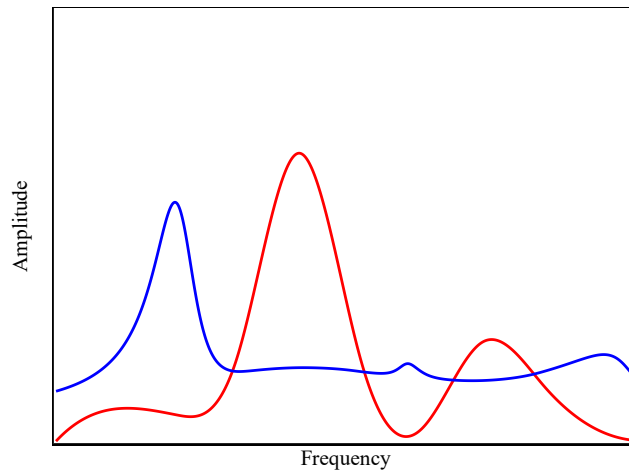
Figure 3-3: Hypothetical on-bridge unfiltered (red) and filtered (blue) spectra.
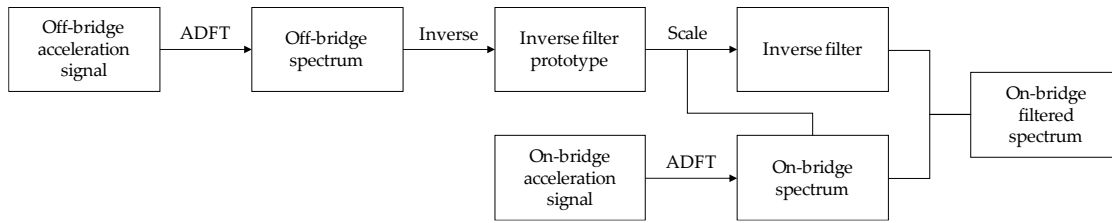
Figure 3-4: Flowchart of the proposed inverse filtering methodology.

3.3. EXPERIMENTAL SETUP

The experimental setup in this chapter is similar to the experiment presented in the previous chapter to provide a clear comparison of the performance of the proposed methodology. A pin-roller bridge is considered, together with a robot car maintaining three different speed levels while using three different spring types, similar to the values mentioned in Chapter 2, to mimic different vehicles passing over the bridge. In addition, since the inverse filtering methodology requires off-bridge data to design the filter, an off-bridge setup is also considered as shown in Figure 3-5. As seen, a similar plate resting on the ground is used to eliminate the effect of surface roughness effects for this stage of the analysis. Since the plate may still vibrate due to imperfections of the floor surface, two masses were used at both ends of the plate to restrain it from any flexural vibrations.
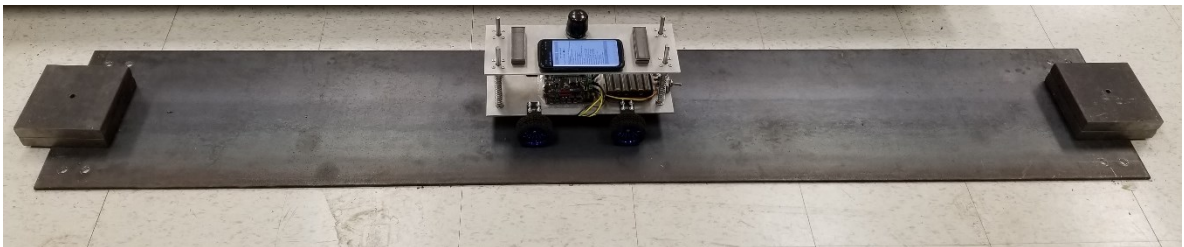
Figure 3-5: Setup for simulating the off-bridge condition.

3.4. RESULTS

In this section, the proposed inverse filtering-based method is applied to the data collected in the experiments. First, the off-bridge data is collected and the inverse filter prototype is developed for each case. Later, the filter is verified by applying it to the off-bridge data. Finally, the filter is

applied to the on-bridge data in order to identify the fundamental bridge frequency. Note that car speeds of 0.2, 0.3, and 0.4 m/s with the spring stiffness values of 425, 615, and 726 N/m (for Spring A, Spring B, and Spring C, respectively) are employed in the experiments, resulting in a total of 9 cases.

3.4.1. Filter Design

In this section, the off-bridge data collected from the robot car while moving on the off-bridge setup, shown in Figure 3-5, are presented. The total duration of the off-bridge signal varied between 4 to 8 seconds for the three speed cases. Therefore, to reduce the local effects of the beam and account for longer duration signals, three trials of off-bridge data were collected in this part. ADFT spectrums of the acceleration data recorded by sensor and smartphone are shown in Figure 3-6 and Figure 3-7, respectively. These figures consist of three rows and three columns representing different speeds and suspension stiffness values. In each plot, trials are illustrated using gray curves and their average is shown with the black curve. As seen, major peaks which are mainly due to motor vibration and moving frequency of the car are mostly dependent on the speed of the car. In addition, an increase in the speed results in higher amplitude for major frequencies. As expected, the data recorded on the sensor show higher resolution with respect to the smartphone due to the higher accuracy of the device, resulting in capturing low-frequency harmonics with higher accuracy. However, the smartphone is successful in capturing major peaks, which are the focus of the proposed method. In fact, the designed filter for each device will be based on the spectrum of that device and thus will be unique.
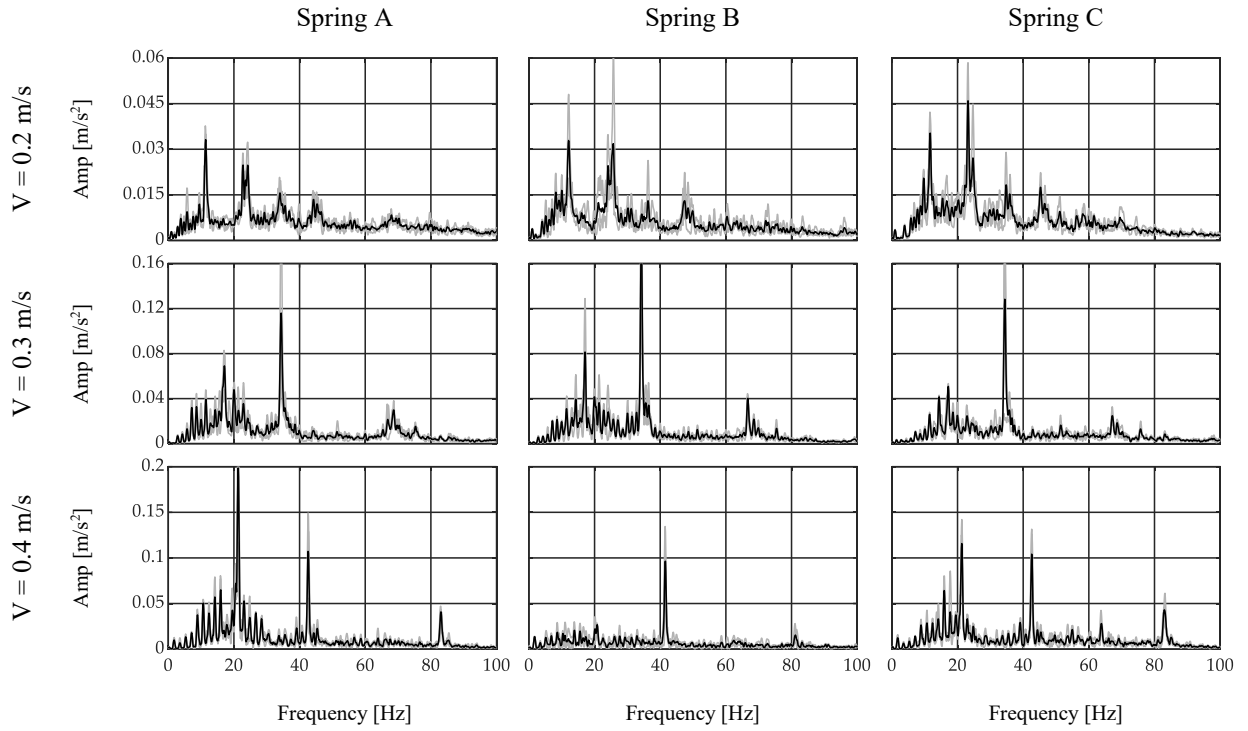
Figure 3-6: ADFT spectrums of off-bridge signals recorded by the sensor.
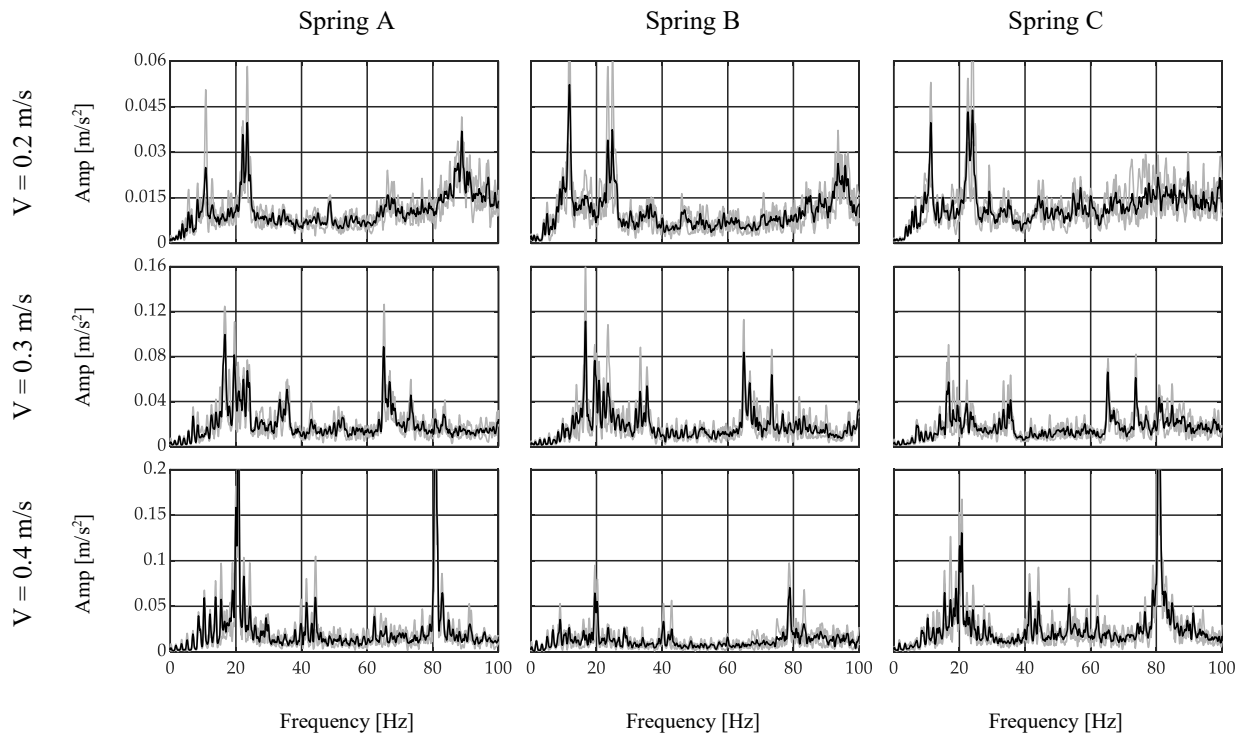
Figure 3-7: ADFT spectrums of off-bridge signals recorded by the smartphone.

As explained in the preceding sections, the off-bridge spectrum is used to form the inverse

filter prototype, which is illustrated in Figure 3-8 and Figure 3-9 for the sensor and smartphone

39

data, respectively. As seen, filter shapes are amplifying low-amplitude frequencies in off-bridge spectrums and suppressing high-amplitude ones. However, as illustrated in Figure 3-8 and Figure 3-9, filter shapes of the sensor and the smartphone have major differences which makes it impossible to use a general filter for all devices even in the same car. In fact, this is one of the major advantages of the proposed method that considers each device in each car as a separate data source and creates a unique filter for it. In addition, it can be seen that the order of the amplitudes of the filter prototypes, i.e. y-axes values in Figure 3-8 and Figure 3-9, are inverse of the order of off-bridge spectrum amplitudes, i.e. y-axes values in Figure 3-6 and Figure 3-7. Thus, it seems reasonable to scale the filter before applying to the on-bridge spectrum to avoid numerical problems.
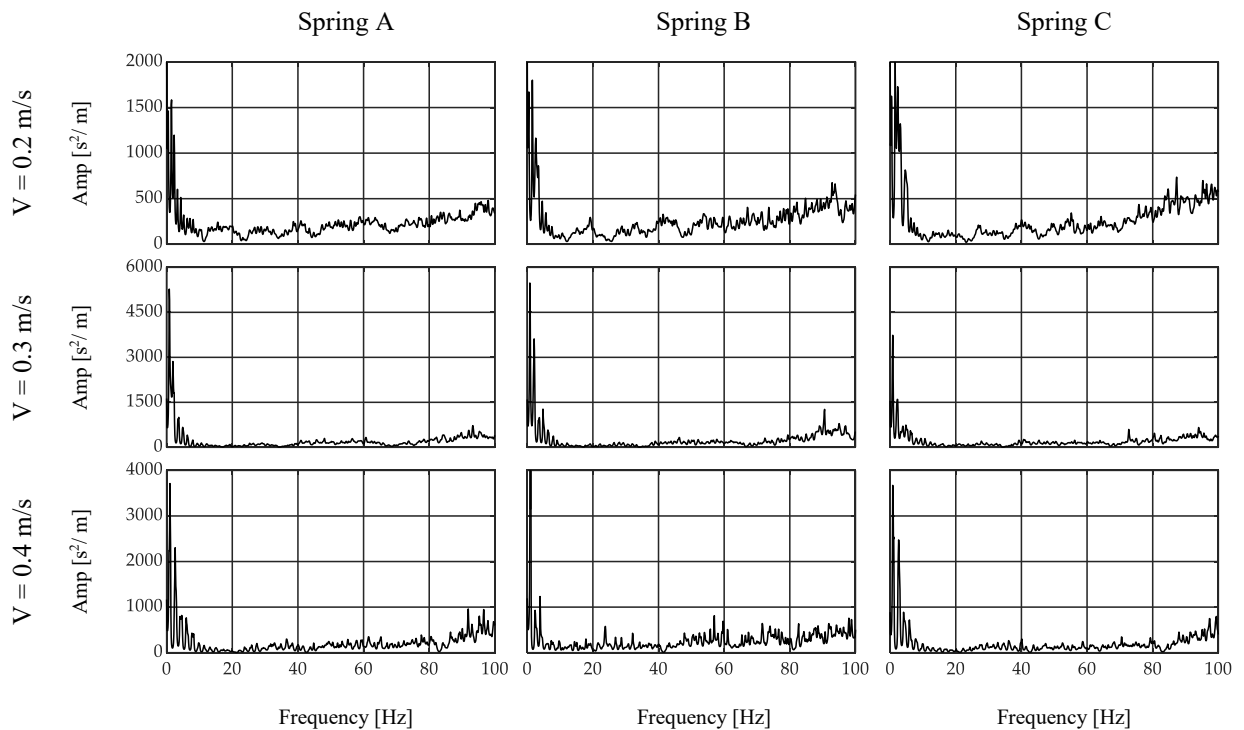
Figure 3-8: Inverse filter prototype based on collected signals by the sensor.
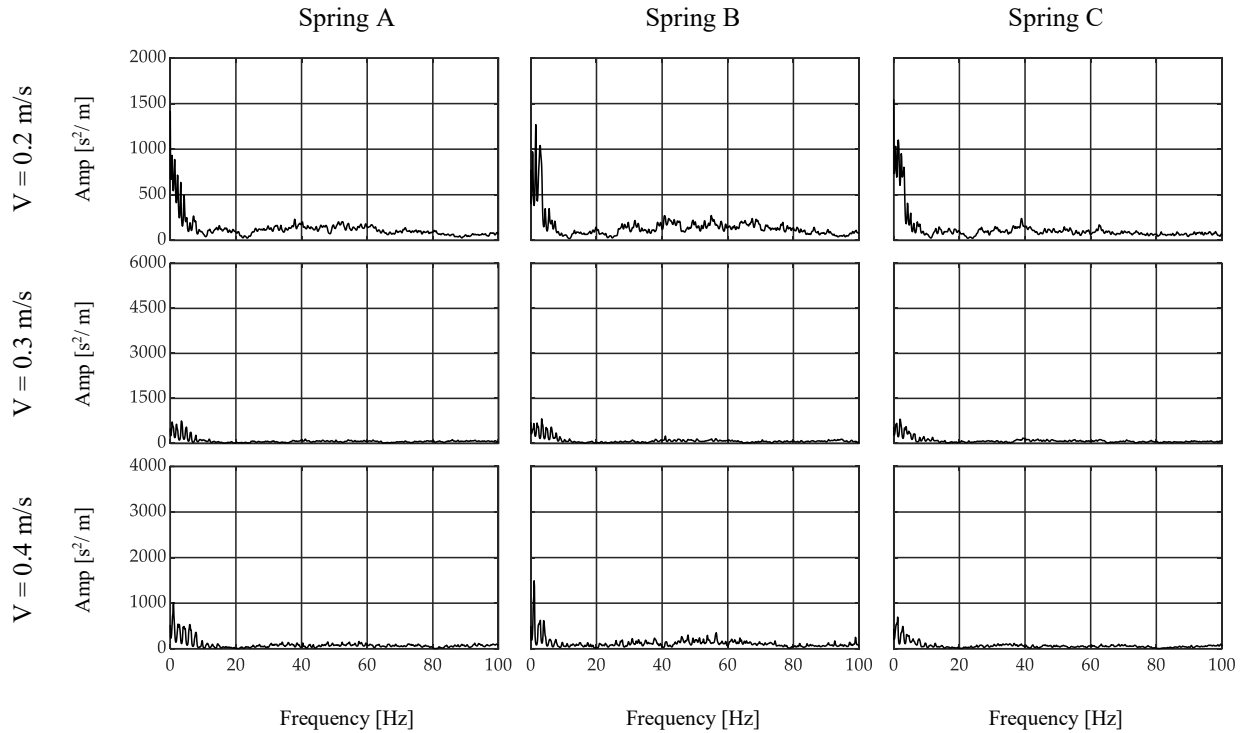
Figure 3-9: Inverse filter prototype based on collected signals by the smartphone.

3.4.2. Filter Verification

Before applying the inverse filter to the on-bridge data, the performance of the filter is verified by applying it to unseen off-bridge data, i.e. new off-bridge data that was not used in the filter development phase. It is expected that the designed filter should remove all major car-related frequencies from the spectrum and no major preference should be present between the frequencies in the filtered off-bridge spectrum. To this end, unfiltered and filtered spectrums of off-bridge acceleration signals are shown in Figure 3-10 and Figure 3-11 for the sensor and smartphone data, respectively. In these figures, the original unfiltered spectrums are illustrated by gray curves and the filtered ones are in black. As seen, the filtered data are almost considered as white noise with no major peaks, which verifies the successful performance of the inverse filter in removing car-related frequency content. In addition, the performance of the filter is stable for all combinations of speed and suspension stiffness which proves the robustness of the proposed method. As

expected, the performance of the filter is stronger using the sensor and filtered spectrums have lower variations. However, Figure 3-11 demonstrates that the filter designed by smartphone-collected data is capable of eliminating most of the major car-related frequency content, which would be used to detect any external frequency content when another vibration source, specifically bridge data, is added to the signal.
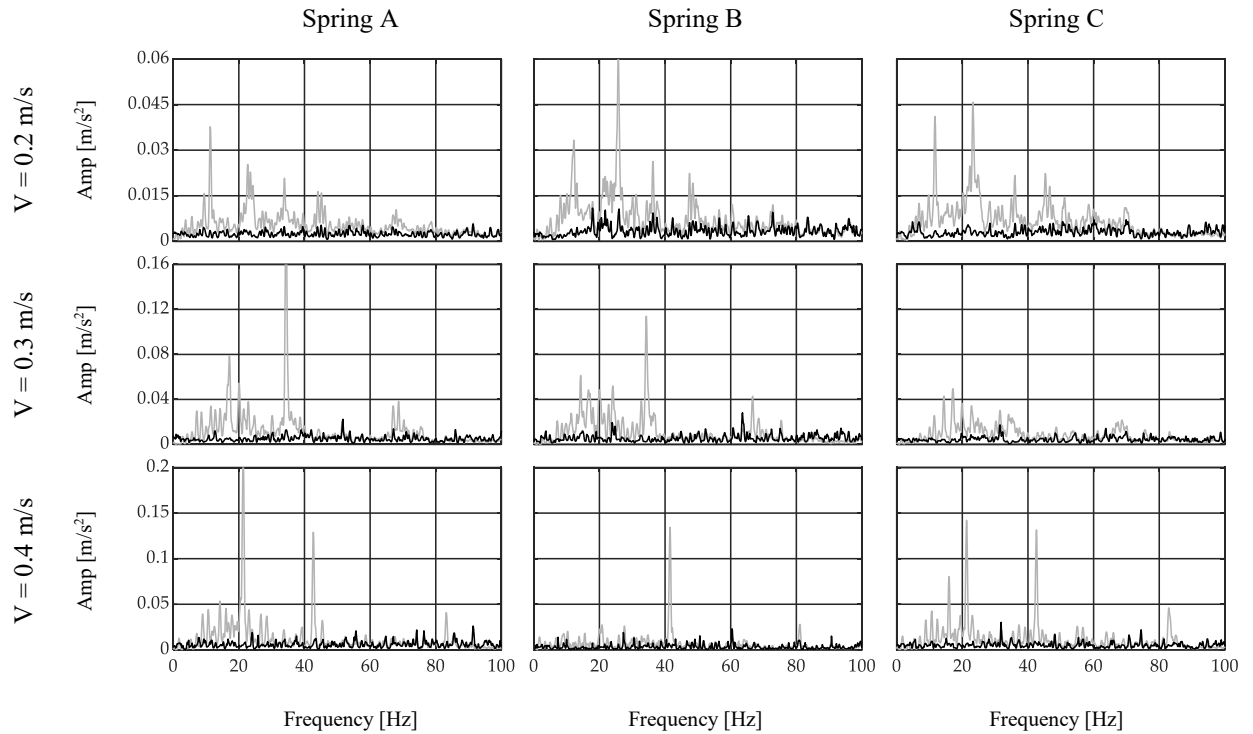
Figure 3-10: Unfiltered (gray) and filtered (black) spectrums of off-bridge data collected by the sensor.
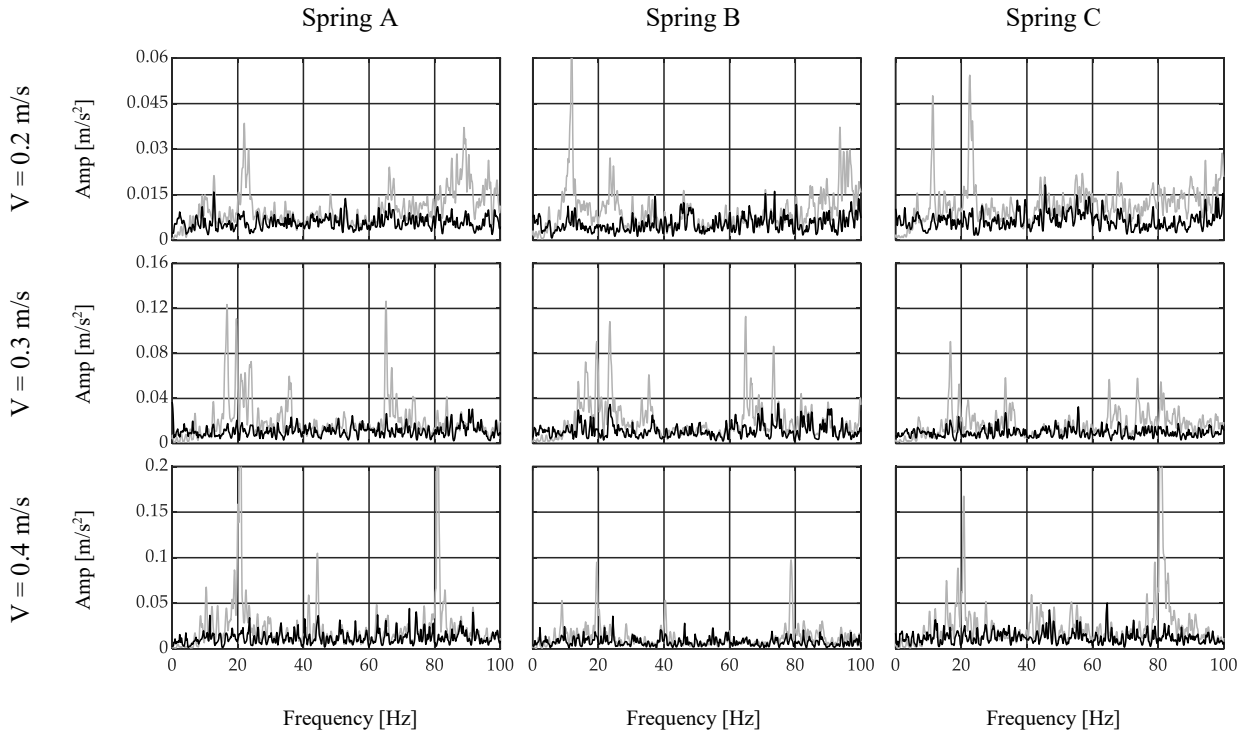
Figure 3-11: Unfiltered (gray) and filtered (black) spectrums of off-bridge data collected by the smartphone.

3.4.3. Filter Application

In this section, the car moves over the bridge and the developed inverse filters are applied to the collected acceleration signals, i.e. on-bridge signals. Figure 3-12 shows the unfiltered and filtered spectrums of on-bridge signals in black and red curves, respectively, for sensor-collected data, while Figure 3-13 shows the same for the smartphone data. In these figures, a frequency range of 0~20 Hz is considered to focus on the fundamental frequency of the bridge. In addition, the fundamental frequency of the bridge is marked with black dashed lines in both figures. This frequency was identified by a separate test by applying initial displacement at the center of the bridge and recording and analyzing the responding free vibration of the bridge. As seen, filtered spectrums, shown with red curves, amplify the fundamental frequency of the bridge, while detecting the frequency of the bridge among all other peaks is challenging through unfiltered spectrums, shown with black curves. In addition, comparing Figure 3-12 and Figure 3-13

demonstrates that the smartphone with lower accuracy performs similarly in detecting the fundamental frequency of the bridge compared to the sensor. The reason is that the inverse filter was designed based on the performance of the device and hence eliminated device errors. Furthermore, considering different combinations of speed and suspension stiffness evidences the robustness of the proposed methodology against car features. Since the duration of the signals was relatively short in this experiment, i.e. 4 to 6 seconds, recorded data may not be able to model the general pattern of the spectrum. It is expected that in real-life conditions, longer signals may improve the performance of the ADFT spectrum and the resulting inverse filter. However, it is also acknowledged that more challenges will be added to the problem in such real-life applications, e.g. surface roughness or speed changes between off-bridge and on-bridge conditions, which will be addressed in the following chapter.
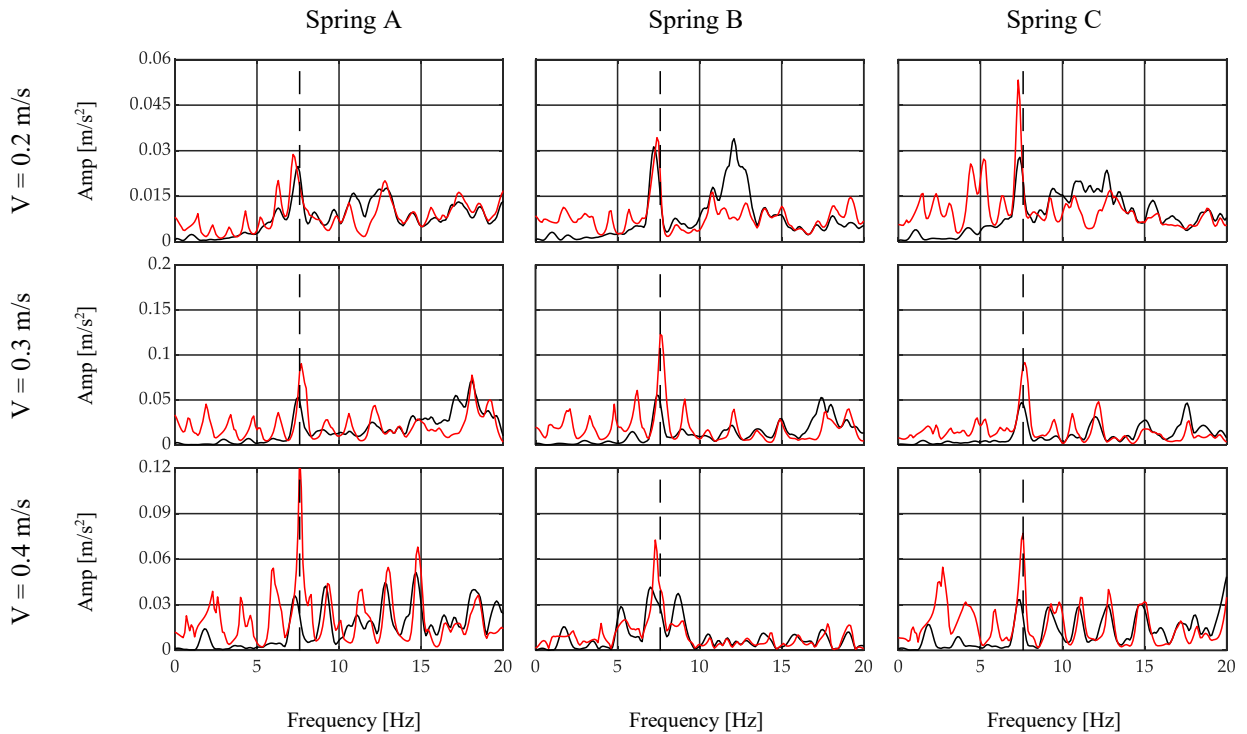
Figure 3-12: Unfiltered (black) and filtered (red) spectrums of on-bridge data collected by the sensor.
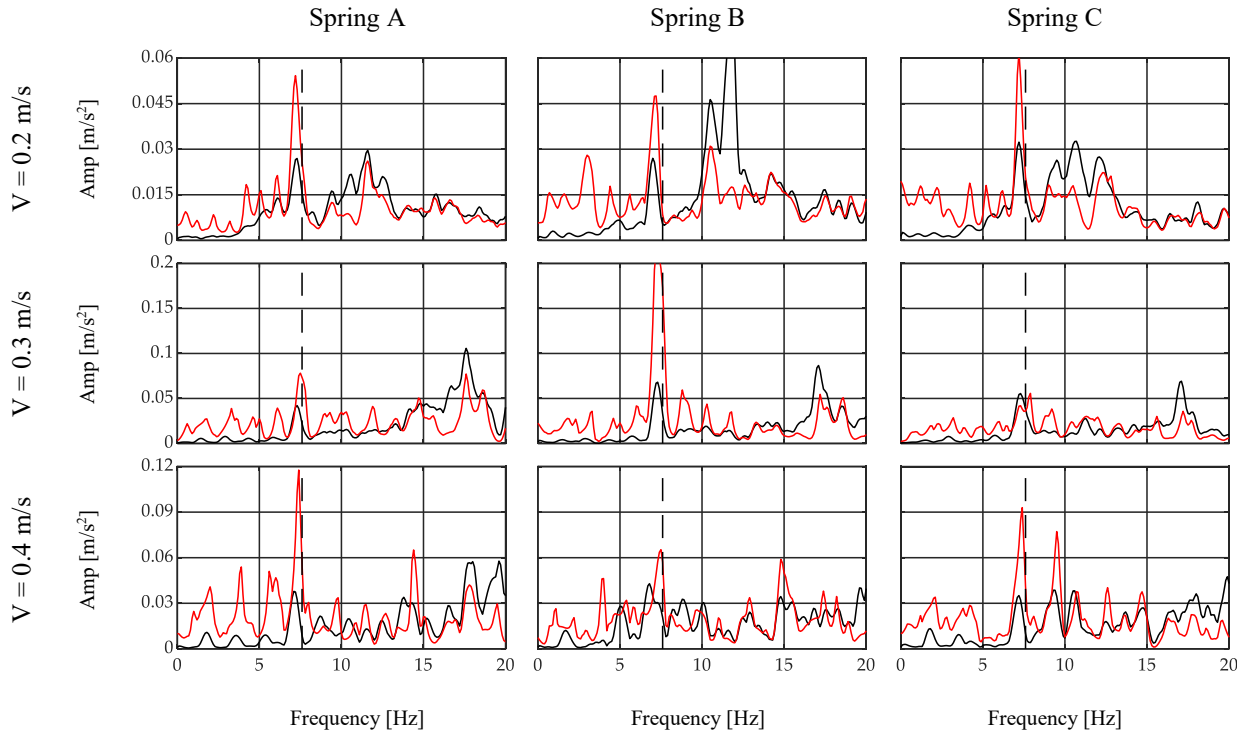
Figure 3-13: Unfiltered (black) and filtered (red) spectrums of on-bridge data collected by the smartphone.

The experimental results illustrated in Figure 3-12 and Figure 3-13 provide further insight toward indirect monitoring of bridges using frequency analysis of a passing vehicle. For instance, lower speeds provide longer recorded signals, which results in an enriched spectrum with more bridge-vehicle content than higher speeds. Comparing each row of Figure 3-12 and Figure 3-13 shows that the presence of the bridge frequency in the spectrums is stronger at the first rows for lower speeds, while at higher speeds, especially in third rows, bridge frequency presence is faded. Furthermore, the accuracy of the sensor in recording acceleration signals yields closer frequencies to the exact bridge frequency as seen in Figure 3-12. However, smartphone results show more shifted frequencies in Figure 3-13. In addition, it should be noted that there are small harmonic peaks emerged in the filtered spectrums of both the sensor and the smartphone, which are due to the inconsistency in the speed of the robot car among off-bridge and on-bridge conditions. The speed of the robot car in this experiment is controlled through the voltage of the motor and the

voltage value is kept constant during each experiment, which would warrant constant speed on a flat surface. However, the deformation of the bridge deck affects the speed of the robot car, unlike the off-bridge condition where the surface is perfectly flat. Since the current methodology does not account for the effect of the speed change of the car, harmonics of the altered speed emerge as new peaks in the filtered spectrums, even though they are not significant enough to overshadow the bridge frequency.

In order to quantify the performance of the inverse filtering method on bridge frequency identification, a peak scoring analysis is conducted based on amplitude and prominence using MATLAB. The prominence of a peak is defined to measure how the peak stands out with respect to other adjacent peaks considering its intrinsic height and location. The prominence of an isolated peak with a low amplitude may be higher than another peak that has a larger amplitude but is among a range of tall peaks. On the other hand, two peaks with similar prominence values but with a notable amplitude difference are not equally significant in a spectrum. Hence, both the prominence and amplitude are considered in the scoring criterion of this study. For each spectrum, the prominence and amplitude scores of all peaks are scaled to 100. Then, the scores are averaged among all passes of the car over the bridge. For simplicity, only the smartphone data are considered for peak analysis. The histogram of the peak analysis of the unfiltered and inverse filtered spectrums are provided in the upper and lower plots of Figure 3-14, respectively. In both plots, the fundamental frequency of the bridge is shown with vertical dashed lines. As seen, considering different cars passing over the bridge at different speeds, the filter can almost double the chance of detecting the frequency of the bridge correctly. In fact, for the performed lab experiments in this chapter, in 100% of the time, the peak with the maximum amplitude and the maximum

prominence was the fundamental bridge frequency, which evidences the strong performance of the proposed inverse filtering method.
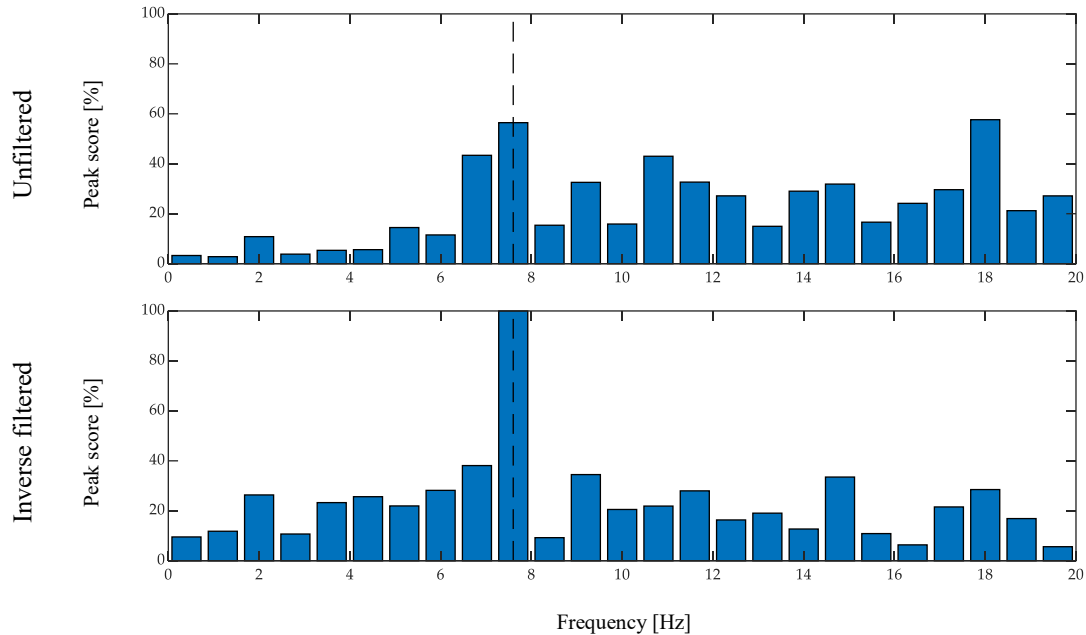
Figure 3-14: Histogram of averaged peak scores of unfiltered and inverse filtered on-bridge spectrums.

3.5. CHAPTER CONCLUSION

This chapter proposes a methodology for identifying the fundamental frequency of a bridge by using acceleration signals recorded on cars passing over the bridge. While most studies focus on processing on-bridge data alone, this study suggests the application of off-bridge signals to filter the on-bridge data. The spectrum of the off-bridge data is used to design a specific inverse filter which then could be applied to the on-bridge data. This way, the frequency content of the car is expected to be removed from the on-bridge data, leaving those of the bridge. To verify the performance of the methodology, a lab-scale experiment, including a robot car and a simply-supported bridge, was performed considering nine combinations of speed and suspension stiffness values. The main highlights and outcomes of this chapter can be listed as: 1) For the first time in the literature, an inverse filtering-based method for indirect frequency identification of bridges is developed; 2) The experiment results demonstrate that inverse filtering provides promising results

in suppressing car-related frequencies and amplifying bridge frequency; 3) The filter is uniquely designed for each device in each car and thus is robust against their features and there is no need to consider the properties of the car or data acquisition devices; 4) The results show that although smartphones have relatively lower accuracy than standalone accelerometers, the proposed inverse filter is able to overcome such challenges by designing unique filter based on the accuracy of each device.

It is expected that as long as the fundamental frequency of the bridge is not close to the major frequencies of the car, the filter would be able to successfully extract the frequency of the bridge. In addition, due to the non-linear coupling of vehicle and bridge vibrations, it is expected that shifted frequencies of the bridge may affect the identified frequency for short-span bridges. In a real-life situation with a variety of cars with different frequencies passing over the bridge, this method is expected to be practical once applied to large crowdsensed data. Furthermore, the proposed inverse filtering approach is efficient when the speed of the car and the surface roughness level are similar in the off-bridge and on-bridge conditions. Both factors significantly affect the pattern of the acceleration spectrum recorded on the car and their variations need to be addressed in order to achieve a real-life applicable inverse filtering technique, which is the topic of the next chapter.

Chapter 4. METHODOLOGY ENHANCEMENT

4.1. OVERVIEW

Following the limitations of the inverse filtering methodology developed in the previous chapter, including the effect of speed and road roughness variations, this chapter aims at addressing such issues in the methodology to be applicable under real-life conditions. A novel approach of constructing a database of vehicle vibrations for different speeds is presented to account for the vehicle speed effect on the performance of the method. In addition, an energy-based surface roughness criterion is proposed to consider surface roughness influence on the identification process. The successful performance of the methodology is investigated for different vehicle speeds and surface roughness levels. While most indirect bridge monitoring studies are investigated in numerical and laboratory conditions, this study proves the capability of the proposed methodology for two bridges in a real-life scale. Promising results collected using only a smartphone as the data acquisition device under real-life conditions corroborate the fact that the proposed inverse filtering methodology could be employed in a crowdsensed framework for monitoring bridges at a global level.

In the following, first, the process of creating the database and classification of the data is explained. Later, the new enhanced methodology will be put into practice in real-life conditions to assess its performance.

4.2. DATABASE DEVELOPMENT AND ANALYSIS

This section explains the procedure of creating and analyzing the database of drive-by vibrational data in the proposed methodology.

4.2.1.   On-Bridge Data Extraction

The first step in the data analysis is to extract on-bridge segments of the acceleration signal. Based on the GPS coordinates of the start and end points of the target bridges, the time frames where the vehicle was moving on the bridge are determined. The corresponding on-bridge acceleration signals are then extracted according to those time frames. In Figure 4-1, one sample of GPS data and the captured bridges in Edmonton are shown on the map. The red line represents the target on-bridge segments and the green lines are the rest of the data, considered as off-bridge in the analysis.

<center>(a)   (b)</center>
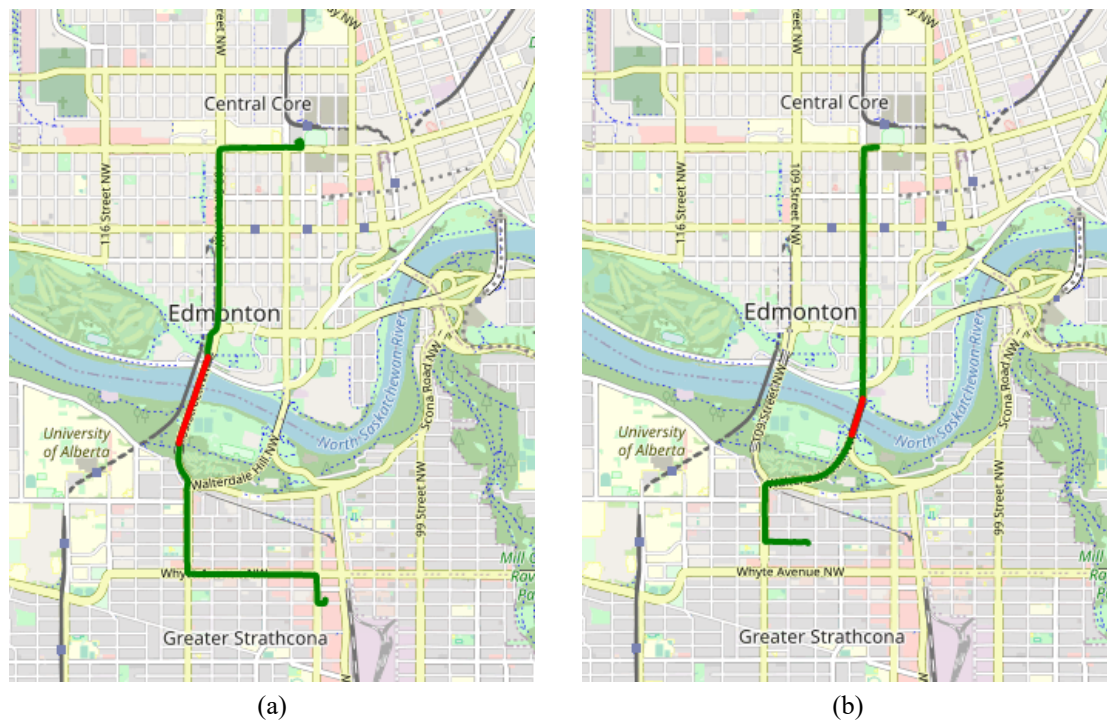
Figure 4-1: Detecting on-bridge (red line) and off-bridge (green line) segments using GPS history for two samples of (a) the High Level Bridge and (b) the Walterdale Bridge in Edmonton[1].

4.2.2.   Speed Categorization

In order to account for the effect of the speed variations on the inverse filtering process, the procedure of speed categorization is applied to create the database for discretized speed values. In

---

[1] The map is the courtesy of openstreetmap.org.

the first step, the continuous values are changed to discrete speeds. In this study, equal speed bins of 2.5 km/h wide with centers at multiples of 2.5 km/h are considered and the center values are assigned to all speeds that lie within the range of a bin. Furthermore, as the sampling frequency of the GPS sensor and hence that of the speed data is 1 Hz, i.e., one data point per second, there is a chance of a speed change between the two consecutive data points. To account for this possibility, the minimum constant speed threshold is considered as the minimum consecutive time steps where the discretized speed is constant. Therefore, the possibility of a sudden speed change between the data points is reduced. The minimum constant speed threshold used in this study is three seconds. Hence, only the time frames where at least four consecutive discretized speed values are equal will be stored in the database. The process of speed categorization for a sample of speed data is illustrated in Figure 4-2. The shaded area in Figure 4-2b represents the selected constant speed segments, which are stored in the database to be employed later in the inverse filtering process.
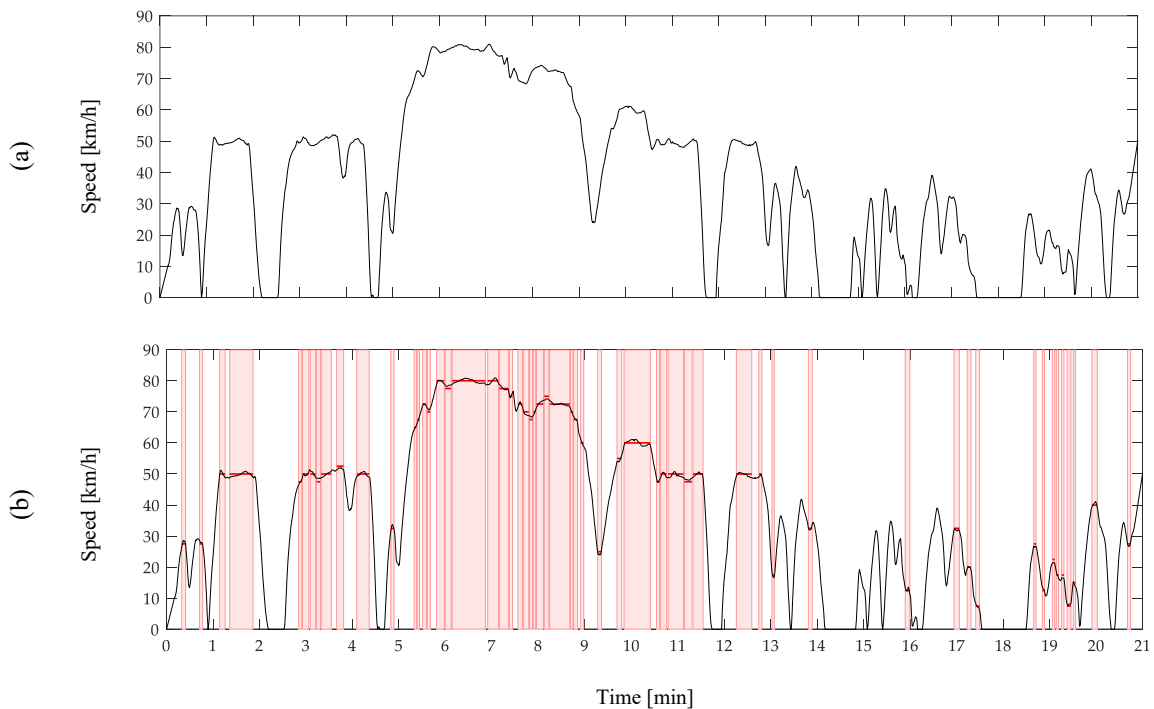
Figure 4-2: A sample of (a) the continuous raw speed data and (b) the categorized constant speed time frame selection for the database.

4.2.3. Roughness Level Estimation

In addition to the effect of speed variations, the roughness level of the road has a significant effect on the performance of the inverse filtering method. In order to account for the variation in the roughness level, a roughness level criterion is proposed in this study, which is defined based on the average energy level of the vertical acceleration signal. It is expected that when a car is moving over a rough surface, the average energy level of the vertical acceleration would be higher in comparison with a smooth surface. Previous studies [75], [76] have shown that the power spectral density (PSD) of a vehicle's vertical acceleration correlates closely to the road roughness. Regarding crowdsensing-based monitoring methods, some recent studies were focused on the application of smartphones for surface roughness estimations [77], [78] or detection of road defects, such as potholes [79], [80].

In this study, the mean square of the acceleration values is employed as a measure of the energy level and therefore the surface roughness criterion (SRC). This criterion is later used for matching the off-bridge and on-bridge signals required for the inverse filtering application. This idea is presented in Figure 4-3, which consists of two columns. In each column, the upper plot shows the on-bridge acceleration signal recorded on the High Level Bridge and the lower one represents the corresponding off-bridge signal with a similar estimated roughness level, all recorded at the same speed of 50 km/h. In column (a), which represents a relatively low roughness level, the SRC is close to 0.3 $(m/s^2)^2$ while this criterion is close to 0.64 $(m/s^2)^2$ for column (b), representing a relatively high roughness level. As seen, employing the proposed SRC makes it possible to account for the effect of the surface roughness. The advantage of the SRC in increasing the performance of the inverse filter in terms of selecting the corresponding on-bridge and off-bridge signals will be discussed in more detail in the Discussion Section of this chapter.

Unlike on-bridge acceleration data, which are limited due to the length of a bridge, there are more off-bridge data available in the database per each vehicle speed. Thus, instead of considering all speed categorized off-bridge data as one signal, different windows of those data are analyzed to find the best matching surface roughness level. In this study, windows of three seconds long with a 25% overlap are considered, which are applied to the off-bridge database and the best matching SRC window is selected for the inverse filtering step. This process is illustrated in Figure 4-4, where a sample of the off-bridge acceleration signal is presented and two windows with a relatively large SRC difference are depicted. As a result, based on the on-bridge data, the window with the closest SRC, i.e., the best matching roughness level, is selected for the inverse filtering process.
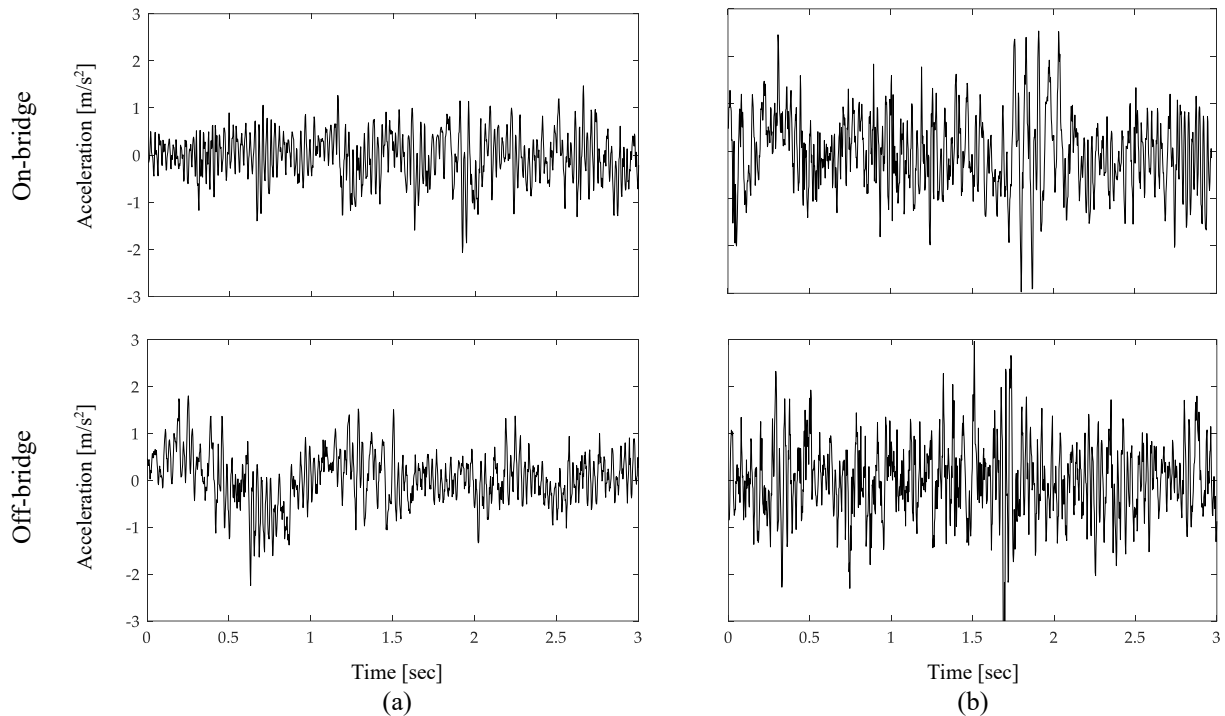
Figure 4-3: A sample of on-bridge and corresponding off-bridge acceleration signals for two different surface roughness levels of (a) low and (b) high, recorded under the same speed of 50 km/h.
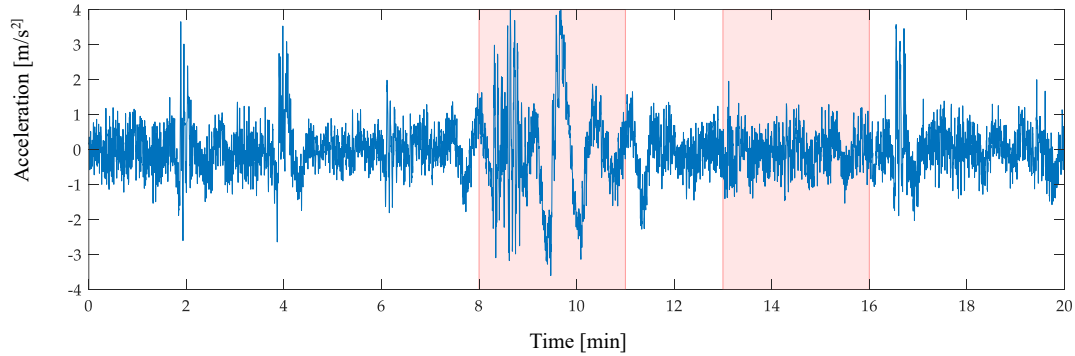
Figure 4-4: A sample of an off-bridge signal and two selected windows with surface roughness criterion (SRC) values of 2 $(m/s^2)^2$ (left) and 0.3 $(m/s^2)^2$ (right) recorded under the constant vehicle speed of 50 km/h.

4.2.4.   Inverse Filtering Application

In the final step, the inverse filtering technique will be applied to detect the bridge frequency. To this end, first, the bridge detection is performed and all acceleration data are divided into on-bridge and off-bridge classes. All of the off-bridge acceleration signals will then go through the speed categorization process to extract constant speed acceleration signals and build the database of the off-bridge signals. Afterwards, the speed categorization of the on-bridge signals will be conducted. Then, the SRC will be calculated for each constant speed segment of the on-bridge signals. The matching speed-categorized segments of the off-bridge data are then recalled from the database and the SRC will be calculated for different windows and the off-bridge segment with the closest roughness level will be selected. If the difference between the on-bridge and off-bridge SRCs is more than 5%, that on-bridge segment will be dropped out of the process. In other words, if an on-bridge signal is recorded on a vehicle moving on a surface with a specific roughness level that was not previously experienced by the same vehicle under the same speed during its off-bridge history, that on-bridge signal will not be suitable for the inverse filtering analysis and will be neglected. Finally, the corresponding on-bridge and off-bridge signals will be transformed into a frequency domain using a discrete Fourier transform and the inverse filtering technique will then be employed. The flowchart of the proposed method is presented in Figure 4-5.
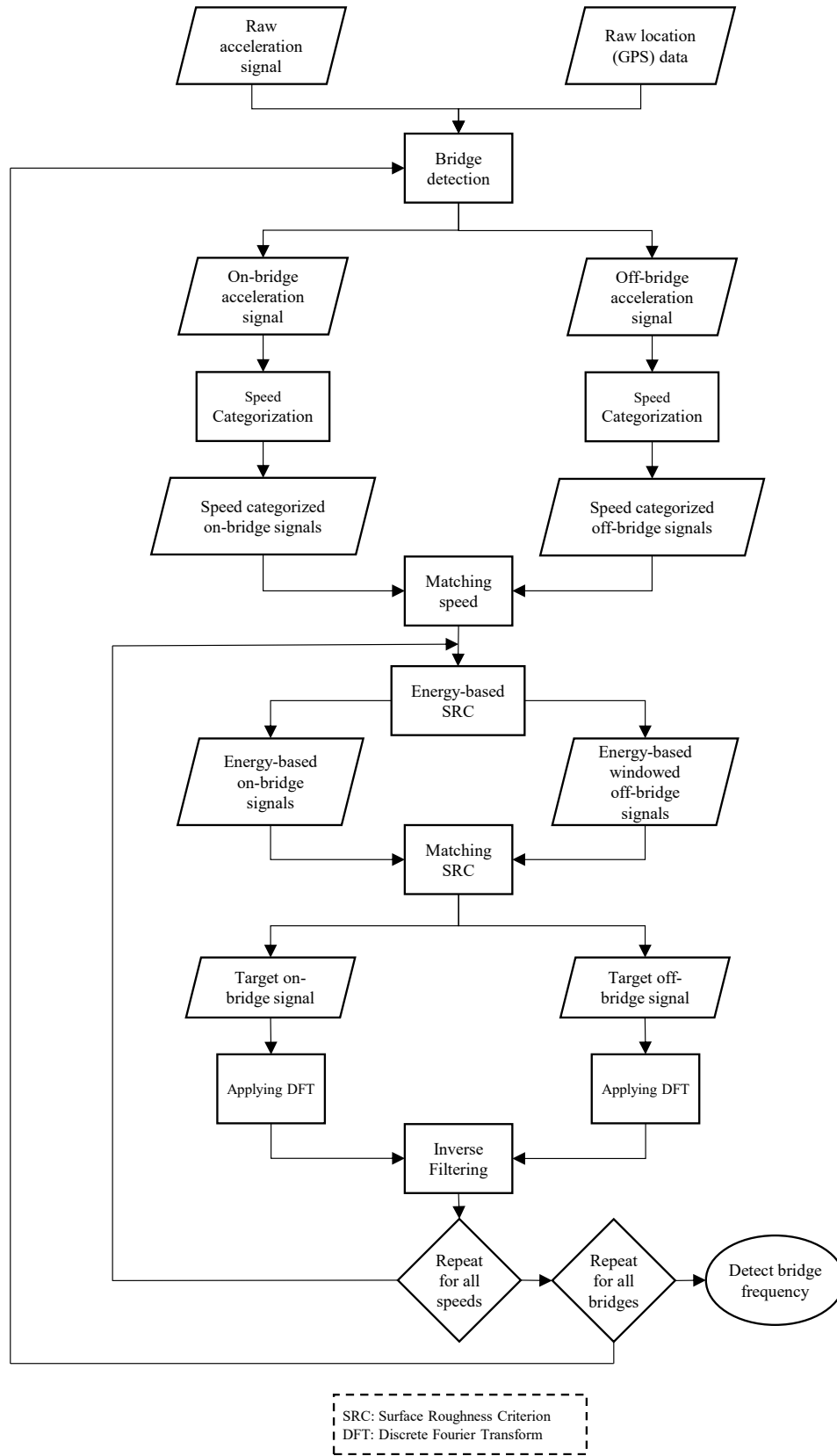
Figure 4-5: Flowchart of the proposed enhanced inverse filtering methodology for bridge frequency detection in real-life conditions.

4.3. REAL-LIFE EXPERIMENTS

In this section, the experimental setup for testing the proposed methodology in real-life practice is presented. Two different bridges in Edmonton, Alberta, Canada, i.e., the High Level Bridge, a steel truss bridge with a length of 777 m built in 1913 and the Walterdale Bridge, a through-arch steel bridge with a total length of 214 m built in 2017, shown in Figure 4-6, are considered. Both bridges span over the North Saskatchewan River that passes through the city.

| (a) | (b) |

Figure 4-6: (a) The High Level Bridge and (b) the Walterdale Bridge that are considered in this study.

The fundamental frequencies of the bridges were identified through a frequency analysis of the recorded vibration under normal loading conditions using on-bridge sensors. In that test, one-minute-long acceleration signals of bridge vibrations were recorded at one-quarter, one-third, and one-half of the length of the bridge using a standalone wireless accelerometer under the sampling frequency of 512 Hz and the first peak among all of those spectra was detected as the fundamental frequency. The identified frequencies were detected as 2.8 Hz for the High Level Bridge and 2.1 Hz for the Walterdale Bridge. The spectra representing the middle point vibrations of the two bridges are shown in Figure 4-7. Note that these vibrational data were collected on a sunny summer day under a temperature of 20~26 °C. It is expected that the fundamental frequency of the bridges would slightly change in different environmental conditions, the effect of which is

not in the scope of this study. However, these effects could be implemented in future studies through integrating artificial intelligence methods [81]–[83].
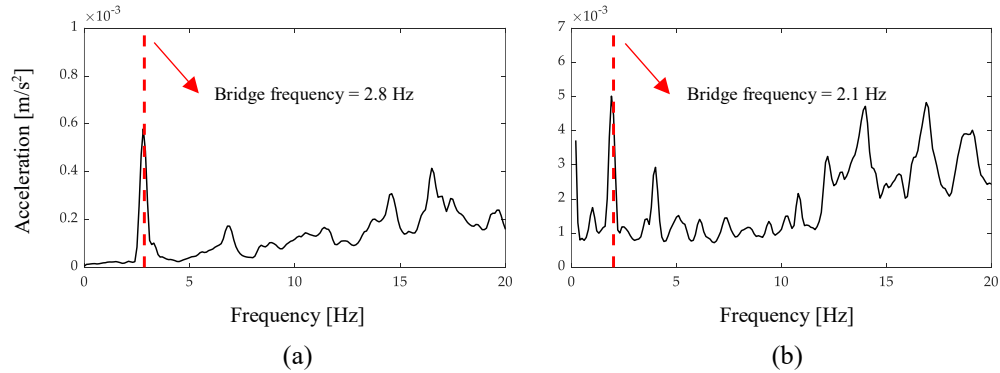
Figure 4-7: A sample of the ambient vibration spectrum of (a) the High Level Bridge and (b) the Walterdale Bridge recorded at the middle point of the bridges.

The required data for the proposed methodology consist of the vertical acceleration, as the main vibrational signal, and the GPS, which will be used to determine the location of the vehicle and its speed. In this research, an academically developed smartphone application called phyphox [84], which was created at the 2nd Institute of Physics of the RWTH Aachen University, is employed. This application provides recordings of all of the smartphone sensors of which the accelerometer and GPS recordings are used in this study. The user interface of the application is shown in Figure 4-8. In addition, the smartphone device used in this research is a Samsung Galaxy Note 10 Plus with a sampling frequency of 400Hz for the accelerometer and 1 Hz for the GPS sensor. The vehicle where all of the recordings were conducted is a Honda Civic sedan. The placement of the smartphone inside the vehicle is also shown in Figure 4-8c.

(a)	(b)	(c)
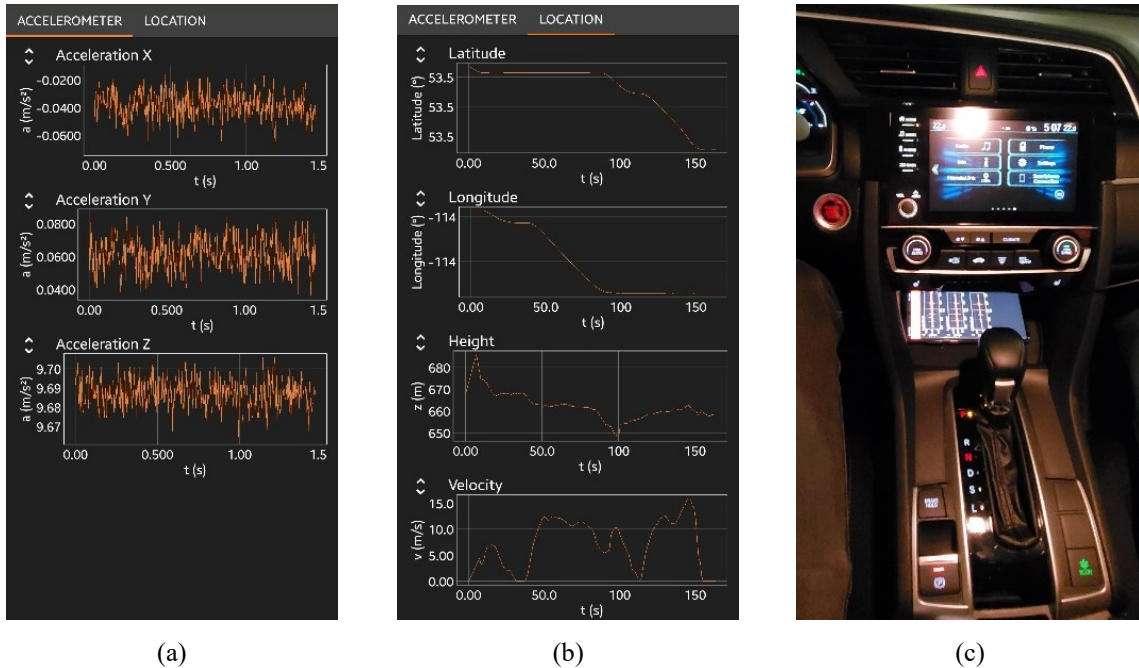
Figure 4-8: The user interface of the phyphox [84] application while recording (a) acceleration and (b) GPS data together with (c) the placement of the smartphone in the vehicle.

4.4. RESULTS

The inverse filtered spectra for the High Level Bridge and the Walterdale Bridge are presented in Figure 4-9 and Figure 4-10, respectively. Each figure consists of four plots organized in two rows, representing different speed ranges of 40~50 and 50~60 km/h, and two columns, representing different surface roughness levels with the SRC ranges of 0~0.5 and 0.5~1 $(m/s^2)^2$. In each plot, the original unfiltered on-bridge spectrum is illustrated with the blue color while the black color represents its inverse filtered spectrum. Note that the dashed red line denotes the fundamental frequency of the bridge. As seen, in most on-bridge cases, it is impossible to detect the bridge frequency with the raw unfiltered data due to the presence operational effects. However, the enhanced inverse filtering methodology demonstrates a promising performance in detecting the fundamental frequency of the bridge. It should be noted that these data were collected on different days and the variations in environmental conditions, specifically the temperature, would cause a slight difference in the detected frequencies, which could be addressed in future studies.

$0 < SRC < 0.5 \; [(m/s^2)^2]$ $\qquad\qquad$ $0.5 < SRC < 1 \; [(m/s^2)^2]$
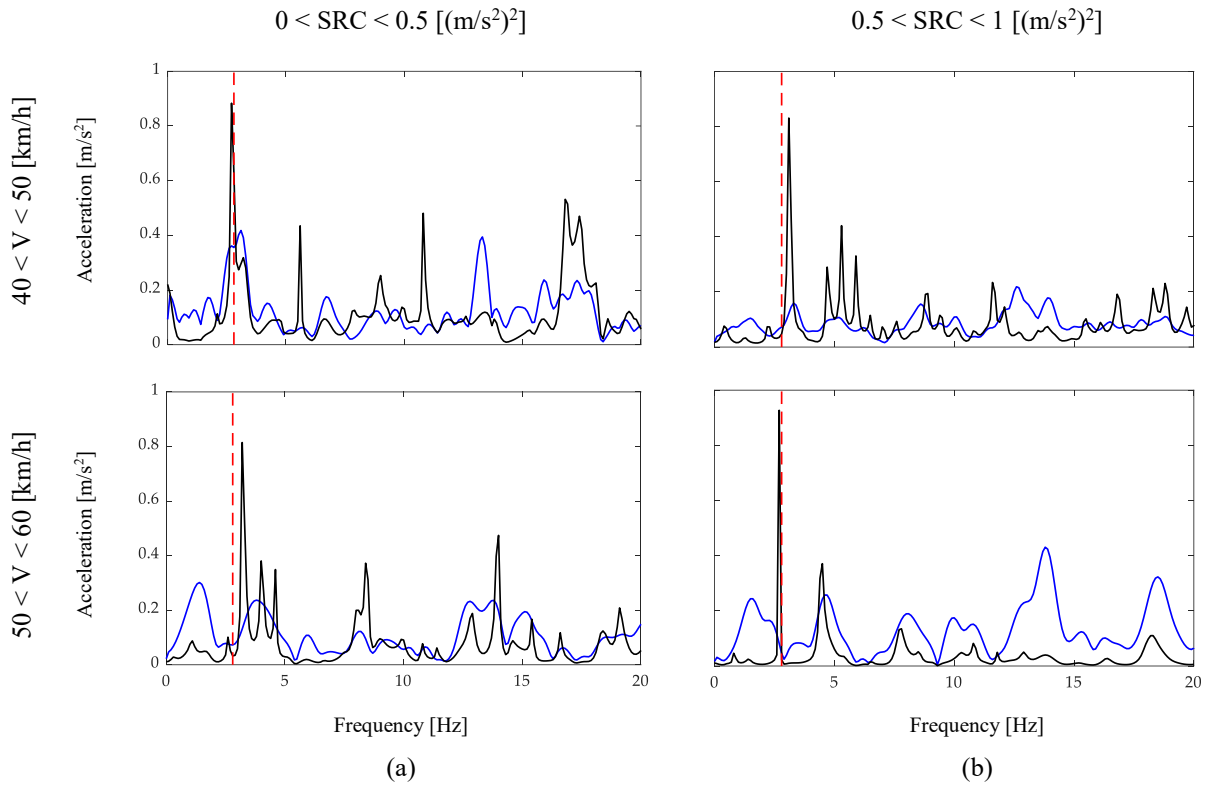
Figure 4-9: On-bridge spectra (blue) and their corresponding inversed filtered spectra (black) for the High Level Bridge considering different vehicle speeds and surface roughness conditions.

$0 < SRC < 0.5 \; [(m/s^2)^2]$ $\qquad\qquad$ $0.5 < SRC < 1 \; [(m/s^2)^2]$
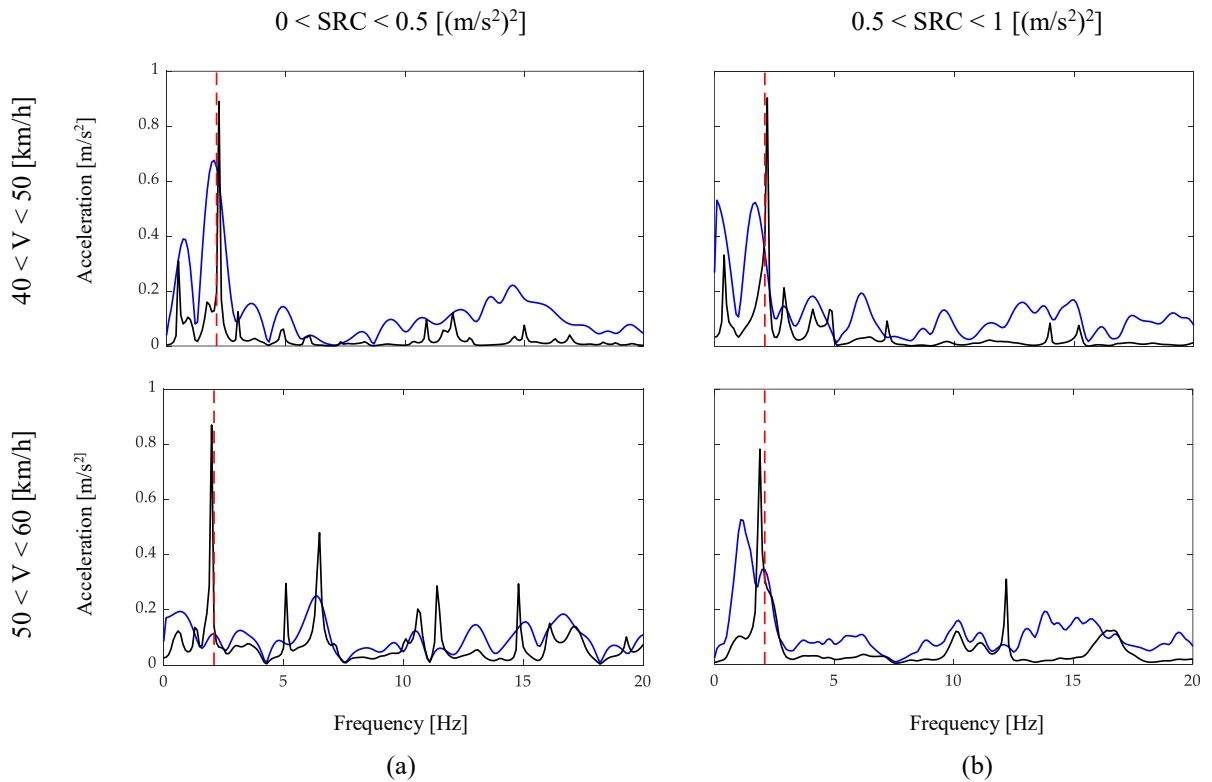
Figure 4-10: On-bridge spectra (blue) and their corresponding inversed filtered spectra (black) for the Walterdale Bridge considering different vehicle speeds and surface roughness conditions.

59

4.5. DISCUSSION

Following the successful performance of the proposed methodology in the previous section, its effectiveness against two major factors in the indirect bridge frequency identification, i.e., vehicle speed and road roughness, is investigated in this section.

4.5.1. Effect of the Speed

As mentioned before, the vehicle speed is one of the significant factors affecting the recorded vertical acceleration and its spectrum. To investigate this effect, a pair of off-bridge spectra recorded on a similar surface roughness level but at different speeds of 55 km/h and 52.5 km/h are employed as input for creating an inverse filter for an on-bridge spectrum recorded at the speed of 55km/hr on a similar surface roughness level on the Walterdale bridge. Figure 4-11 represents the off-bridge and inverse filtered spectra of the matching speed case, i.e., using the database speed-matching process, while Figure 4-12 illustrates spectra of those with different speeds. All of these spectra were recorded on a similar vehicle and under similar surface conditions with an SRC value of 0.7 $(m/s^2)^2$. Note that the fundamental frequency of the bridge is shown with a dashed line. Comparing these two figures shows that a slight difference between the vehicle speeds translates to a significant effect on the vibrational data and major irrelevant peaks occurred in the speed-variant inverse filtered spectrum. This is due to the fact that major vibrational sources including the moving frequency of the vehicle and engine vibrations were all speed-dependent and a slight change in the speed of the vehicle changed the position of the major peaks in the spectrum, which was magnified in the inverse filtering process. This substantiates the fact that creating a speed-dependent database of the off-bridge signals is crucial for the successful performance of the inverse filtering for frequency identification of bridges.
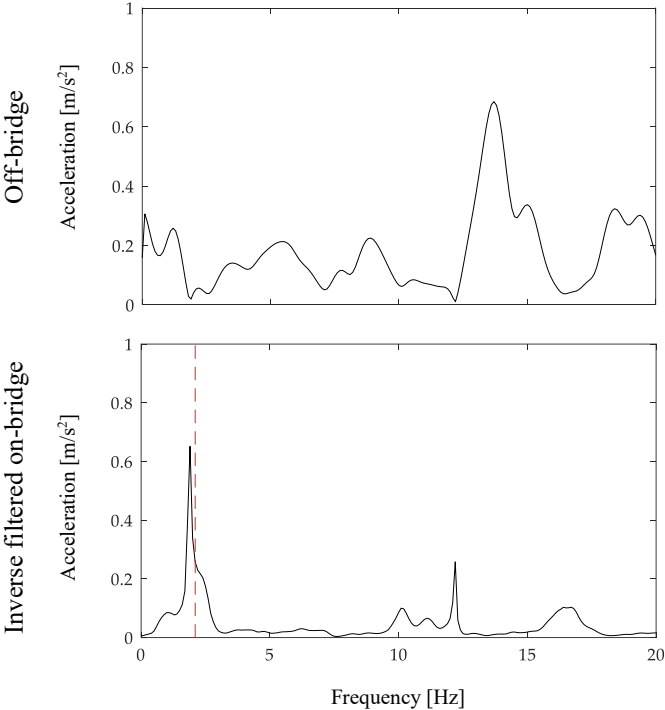
Figure 4-11: A sample of off-bridge data and its resulting inverse filtered spectra using the database speed-matching process.
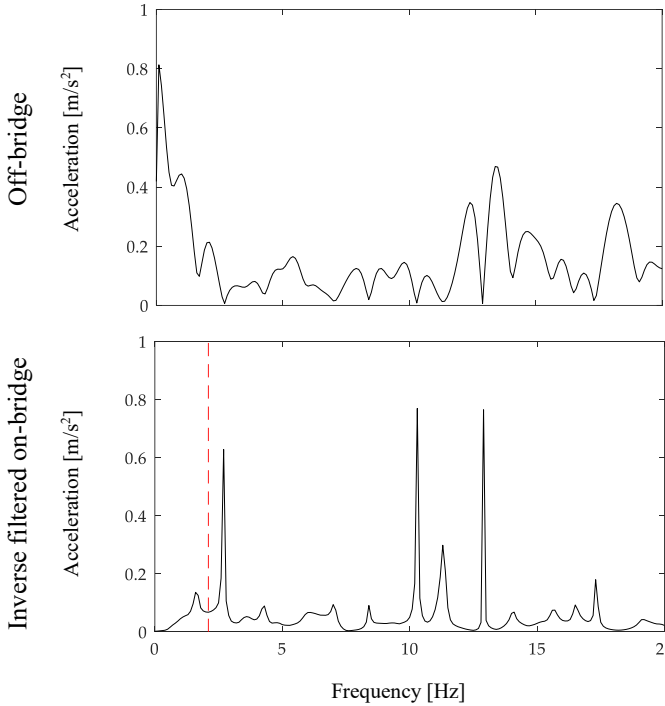
Figure 4-12: A sample of off-bridge data and its resulting inverse filtered spectra without using the database speed-matching process.

4.5.2. Effect of the Surface Roughness

Surface roughness was the other important factor in the performance of the inverse filtering. The proposed energy-based SRC discussed in Section 4.2.3 played a significant role in the successful performance of the inverse filtering. To assess its influence, a pair of off-bridge spectra recorded under a similar speed of 50 km/hr but on different surface roughness levels with SRCs of 0.7 $(m/s^2)^2$ and 0.42 $(m/s^2)^2$ are employed as input for creating an inverse filter for an on-bridge spectrum recorded on a surface with an SRC of 0.7 $(m/s^2)^2$ on the Walterdale bridge. Figure 4-13 represents the off-bridge and inverse filtered spectra of the matching roughness case, i.e., using the database roughness-matching process, while Figure 4-14 illustrates spectra of those with different roughness levels. All of these spectra were recorded on a similar vehicle and at the same speed of 50 km/hr. Note that the fundamental frequency of the bridge is shown with a dashed line. Figure 4-14 demonstrates that although the speed of the vehicle in both the on-bridge and off-bridge spectra was similar, the inverse filtering was unable to extract the bridge frequency due to the difference in surface roughness levels. In fact, the surface roughness is one of the sources that significantly affect the frequency content and hence the shape of the spectrum of the recorded acceleration signals. As a result, any comparison among the frequency contents of the on- and off-bridge spectra needs to be under similar or close surface roughness conditions. The successful performance of the inverse filtering in the previous section demonstrated that the proposed SRC was efficient in detecting these similar surface conditions. In addition, the results in Figure 4-13 show that the methodology performed effectively for relatively high surface roughness levels despite the fact that vehicle features dominate vibrations over such surfaces, making the bridge frequency identification challenging.
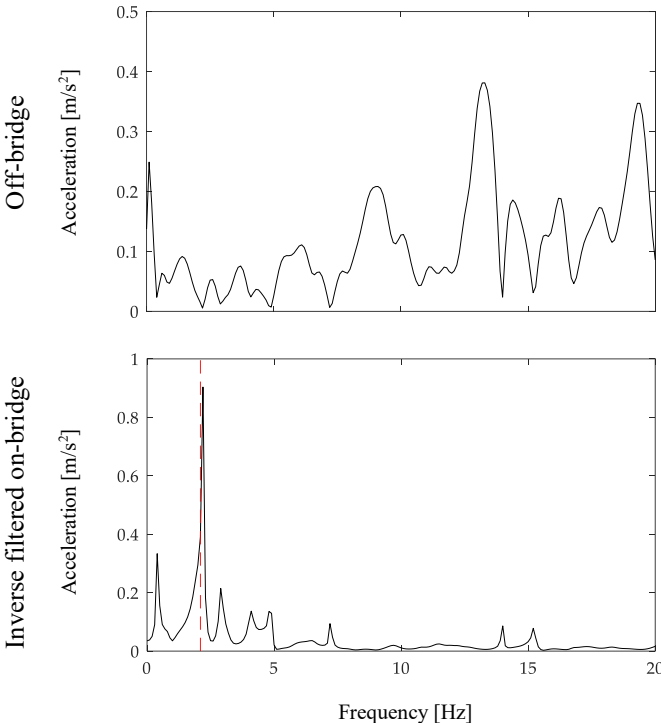
Figure 4-13: A sample of off-bridge data and its resulting inverse filtered spectra using the database roughness-matching process.
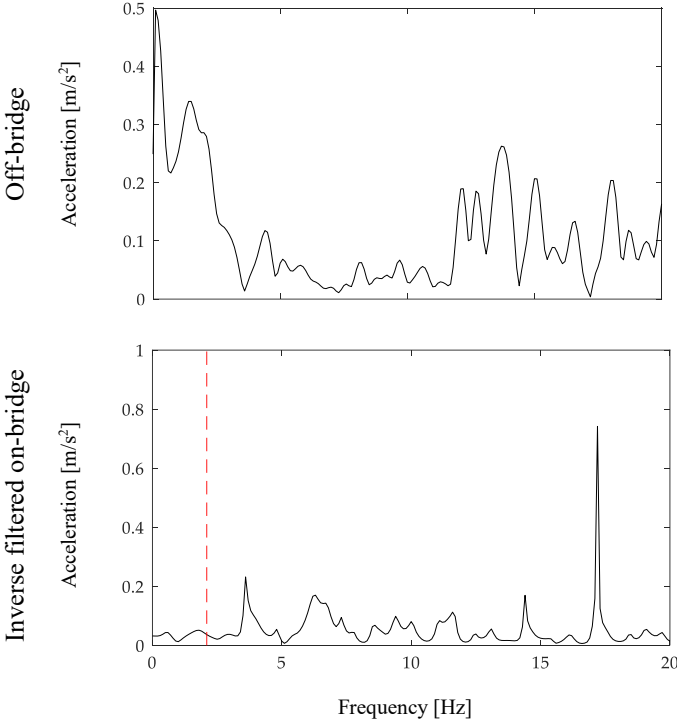
Figure 4-14: A sample of off-bridge data and its resulting inverse filtered spectra without using the database roughness-matching process.

4.6. CHAPTER CONCLUSION

This chapter presented an enhanced inverse filtering methodology for the real-life applications of the drive-by frequency identification of bridges using smartphones through a new framework. Two major limitations of the previously proposed methodology were addressed here. First, it was proposed that by developing a database of off-bridge acceleration signals per different vehicle speeds, it would be possible to consider speed variations between off- and on-bridge signals. In addition, a surface roughness criterion was defined based on the average energy level of the acceleration signal. Thus, the challenge of discrepancies between surface roughness levels of off- and on-bridge conditions was also eliminated. The successful performance of the proposed approach for two full-scale bridges demonstrated the capability of the application for future bridge monitoring purposes. As all of the required data including the acceleration signals and the GPS data were collected from a smartphone, the implementation of the proposed method through a crowdsensed framework would significantly reduce the cost of monitoring a plethora of bridges in future smart cities. It should be noted that such methods can easily be extended to the embedded sensors in autonomous and connected vehicles.

It is worth noting that the proposed methodology focused on detecting the fundamental frequency of the bridge only and further improvement is needed to detect other dynamic features. Moreover, there were other important factors affecting the identification process, specifically environmental effects, such as temperature changes. These factors can drastically change the bridge frequency and should be considered for health monitoring purposes.

Chapter 5. EXTENSION OF APPLICATION

5.1. OVERVIEW

In previous chapters, the proposed inverse filtering for the elimination of operational effects was applied to detecting the fundamental frequency of the bridge. However, bridge health monitoring is not limited to the identification of its modal parameters. For instance, O'Brien et al. [28] utilized Moving Force Identification (MFI), a method based on finding the time history of forces applied to the bridge, to detect damage on the bridge. Zhang et al. [29] employed Operating Deflection Shape Curvature (ODSC) method. Yin and Tang [30] used Proper Orthogonal Decomposition (POD) to calculate the difference between the displacement responses of a vehicle passing damaged and healthy bridges. In addition, multiple studies [31]–[33] focused on the application of wavelet transform for bridge damage detection. Recently, a novel damage detection approach based on Mel-frequency cepstral analysis has been proposed for indirect bridge monitoring [34], [35].

Cepstrum, first introduced by Childers et al. [85], is defined as the inverse Fourier transform of the logarithm of the spectrum of a signal. Initially developed to study seismic echoes from earthquakes and explosions, it became a well-known audio processing [86]–[88] tool. Mel-frequency Cepstral (MFC) analysis is among the most popular cepstral-based signal processing methods, which efficiency in speech recognition has been widely investigated [89]–[91]. Instead of focusing on the peak analysis, such as natural frequency detection, MFC analysis extract patterns in the spectrum of a signal through extracting MFC features, called Mel frequency Cepstral Coefficients (MFCCs). In other words, MFCCs are a vector of features representing patterns in the spectrum of a signal. MFC has been employed in SHM studies in recent years. For instance, Zhang et al. [92] proposed a delamination detection method using MFFCs to remove

noise and subjectivity. Moreover, Balsamo et al. [93] employed MFCCs as damage features and showed that the accuracy in damage detection is higher using MFCCs compared to using auto-regressive coefficients. Regarding indirect bridge monitoring, Mei et al. [45] used extracted MFCCs and detected damage on the bridge by applying Principal Component Analysis (PCA), which provided insights toward both the presence and severity of the damage.

This chapter concentrates on the detection of damage on the bridge using Mel-frequency cepstral analysis considering the elimination of operational effects. The proposed approach is built upon two main methods: Inverse filtering and Mel-frequency cepstral analysis. Inverse filtering is first applied to suppress the operational effects in drive-by vibrations. Later, an abnormality index is defined based on the distribution of MFCCs compared to a baseline healthy case, representing the change in the bridge dynamic state. In the following, first, the methodology is explained in detail. Afterwards, the performance of the method in eliminating operational effects is investigated through laboratory experiments and also under real-life conditions. Then, the damage detection capability of the proposed method is assessed in laboratory conditions.

5.2. MEL-FREQUENCY CEPSTRAL ANALYSIS

Cepstral analysis, as a powerful method in speech recognition and natural language processing, is defined as the inverse Fourier transform of the logarithm of the spectrum of a signal. Mel-frequency cepstral analysis is one of the methods employed in the cepstral environment. The outputs of Mel-frequency cepstral analysis are a series of features called Mel-frequency cepstral coefficients, herein MFCCs. These features represent important patterns in the frequency content of the signal, which is a major improvement compared to peak detection. In addition, MFCCs are extracted with a higher focus on the lower frequencies, which are desired from the bridge health monitoring point of view.

The process of extracting MFCCs from acceleration signals in this study is presented in Figure 5-1. After transforming acceleration signals into the frequency domain using Fourier transform, the spectrum is transformed into the Mel-frequency environment. The relationship between Mel-scale and Hertz-scale in speech recognition applications is designed based on the frequencies detectable by the human hearing system, which ranges between 2000~5000 Hz [94]. Since this frequency range is far from the major frequency content of bridge structures, an adapted version of the Mel-scale is proposed in the literature [93], as provided in the equations below:

$$\begin{cases} m = M(f) = 5\ln\left(1 + \dfrac{f}{5}\right) \\ f = M^{-1}(m) = 5\left(e^{m/5} - 1\right) \end{cases} \tag{5-1}$$

Eq. (5-1) shows relationships for converting Hertz-scale, denoted by f, to Mel-scale, denoted by m, and vice versa. The main purpose of this relationship is to relate evenly distributed Mel-frequencies with exponentially increasing intervals of Hertz-scale, leading to more focus on lower frequencies. The following equation locates those unevenly spaced points:

$$f_i = M^{-1}\left(M(f_1) + (i-1) \times \frac{M(f_n) - M(f_1)}{n-1} \right) \tag{5-2}$$

In Eq. (5-2), f_i is the ith frequency selected unevenly from Hertz-scale that corresponds to the ith evenly scaled Mel-scale frequency, and n is the number of key frequencies selected from the frequency range of $f_1 \sim f_n$. Note that the number of key frequencies will later contribute to the number of coefficients of MFCCs. This relationship is illustrated in Figure 5-2 for 20 key frequencies in the range of 0-50 Hz. It can be seen that the frequency intervals are increasing exponentially in Hertz-scale while being constant in Mel-scale.
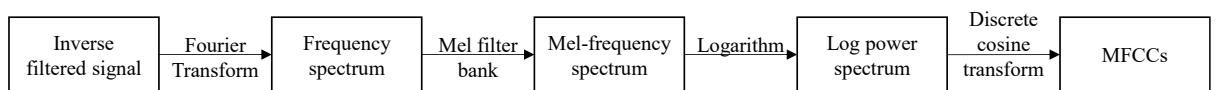
Figure 5-1: The process of MFCCs extraction.
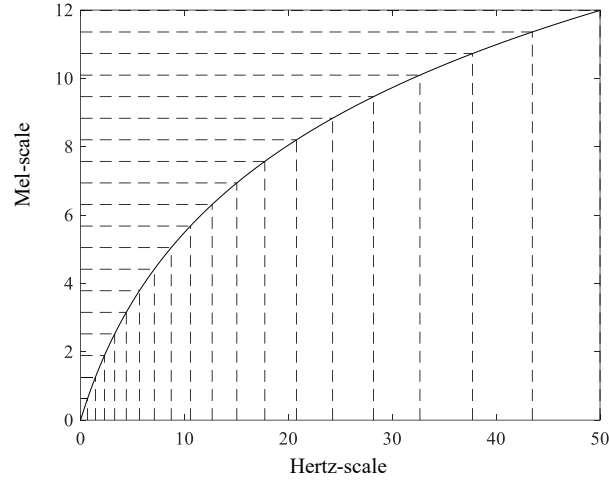
Figure 5-2: Relationship between Hertz and Mel scale.

In the next step, the Mel filter bank is built at the selected key frequencies through a series of triangular filter shapes using the following equation:

$$H_i[k] = \begin{cases} 0 & k < f_{i-1} \\ \dfrac{2(k - f_{i-1})}{(f_{i+1} - f_{i-1})(f_i - f_{i-1})} & f_{i-1} \leq k < f_i \\ \dfrac{2(f_{i+1} - k)}{(f_{i+1} - f_{i-1})(f_{i+1} - f_i)} & f_i \leq k < f_{i+1} \\ 0 & k \geq f_{i+1} \end{cases}, i = 2, 3, ..., n-1 \qquad (5\text{-}3)$$

The function $H_i(k)$ in Eq. (5-3) represents the ith triangular filter bank at the corresponding key frequency. The filter bank plot corresponding to selected key frequencies in Figure 5-2 is demonstrated in Figure 5-3. It can be observed that the filter amplitude decreases with frequency, which is in accordance with prioritizing lower frequencies. The filter bank is then applied to the frequency spectrum of the signal, calculating the total energy for each filter as follows:

$$E[i] = \sum_k H_i[k] X_{\text{on}}^{\text{f}}[k], i = 2, 3, ..., n-1 \qquad (5\text{-}4)$$

where X_{on}^{f} is the frequency spectrum of the on-bridge acceleration signal after inverse filtering according to the details provided in the previous chapters.
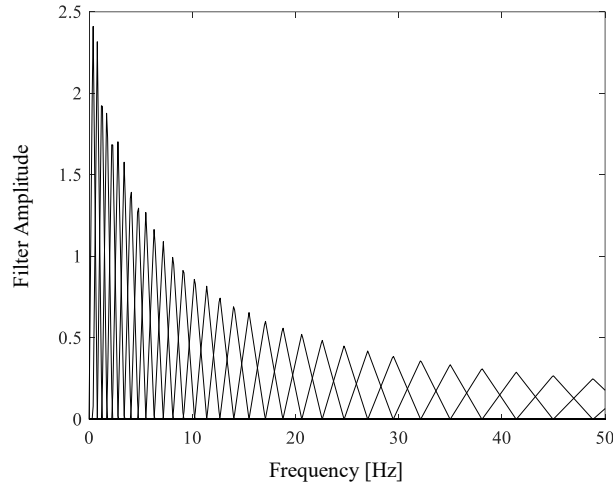
Figure 5-3: Mel filter bank.

Following the process shown in Figure 5-1, the next step is taking the logarithm of the total energy for each filter at each of the Mel frequencies. Then, the discrete cosine transform of the logged energies will lead to MFCCs:

$$C_j = \sum_{i=2}^{n-1} \log E[i] \cos\left[\frac{\pi}{\pi-2}\left(i-\frac{3}{2}\right)j\right], j = 1, 2, ..., n-2 \tag{5-5}$$

where C_j is the jth coefficient of MFCCs. As mentioned before, the number of MFCCs depends on the number of filters, i.e., the number of key frequencies. The extracted MFCCs will then be used to create an abnormality index, which is explained in the following.

5.3. ABNORMALITY INDEX

As mentioned before, MFCCs are expected to capture the pattern in a spectrum. Thus, major changes in the captured MFCCs could be a representation of a pattern change in the sources of vibrations. Without applying inverse filtering, it is expected that the captured pattern is mostly due to operational effects, i.e., vehicle and road parameters, rather than the bridge structures. However, after applying inverse filtering, it is expected that the presence of the bridge frequency content will be improved. Hence, the difference between the MFCCs of the two scenarios demonstrates a

change in the frequency content of the main source, i.e., the bridge. Therefore, the Euclidean distance of the MFCCs is considered as follows:

$$DC_u = \sqrt{\sum_{j=n_1}^{n_2} \left(C_{j,u} - C_{j,b} \right)^2} \tag{5-6}$$

In Eq. (5-6), DC_u is the "Difference of Coefficients" for the unknown case, $C_{j,b}$ is the jth coefficient of the baseline case, and $C_{j,u}$ is the jth coefficient of the unknown case. Practically, only some of them are selected for further analysis, which is shown by the range of $n_1 \sim n_2$ in Eq. (5-6).

Ideally, if the inverse filtering was capable of removing 100% of the operational effects from the drive-by spectrum, the DC would be zero considering the healthy bridge as the unknown case. However, due to errors in the estimation of the surface roughness and the effect of continuously varying speed of the vehicle, the elimination of operational effects is not completely perfect and the DC will not get theoretically zero. In order to account for the remaining effects of the operational factor, the distribution of the DCs calculated from the passage of multiple vehicles over the bridge is considered. In other words, the change in the distribution of DCs of vehicles passing over a bridge would be an index for an abnormality in the bridge structure. A sample of the distribution of DC parameters for a real-life case study is presented in Figure 5-4.
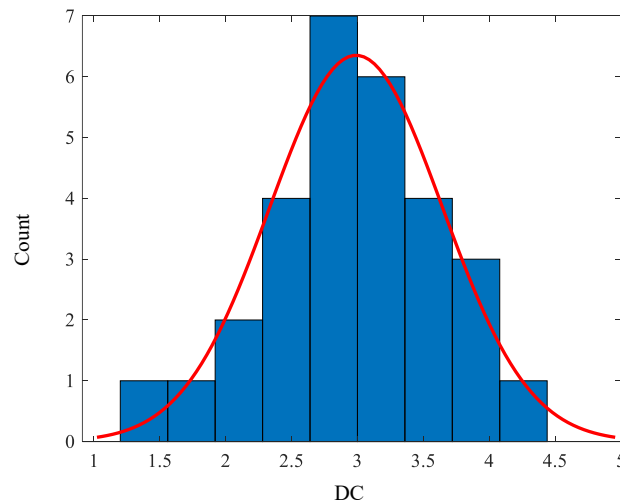
Figure 5-4: A sample of the distribution of DC parameters for a real-life case study on the High Level Bridge.

Quantification of the distribution comparison is achieved using the Z test through the following formula:

$$Z = \frac{|\mu_2 - \mu_1|}{\sqrt{\sigma_2^2 + \sigma_1^2}}$$
(5-7)

where μ_1 and μ_2 are the means, and σ_1 and σ_2 are the standard deviations of the fitted normal distributions of DC for two different scenarios. In fact, the Z test will show how the distribution of DCs has changed between two specific points in time and hence will be denoted as the abnormality index in this study. To assess the capability of the proposed method for detecting changes in bridge state, first, a series of laboratory and real-life experiments are conducted with the focus on the elimination of operational effects. Later, the performance of the method for damage detection is investigated.

5.4. ELIMINATING OPERATIONAL EFFECTS

This section focuses on the application of the proposed methodology in eliminating operational effects from indirectly recorded vibrations. As mentioned before, vehicle features, including speed, suspension system, engine vibrations, etc, as well as road roughness significantly dominate the vibrations recorded on the passing vehicle. The performance of the proposed approach in eliminating such effects is assessed in the following sections using first laboratory experiments and then real-life experiments.

5.4.1. Laboratory Experiments

Experimental setup

In order to investigate the capability of the methodology in suppressing operational effects, controlled laboratory experiments are conducted. The setup includes the similar custom-designed and -built robot car used in the experimental study of Chapter 2, capable of maintaining different

suspension levels and speed values representing a variety of the vehicles passing over a bridge, which is shown in Figure 5-5. Likewise, a steel plate resting on a pin-roller support system employed in the experimental study of Chapter 2 is used as the bridge model, as presented in Figure 5-6. Note that the off-bridge simulation required for the design of the inverse filter was conducted using the robot car moving on the same steel plate resting on the floor, as the effect of the road roughness change was not the focus of this controlled experiment. Furthermore, the features of the robot car and the bridge are presented in Table 5-1. As seen, three different suspension levels and three different speed values yield nine unique combinations of vehicle features, which results are presented in the following section.
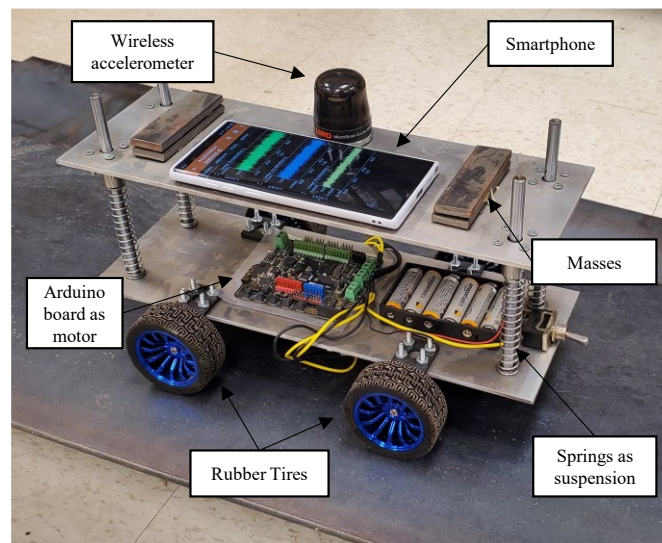
Figure 5-5: The custom-designed and -built robot car used in the experiment.

Figure 5-6: Bridge model employed in the experimental study.

Table 5-1: Features of different elements of the experimental setup.

Element	Parameter	Value
Robot Car	Plate Dimensions (mm)	350×125×3.1
	Total Weight (kg)	2.3
	Top Plate Weight (kg)	1.3
	Spring Coefficient (N/m)	425, 615, 726
	Speed (m/s)	0.2, 0.3, 0.4
Bridge	Steel Grade	W44
	Modulus of Elasticity (GPa)	200
	Yield Strength (MPa)	250
	Deck Dimensions (mm)	2000×330×12.7
	Deck Weight (kg)	60

Results

In this section, the abnormality index explained in the Methodology Section is calculated for four trial series of the robot car travels over the bridge considering a unique baseline case. Each trial consists of three travels for nine unique combinations of car features, resulting in 108 robot car travels in total. Note that at this point of the study, the bridge is undamaged for the unknown trials as the focus is on assessing the elimination of operational effects only. In other words, the baseline and unknown cases for comparing MFCCs and calculating the abnormality index are both undamaged bridges.

Figure 5-7 illustrates the fitted normal distributions for DC parameters of two separate trials. Figure 5-7a shows the distributions without filtering while Figure 5-7b shows the results with inverse filtering. As seen, there is a slight difference in the distribution of DC parameters while the filter has not been applied, which is minimized after applying inverse filtering. In addition, the distributions have been narrower in the filtered versions as the presence of operational effects has been reduced. Note that the experiment has been conducted in controlled ideal conditions, such as similar surface roughness levels, and these differences are expected to be more significant under real-life conditions, as discussed in the next part of this section.

(a)   (b)
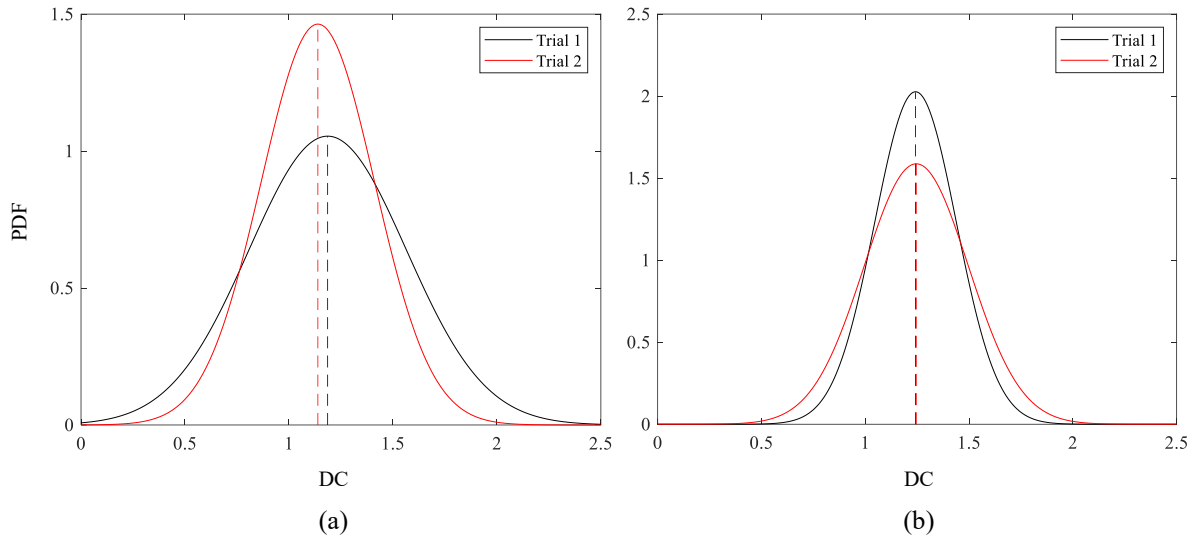
Figure 5-7: Fitted normal distribution of DC parameter for two cases (a) without filtering and (b) with inverse filtering.

To quantify the distribution comparison, the abnormality index calculations are presented in Table 5-2 for all six possible scenarios out of four trials. In fact, the index for each scenario is calculated by performing the Z test between the distributions of two different trials for the healthy bridge. As seen, the inverse filter significantly reduces the abnormality index, 89% on average, which is expected due to the elimination of operational effects, including the suspension and speed effects. It will be shown in the Damage Detection section that the proposed inverse filtering-based methodology and abnormality index are very effective for damage detection of bridges using indirect monitoring under operational effects.

Table 5-2: Abnormality index for trial cases in the healthy bridge condition.

Scenario	Unfiltered	Inverse Filtered
1	0.11	0.038
2	0.26	0.023
3	0.09	0.008
4	0.13	0.020
5	0.37	0.037
6	0.48	0.037
Average	0.24	0.027

5.4.2. Real-life Experiments

Experimental setup

In this section, the performance of the proposed method in eliminating operational effects is investigated in real-life conditions. Five different bridges in the city of Edmonton, Alberta, Canada are studied as detailed in Table 5-3. All bridges span over the North Saskatchewan River and their locations are shown in Figure 5-8. To account for the effects of vehicle and device types, four different smartphones mounted on four different vehicles were employed in this study, which details are presented in Table 5-4. The pictures of the two of the cars, as well as a sample of the placement of the smartphone, is shown in Figure 5-9. As seen, the vehicles are a combination of Sedan and SUV types, and smartphones are from different models, with accelerometers of the different maximum sampling frequencies of 200~500 Hz.
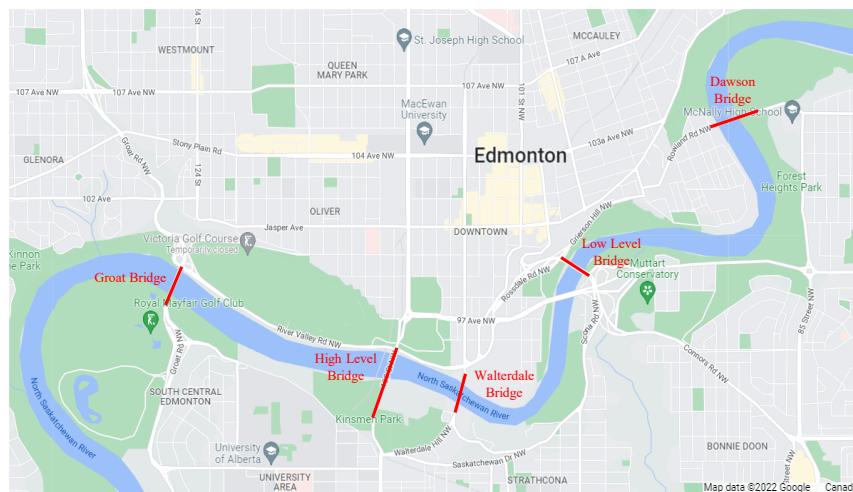
Figure 5-8: Location of the bridges studied in the real-life experiment.

Table 5-3: Details of the bridges studied in the real-life experiment.

Bridge name	Details		Picture
Groat Bridge	Length	315 m	
	System	Steel Girder	
	Year built	1955	
	Last rehabilitation	2020	
High Level Bridge	Length	777 m	
	System	Steel Truss	
	Year built	1913	
	Last rehabilitation	1995	
Walterdale Bridge	Length	214 m	
	System	Steel Through-arch	
	Year built	2017	
	Last rehabilitation	-	
Low Level Bridge	Length	213 m	
	System	Steel Truss	
	Year built	1900	
	Last rehabilitation	2006	
Dawson Bridge	Length	236 m	
	System	Steel Truss	
	Year built	1912	
	Last rehabilitation	2010	

Table 5-4: Vehicle and smartphone devices employed in the real-life experiment.

Vehicle model	Vehicle type	Smartphone model	Maximum sampling frequency (Hz)
Honda Civic (1)	Sedan	Samsung Galaxy Note 10+	400
Honda Civic (2)	Sedan	BlackBerry Priv	200
Honda Pilot	SUV	Huawei Mate 20 Pro	500
Toyota Rav4	SUV	Samsung Galaxy S10	415

Figure 5-9: Pictures of two of the vehicles as well as smartphone placement inside a vehicle

Results

In the experiments, all the vehicles travel each bridge twice. In comparison to the laboratory experiments where more data were available, in real-life experiments, due to the limited amount of data, the considered baseline case is the direct bridge measurements. Fixed accelerometers were mounted on each bridge and their acceleration data were used for the baseline case. Later, with the collection of drive-by data from vehicles, the abnormality index is calculated compared to the baseline data. This way, it would be possible to concentrate on the elimination of operational factors, as the baseline case is direct bridge vibrations and contains no operational effects.

Each case of this study includes the data extracted from one Sedan and one SUV vehicle passing over each bridge. The distribution of DCs for each case is shown in Figure 5-10. The figure consists of five rows, presenting results for each bridge, and two columns. In column (a), the boxplot presentation of the distributions is provided, which is the five-number summary of each case, i.e., the minimum, first quartile, median, third quartile, and maximum. Each plot in column

(a) shows four distributions, two data cases denoted by C1 and C2, and unfiltered vs. inverse filtered results denoted by (U) and (F), respectively. Column (b) presents the fitted normal distribution for DCs for each case, where black curves represent distributions using unfiltered data and red curves represent those of inverse filtered. As illustrated in Figure 5-10, without applying the inverse filtering method, for almost all bridges studied here, the change in the distribution of DCs is significant. Since the MFCCs used in the calculation of DCs are the representors of the patterns in the spectrum of a signal, these substantial changes in the frequency content could result in a false abnormality detection of the bridge, which is in fact due to the effect of the operational factors. However, since the bridges are not damaged during this study, it is expected that a robust method of filtering out operational effects produces similar distributions, which is seen in Figure 5-10. Moreover, the inverse filtering is notably reducing the DC values in comparison to the unfiltered cases, which further corroborates the fact that undesired operational effects are less significant in the inverse filtered data.

In order to quantify the results, the proposed abnormality index is calculated for this study and presented in Table 5-5. As expected, the abnormality index is significantly reduced using the inverse filtering method. In addition, the order of abnormality index using inverse filtering in the real-life study is comparable to the laboratory experiment, i.e., order of magnitude of 10^{-2}, which shows the successful performance of the method in eliminating operational effects even in real-life conditions with challenging factors compared to a controlled laboratory environment. Using the results provided in this section, it can be concluded that without applying the inverse filtering method, the Mel-frequency cepstral analysis is not capable of capturing patterns related to bridge dynamics in the mixed drive-by vibrations, as the bridge features are barely detectable in the significant presence of vehicle and road roughness effects under real-life conditions.
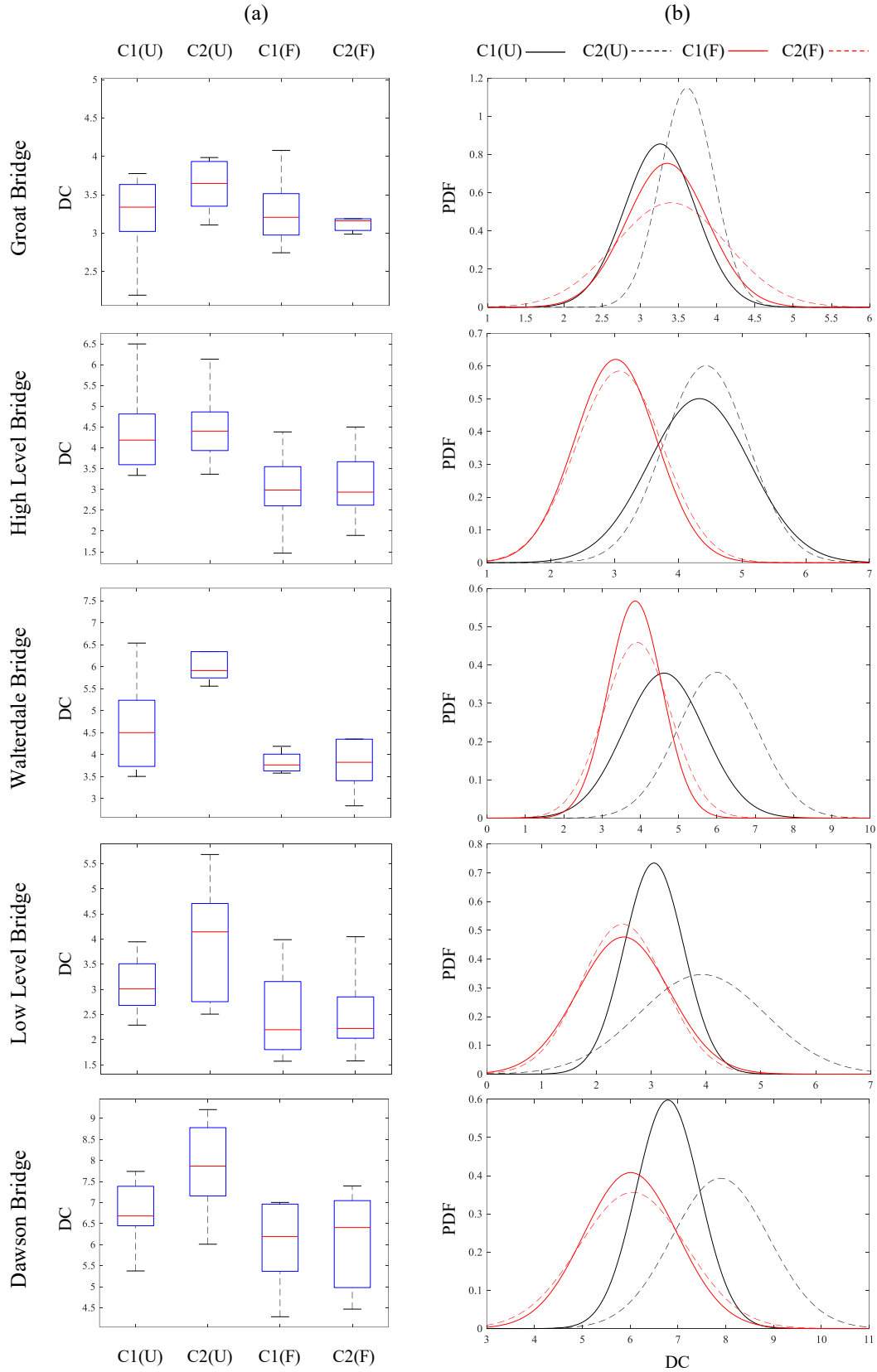
Figure 5-10: Distribution of DC parameters for each case (C1, C2) without filtering (U) and using inverse filtering method (F) plotted using boxplots (a) and fitted normal distributions (b).

Table 5-5: Abnormality index for real-life study.

Bridge	Unfiltered	Inverse filtered
Groat Road	0.606	0.056
High Level	0.099	0.061
Walterdale	0.936	0.043
MacDonald	0.688	0.015
Low Level	0.905	0.027

5.5. DAMAGE DETECTION

This section covers the application of the proposed methodology for bridge damage detection. Due to the unavailability of the data for a real-life damaged bridge, the damage detection study is only investigated through a laboratory experiment. The experimental setup is similar to Section 5.4.1. However, in addition to the healthy bridge case, four damaged cases are considered. The damage in the bridge is modeled using the reduction in the cross-sectional area of the bridge deck at different locations. The details of all bridge cases are presented in Table 5-6. The damage cases are designed so that both the effect of the damage severity and location are considered. Note that the steel plates used for all damage cases are similar in material and dimensions, except for the cross-sectional area reduction.

Table 5-6: Details of the bridge cases in the laboratory experiment for damage detection analyses.

Damage case	Damage location	Cross-sectional area reduction	Picture
B	No damage (Baseline)	-	
C1	Center	15%	
C2	Center	30%	
Q1	Quarter	15%	
Q2	Quarter	30%	

The distribution of DCs for damage cases at the center and quarter of the bridge length are presented in Figure 5-11 and Figure 5-12, respectively. The rows in those figures represent results using unfiltered vs. inverse filtered signals, while the columns, similar to Figure 5-10, illustrate the boxplot and fitted normal distributions of the DCs. Note that each figure contains one distribution for the baseline case, i.e., healthy bridge, which will be used as a benchmark for damage detection. As seen in the first rows of Figure 5-11 and Figure 5-12, it is barely possible to detect a shift in the distribution of the DCs, representing a change in the pattern of the frequency spectrum. It is noteworthy that such small shifts can occur in the healthy conditions of the bridge, according to the results seen in Section 5.4.1. However, the second rows of Figure 5-11 and Figure 5-12 demonstrate a considerable shift between damage cases, which increases with the severity of the damage, substantiating the effect of inverse filtering for improving damage detection accuracy.
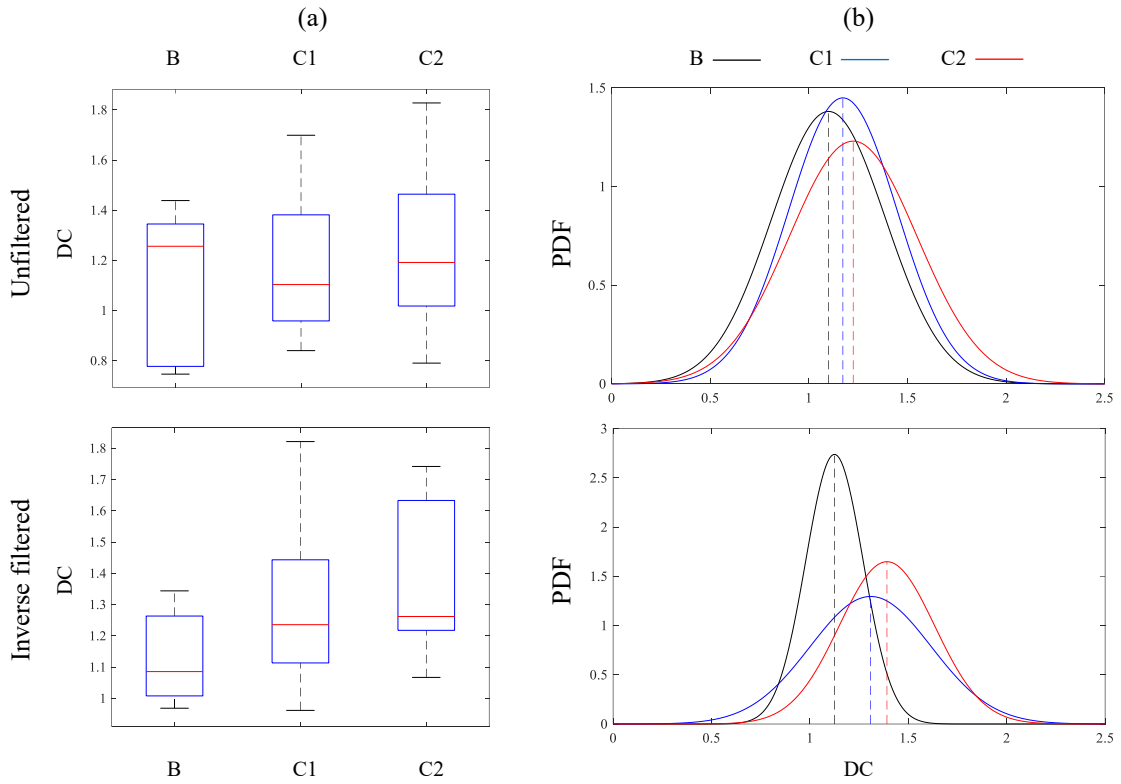
Figure 5-11: Distribution of DC parameters for the baseline and damage cases at the center (B, C1, and C2) plotted using boxplots (a) and fitted normal distributions (b).
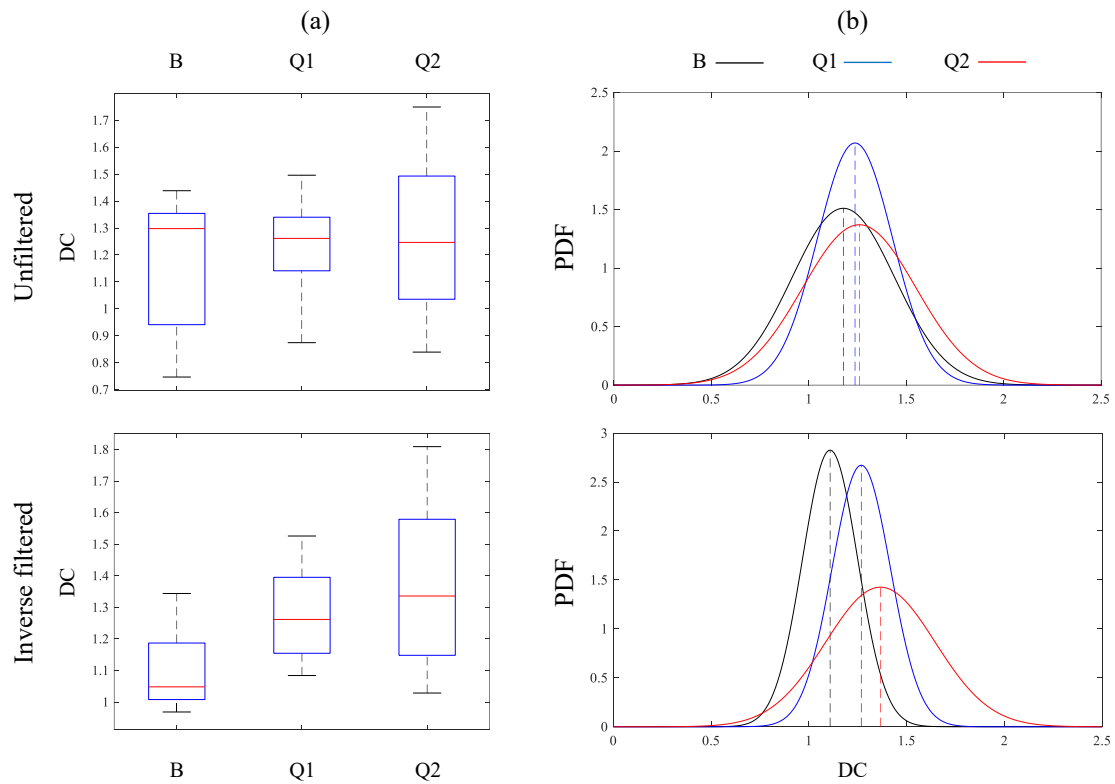
Figure 5-12: Distribution of DC parameters for the baseline and damage cases at the quarter (B, Q1, and Q2) plotted using boxplots (a) and fitted normal distributions (b).

Quantification of the damage detection performance is conducted using the proposed abnormality index, which results are presented in Table 5-7. The abnormality indices are calculated through comparing the distribution of DCs in the healthy baseline case with each damage case. Although the indices are increasing with damage severity in the unfiltered analysis, comparing the index values with those of the healthy cases in Section 5.4.1 shows that detecting damage on the bridge is almost impossible. In fact, the abnormality index shows similar levels in healthy and damaged cases without an appropriate filtering method, which supports the notion that the drive-by vibrations are dominated by operational factors. On the other hand, inverse filtered indices are significantly larger in the damaged cases compared to the healthy cases in Section 5.4.1. Therefore, not only does the inverse filtering decreases abnormality indices for healthy cases, it increases those of the damaged cases, yielding far more accurate damage detection.

Table 5-7: Abnormality index for the damage detection study.

Damage case	Unfiltered	Inverse filtered
C1	0.18	0.54
C2	0.29	0.94
Q1	0.18	0.78
Q2	0.21	0.82

5.6. CHAPTER CONCLUSION

This chapter proposes a bridge monitoring method considering operational effect using Mel-frequency cepstral analysis. Since drive-by data are significantly dominated by operational factors, including engine vibrations, suspension system, road roughness, etc., a recently developed inverse filtering method is employed to suppress such factors and magnify bridge dynamic features. In addition, a Mel-frequency cepstral analysis is employed to capture patterns in the frequency spectrum instead of looking for peaks. An abnormality index is proposed, representing a change

in the patterns inside the frequency spectrum, which would be interpreted as a change in the health state of the bridge structure.

The performance of the proposed method was first assessed through controlled laboratory experiments, where a robot car modeled the vehicle and a steel plate resting on a pin-roller boundary condition represented the bridge. Different combinations of suspension stiffness and speed values were considered to account for a variety of vehicles passing over the bridge using the robot car. It was shown that the frequency content of the spectrum would be overshadowed by operational factors without applying inverse filtering. Similar conclusions were made in a real-life study conducted on five major bridges in the city of Edmonton. Four different smartphones mounted on four different vehicles were employed to mimic different device-vehicle combinations in a crowdsensed framework. The main deduction was the importance of applying inverse filtering for detecting patterns related to bridge vibrations in a spectrum. It should be noted that the real-life data collections were performed in low-traffic conditions under maximum posted speed limits of 50 and 60 km/hr. It is expected that under heavy-traffic conditions, due to the presence of more vehicles on the bridge, the excitation level of the bridge would be increased, which leads to a stronger presence of the bridge features in the recorded mixed signals. In addition, lower speeds of the vehicles under heavy-traffic conditions lead to more on-bridge data availability, which is favorable for the proposed methodology.

The laboratory experiments were then extended to investigate the damage detection capability of the proposed method. Four damage cases were considered through two levels of cross-sectional area reduction at the center and quarter length of the bridge deck. The proposed abnormality index was capable of detecting the damage in all cases and was sensitive to the severity of the damage. The comparison of the abnormality index between healthy and damaged

cases corroborated the fact that without an appropriate filtering method, the index results in similar levels for both healthy and damaged conditions, which substantiates the dominancy of operational effects on the drive-by vibrations.

Chapter 6.   CONCLUSIONS AND FUTURE WORKS

6.1.   SUMMARY OF OUTCOMES

This thesis takes a step toward crowdsensing-based indirect bridge monitoring framework through addressing operational effects. Smartphones of the passengers inside vehicles are employed as data acquisition devices and the data recorded by their accelerometer and GPS sensors are used to detect multiple bridge states. In a real-life experiment, five full-scale bridges were studied using data recorded by four different smartphones mounted on four different vehicles and it was shown that the proposed inverse filtering method can eliminate the operational effects. Hence, the proposed method has the potential for implementation in a crowdsensed framework to detect irregularities in bridges in future smart cities.

For the first time in the literature, a novel inverse filtering methodology was proposed for eliminating operational effects from drive-by monitoring of bridges. In chapter 3, the methodology of inverse filtering was developed, which relies on the off-bridge vibrations to create a filter capable of eliminating operational effects. Later in that chapter, the method was assessed for the detection of the fundamental frequency of different bridges in a series of laboratory experiments. In Chapter 4, the proposed inverse filtering approach was enhanced to consider vehicle speed and road roughness variations for real-life applications. Despite the complexity of the real-life environments, the enhanced method was successful in detecting fundamental frequencies of two full-scale bridges in the city of Edmonton using a smartphone mounted on a full-size car. In chapter 5, the application of the method is extended beyond bridge frequency detection and Mel-frequency cepstral analysis is implemented which detects patterns in the frequency spectrum of vibrations instead of focusing on peaks. An abnormality index was proposed to represent the change in the bridge state. It was shown that the method was successful in eliminating operational effects and

the abnormality index was robust against the vehicle, road roughness, and data acquisition device features, both in a laboratory and real-life conditions. The damage detection capability of the proposed method was then conducted considering multiple damage scenarios at different locations with different severities. It was demonstrated that the operational factors play a significant role in the spectrum of drive-by vibrations and without inverse filtering, damage detection would be substantially overshadowed by their effects.

In summary, it is demonstrated in this thesis that crowdsensing-based monitoring of bridges using smartphones is promising and can provide a low-cost efficient pre-screening tool for transportation infrastructure management decision-makers to increase the sustainability and resiliency of our future smart cities.

6.2. LIMITATIONS AND RECOMMENDATIONS FOR FUTURE RESEARCH

Although this thesis proposes a novel method aiming at employing crowdsensing-based frameworks for bridge health monitoring, there are more challenges that need to be addressed in the future in order to achieve a robust universal approach that could be applied to any metropolitan around the world. The recommendations for future studies are listed in the following:

1) Since bridges are exposed structures, there are other factors affecting their vibrational response, especially environmental factors such as temperature, humidity, wind, etc. These factors can sometimes drastically affect the detected vibrational features of the bridges. Thus, environmental factors need to be implemented in conjunction with the proposed method to increase the robustness of the indirect bridge monitoring.

2) The damage detection capability of the current method is global, though it could be enhanced to incorporate damage localization as well. Drive-by vibrations are located from different points along the bridge, which provides the opportunity to localize damage

location and severity. Meanwhile, the limited availability of vibrations due to the high speeds of the vehicle, especially for short-span bridges, is a challenge that needs to be addressed in the future.

3) Regarding the crowdsensing implementation of the method in the future, there is an opportunity for recording data from multiple vehicles passing over a single bridge, which will be helpful for improving the accuracy of current methods or even detecting more dynamic features from the bridge, e.g., mode shapes.

4) One of the main concerns of employing crowdsensed frameworks is privacy issues. Since the data are collected from citizens' devices, these issues need to be addressed for the final implementation of the proposed methods in future smart cities.

BIBLIOGRAPHY

[1]   S. Graham, *Disrupted Cities: When Infrastructure Fails*. Routledge, 2009.

[2]   M. Renkow and D. Hoover, "Commuting, Migration, and Rural-urban Population Dynamics," *J. Reg. Sci.*, vol. 40, no. 2, pp. 261–287, 2000.

[3]   R. Faturechi and E. Miller-Hooks, "Measuring the Performance of Transportation Infrastructure Systems in Disasters: A Comprehensive Review," *Journal of Infrastructure Systems*, vol. 21, no. 1, p. 04014025, 2015.

[4]   W. Serrano, "Digital Systems in Smart City and Infrastructure: Digital as a Service," *Smart Cities*, vol. 1, no. 1, pp. 134–153, 2018.

[5]   M. Angelidou, A. Psaltoglou, N. Komninos, C. Kakderi, P. Tsarchopoulos, and A. Panori, "Enhancing Sustainable Urban Development Through Smart City Applications," *J. Sci. Technol. Policy Manag.*, vol. 9, no. 2, pp. 146–169, 2018.

[6]   B. N. Silva, M. Khan, and K. Han, "Towards Sustainable Smart Cities: A Review of Trends, Architectures, Components, and Open Challenges in Smart Cities," *Sustainable Cities and Society*, vol. 38, pp. 697–713, 2018.

[7]   H. Ham, T. J. Kim, and D. Boyce, "Assessment of Economic Impacts from Unexpected Events with An Interregional Commodity Flow and Multimodal Transportation Network Model," *Transp. Res. Part A Policy Pract.*, vol. 39, no. 10, pp. 849–860, 2005.

[8]   M. C. Wilson, "The Impact of Transportation Disruptions on Supply Chain Performance," *Transp. Res. Part E Logist. Transp. Rev.*, vol. 43, no. 4, pp. 295–320, 2007.

[9]   CIRC, "Canada Infrastructure Report Card 2019," 2019.

[10]   H. Wenzel, *Health Monitoring of Bridges*. John Wiley & Sons, 2009.

[11]   F. N. Catbas, M. Gul, and J. L. Burkett, "Conceptual Damage-Sensitive Features for

Structural Health Monitoring: Laboratory and Field Demonstrations," *Mech. Syst. Signal Process.*, vol. 22, no. 7, pp. 1650–1669, 2008.

[12]   S. Guan, J. A. Bridge, C. Li, and N. J. DeMello, "Smart Radar Sensor Network for Bridge Displacement Monitoring," *J. Bridg. Eng.*, vol. 24, no. 1, p. 04018102, 2019.

[13]   M. Gul and F. Necati Catbas, "Statistical Pattern Recognition for Structural Health Monitoring Using Time Series Modeling: Theory and Experimental Verifications," *Mech. Syst. Signal Process.*, vol. 23, no. 7, pp. 2192–2204, 2009.

[14]   N. A. Hoult, P. R. A. Fidler, P. G. Hill, and C. R. Middleton, "Long-Term Wireless Structural Health Monitoring of the Ferriby Road Bridge," *J. Bridg. Eng.*, vol. 15, no. 2, pp. 153–159, 2010.

[15]   K. H. Hsieh, M. W. Halling, and P. J. Barr, "Overview of Vibrational Structural Health Monitoring with Representative Case Studies," *J. Bridg. Eng.*, vol. 11, no. 6, pp. 707–715, 2006.

[16]   J. M. Ko and Y. Q. Ni, "Technology Developments in Structural Health Monitoring of Large-Scale Bridges," *Eng. Struct.*, vol. 27, no. 12, pp. 1715–1725, 2005.

[17]   K. Y. Wong, "Instrumentation and Health Monitoring of Cable-Supported Bridges," *Struct. Control Heal. Monit.*, vol. 11, no. 2, pp. 91–124, 2004.

[18]   O. E. Ramadan and V. P. Sisiopiku, "Evaluation of Merge Control Strategies at Interstate Work Zones under Peak and Off-Peak Traffic Conditions," *J. Transp. Technol.*, vol. 06, no. 03, pp. 118–130, 2016.

[19]   C. W. Lin and Y. B. Yang, "Use of a Passing Vehicle to Scan the Fundamental Bridge Frequencies: An Experimental Verification," *Eng. Struct.*, vol. 27, no. 13, pp. 1865–1878, 2005.

[20]   Y. B. Yang, C. W. Lin, and J. D. Yau, "Extracting Bridge Frequencies from The Dynamic Response of a Passing Vehicle," *J. Sound Vib.*, vol. 272, no. 3–5, pp. 471–493, 2004.

[21]   A. Malekjafarian, P. J. McGetrick, and E. J. Obrien, "A Review of Indirect Bridge Monitoring Using Passing Vehicles," *Shock and Vibration*, vol. 2015, 2015.

[22]   A. Elhattab, "Drive-by Bridge Damage Monitoring: Concise Review," *Civ. Eng. Res. J.*, vol. 1, no. 1, 2017.

[23]   Y. B. Yang and J. P. Yang, "State-of-the-Art Review on Modal Identification and Damage Detection of Bridges by Moving Test Vehicles," *Int. J. Struct. Stab. Dyn.*, vol. 18, no. 2. 2018.

[24]   J. Liu, M. Bergés, J. Bielak, J. H. Garrett, J. Kovačević, and H. Y. Noh, "A Damage Localization and Quantification Algorithm for Indirect Structural Health Monitoring of Bridges Using Multi-Task Learning," *AIP Conf. Proc.*, vol. 2102, no. 1, p. 090003, 2019.

[25]   J. Keenahan, E. J. OBrien, P. J. McGetrick, and A. Gonzalez, "The Use of a Dynamic Truck–Trailer Drive-By System to Monitor Bridge Damping," *Struct. Heal. Monit.*, vol. 13, no. 2, pp. 143–157, 2013.

[26]   Y. B. Yang and K. C. Chang, "Extraction of Bridge Frequencies from The Dynamic Response of a Passing Vehicle Enhanced by the EMD Technique," *J. Sound Vib.*, vol. 322, no. 4–5, pp. 718–739, 2009.

[27]   W. M. Li, Z. H. Jiang, T. L. Wang, and H. P. Zhu, "Optimization Method Based on Generalized Pattern Search Algorithm to Identify Bridge Parameters Indirectly by a Passing Vehicle," *J. Sound Vib.*, vol. 333, no. 2, pp. 364–380, 2014.

[28]   A. Malekjafarian and E. J. O'Brien, "Application of Output-only Modal Method in Monitoring of Bridges Using an Instrumented Vehicle," *Civ. Eng. Res. Irel.*, 2014.

[29]   A. K. Pandey, M. Biswas, and M. M. Samman, "Damage Detection from Changes in Curvature Mode Shapes," *J. Sound Vib.*, vol. 145, no. 2, pp. 321–332, 1991.

[30]   V. Arora, S. P. Singh, and T. K. Kundra, "Damped Model Updating Using Complex

Updating Parameters," *J. Sound Vib.*, vol. 320, no. 1–2, pp. 438–451, 2009.

[31]   Y. Zhang, L. Wang, and Z. Xiang, "Damage Detection by Mode Shape Squares Extracted from a Passing Vehicle," *J. Sound Vib.*, vol. 331, no. 2, pp. 291–307, 2012.

[32]   Y. B. Yang, Y. C. Li, and K. C. Chang, "Constructing the Mode Shapes of a Bridge from a Passing Vehicle: A Theoretical Study," *Smart Struct. Syst.*, vol. 13, no. 5, pp. 797–819, 2014.

[33]   Y. Oshima, K. Yamamoto, and K. Sugiura, "Damage Assessment of a Bridge Based on Mode Shapes Estimated by Responses of Passing Vehicles," *Smart Struct. Syst.*, vol. 13, no. 5, pp. 731–753, 2014.

[34]   A. Malekjafarian and E. J. OBrien, "Identification of Bridge Mode Shapes Using Short Time Frequency Domain Decomposition of the Responses Measured in a Passing Vehicle," *Eng. Struct.*, vol. 81, pp. 386–397, 2014.

[35]   Q. Mei, N. Shirzad-Ghaleroudkhani, M. Gül, S. F. Ghahari, and E. Taciroglu, "Bridge Mode Shape Identification Using Moving Vehicles at Traffic Speeds Through Non-Parametric Sparse Matrix Completion," *Struct. Control Heal. Monit.*, e2747, 2021.

[36]   E. J. OBrien, P. J. Mcgetrick, and A. González, "A Drive-by Inspection System via Vehicle Moving Force Identification," *Smart Struct. Syst.*, vol. 13, no. 5, pp. 821–848, 2014.

[37]   Y. Zhang, S. T. Lie, and Z. Xiang, "Damage Detection Method Based on Operating Deflection Shape Curvature Extracted from Dynamic Response of a Passing Vehicle," *Mech. Syst. Signal Process.*, vol. 35, no. 1–2, pp. 238–254, 2013.

[38]   S. H. Yin and C. Y. Tang, "Identifying Cable Tension Loss and Deck Damage in a Cable-Stayed Bridge Using a Moving Vehicle," *J. Vib. Acoust. Trans.*, vol. 133, no. 2, 2011.

[39]   A. Khorram, F. Bakhtiari-Nejad, and M. Rezaeian, "Comparison Studies Between Two Wavelet-based Crack Detection Methods of a Beam Subjected to a Moving Load," *Int. J. Eng.*

Sci., vol. 51, pp. 204–215, 2012.

[40]   P. J. McGetrick and C. W. Kim, "A Parametric Study of a Drive-by Bridge Inspection System Based on the Morlet Wavelet," *Key Eng. Mater.*, vol. 569, pp. 262–269, 2013.

[41]   P. J. McGetrick and C. W. Kim, "An Indirect Bridge Inspection Method Incorporating a Wavelet-based Damage Indicator and Pattern Recognition," *Proc. IX Int. Conf. Struct. Dyn. EURODYN*, pp. 2605–2612, 2014.

[42]   J. Liu, S. Xu, M. Bergés, and H. Y. Noh, "HierMUD: Hierarchical Multi-task Unsupervised Domain Adaptation between Bridges for Drive-by Damage Diagnosis," *arXiv preprint*, arXiv:2107.11435, 2021.

[43]   O. L. Ouabi, P. Pomarede, N. Declercq, N. Zeghidour, M. Geist, and C. Pradalier, "Learning the Propagation Properties of Plate-like Structures for Lamb Wave-based Mapping," *Ultrasonics*, pp.106705, 2022.

[44]   J. Liu, S. Chen, M. Bergés, J. Bielak, J. H. Garrett, J. Kovačević, and H. Y. Noh, "Diagnosis Algorithms for Indirect Structural Health Monitoring of a Bridge Model via Dimensionality Reduction," *Mech. Syst. Signal Process.*, vol. 136, p. 106454, 2020.

[45]   Q. Mei, M. Gül, and M. Boay, "Indirect Health Monitoring of Bridges Using Mel-frequency Cepstral Coefficients and Principal Component Analysis," *Mech. Syst. Signal Process.*, vol. 119, pp. 523–546, 2019.

[46]   M. C. Lucic, X. Wan, H. Ghazzai, and Y. Massoud, "Leveraging Intelligent Transportation Systems and Smart Vehicles Using Crowdsourcing: An Overview," *Smart Cities*, vol. 3, no. 2, pp. 341–361, 2020.

[47]   B. Jan, H. Farman, M. Khan, M. Talha, and I. U. Din, "Designing a Smart Transportation System: An Internet of Things and Big Data Approach*," IEEE Wirel. Commun.*, vol. 26, no. 4, pp.

73–79, 2019.

[48]   V. Astarita, V. P. Giofrè, G. Guido, G. Stefano, and A. Vitale, "Mobile Computing for Disaster Emergency Management: Empirical Requirements Analysis for a Cooperative Crowdsourced System for Emergency Management Operation," *Smart Cities*, vol. 3, no. 1, pp. 31–47, 2020.

[49]   Q. Mei, M. Gül, and N. Shirzad-Ghaleroudkhani, "Towards Smart Cities: Crowdsensing-based Monitoring of Transportation Infrastructure Using In-traffic Vehicles," *J. Civ. Struct. Heal. Monit.,* vol.10, no. 4, pp. 653–665, 2020.

[50]   N. Shirzad-Ghaleroudkhani, Q. Mei, and M. Gül, "A Crowdsensing-based Platform for Transportation Infrastructure Monitoring and Management in Smart Cities," *The Rise of Smart Cities,* Chapter 24, pp. 609–624, 2022.

[51]   P. Mohan, V. N. Padmanabhan, and R. Ramjee, "Nericell: Rich Monitoring of Road and Traffic Conditions using Mobile Smartphones," *Proceedings of the 6th ACM Conference on Embedded Networked Sensor Systems*, pp. 323–336, 2008.

[52]   P. Händel, J. Ohlsson, M. Ohlsson, I. Skog, and E. Nygren, "Smartphone-based Measurement Systems for Road Vehicle Traffic Monitoring and Usage-based Insurance," *IEEE Syst. J.*, vol. 8, no. 4, pp. 1238–1248, 2014.

[53]   R. Bhoraskar, N. Vankadhara, B. Raman, and P. Kulkarni, "Wolverine: Traffic and Road Condition Estimation Using Smartphone Sensors," *4th International Conference on Communication Systems and Networks, COMSNETS*, pp. 1–6, 2012.

[54]   M. Feng, Y. Fukuda, M. Mizuta, and E. Ozer, "Citizen Sensors for SHM: Use of Accelerometer Data from Smartphones," *Sensors (Switzerland)*, vol. 15, no. 2, pp. 2980–2998, 2015.

[55]	Q. Kong, R. M. Allen, M. D. Kohler, T. H. Heaton, and J. Bunn, "Structural Health Monitoring of Buildings Using Smartphone Sensors," *Seismol. Res. Lett.*, vol. 89, no. 2A, pp. 594–602, 2018.

[56]	E. Ozer and M. Q. Feng, "Synthesizing Spatiotemporally Sparse Smartphone Sensor Data for Bridge Modal Identification," *Smart Mater. Struct.*, vol. 25, no. 8, 2016.

[57]	E. Ozer and M. Q. Feng, "Direction-sensitive Smart Monitoring of Structures Using Heterogeneous Smartphone Sensor Data and Coordinate System Transformation," *Smart Mater. Struct.*, vol. 26, no. 4, 2017.

[58]	X. Zhao, R. Han, Y. Yu, W. Hu, D. Jiao, X. Mao, M. Li, and J. Ou, "Smartphone-based Mobile Testing Technique for Quick Bridge Cable–Force Measurement," *J. Bridg. Eng.*, vol. 22, no. 4, p. 06016012, 2017.

[59]	G. Morgenthal, S. Rau, J. Taraben, T. Abbas, and N. Hallermann, "Determination of Stay Cable Forces Using Highly Mobile Vibration Measurement Devices," *Proc. 9th Int. Conf. Bridg. Maint., Safety Manag.*, *IABMAS*, vol. 23, no. 2, pp. 2558–2565, 2018.

[60]	Q. Mei and M. Gül, "A Crowdsourcing-based Methodology Using Smartphones for Bridge Health Monitoring," *Struct. Heal. Monit.*, vol. 18, no. 5–6, pp. 1602–1619, 2019.

[61]	T. J. Matarazzo, P. Santi, S. N. Pakzad, K. Carter, C. Ratti, B. Moaveni, C. Osgood, and N. Jacob, "Crowdsensing Framework for Monitoring Bridge Vibrations Using Moving Smartphones," *Proc. IEEE*, vol. 106, no. 4, pp. 577–593, 2018.

[62]	"Intelligent Transportation Systems - Fehr & Peers." [Online]. Available: https://www.fehrandpeers.com/intelligent-transportation-systems/.

[63]	Y.-B. Yang and J.-D. Yau, "Vehicle-bridge Interaction Element for Dynamic Analysis," *J. Struct. Eng.*, vol. 123, no. 11, pp. 1512–1518, 1997.

[64]   Y. B. Yang and C. W. Lin, "Vehicle-bridge Interaction Dynamics and Potential Applications," *J. Sound Vib.*, vol. 284, no. 1–2, pp. 205–226, 2005.

[65]   P. D. Welch, "The Use of Fast Fourier Transform for the Estimation of Power Spectra: A Method Based on Time Averaging Over Short, Modified Periodograms," *IEEE Trans. Audio Electroacoust.*, vol. 15, no. 2, pp. 70–73, 1967.

[66]   F. J. Harris, "On the Use of Windows for Harmonic Analysis with the Discrete Fourier Transform," *Proc. IEEE*, vol. 66, no. 1, pp. 51–83, 1978.

[67]   Mathworks, "MATLAB, the Language of Technical Computing." 2018.

[68]   Y. L. Ding, H.-W. Zhao, and A. Q. Li, "Temperature Effects on Strain Influence Lines and Dynamic Load Factors in a Steel-Truss Arch Railway Bridge Using Adaptive FIR Filtering," *J. Perform. Constr. Facil.*, vol. 31, no. 4, p. 04017024, 2017.

[69]   H. He, Y. Lv, and E. Han, "Damage Detection for Continuous Bridge Based on Static-dynamic Condensation and Extended Kalman Filtering," *Math. Probl. Eng.*, vol. 2014, 2014.

[70]   K. Erazo, D. Sen, S. Nagarajaiah, and L. Sun, "Vibration-based Structural Health Monitoring Under Changing Environmental Conditions Using Kalman Filtering*," Mech. Syst. Signal Process.*, vol. 117, pp. 1–15, 2019.

[71]   M. Rothenberg, "New Inverse–Filtering Technique for Deriving the Glottal Air Flow Waveform During Voicing," *J. Acoust. Soc. Am.*, vol. 48, no. 1A, pp. 130–130, 1970.

[72]   H. Wakita, "Direct Estimation of the Vocal Tract Shape by Inverse Filtering of Acoustic Speech Waveforms," *IEEE Trans. Audio Electroacoust.*, vol. 21, no. 5, pp. 417–427, 1973.

[73]   O. Michailovich and A. Tannenbaum, "Blind Deconvolution of Medical Ultrasound Images: A Parametric Inverse Filtering Approach," *IEEE Trans. Image Process.*, vol. 16, no. 12, pp. 3005–3019, 2007.

[74]   P. L. Goupillaud, "An Approach to Inverse Filtering of Near‐Surface Layer Effects from Seismic Records," *Geophysics*, vol. 26, no. 6, pp. 754–760, 1961.

[75]   L. Sun, "Developing Spectrum-Based Models for International Roughness Index and Present Serviceability Index," *J. Transp. Eng.*, vol. 127, no. 6, pp. 463–470, 2001.

[76]   R. Hesami and K. J. McManus, "Signal Processing Approach to Road Roughness Analysis and Measurement," *IEEE Reg. 10 Annu. Int. Conf. Proceedings, TENCON*, pp. 1–6, 2009.

[77]   S. Islam, W. G. Buttlar, R. G. Aldunate, and W. R. Vavrik, "Measurement of Pavement Roughness Using Android-based Smartphone Application," *Transp. Res. Rec.*, vol. 2457, pp. 30–38, 2014.

[78]   W. Wang and F. Guo, "RoadLab: Revamping Road Condition and Road Safety Monitoring by Crowdsourcing with Smartphone App," *Transportation Research Board 95th Annual Meeting*, no. 16–2116, 2016.

[79]   M. Byrne, T. Parry, R. Isola, and A. Dawson, "Identifying Road Defect Information from Smartphones," *Road Transp. Res. A J. Aust. New Zeal. Res. Pract.*, vol. 22, no. 1, pp. 39–50, 2013.

[80]   F. Carrera, "Wise Cities: 'Old' Big Data and 'Slow' Real Time," *Built Environ.*, vol. 42, no. 3, pp. 474–497, 2016.

[81]   B. Kostić and M. Gül, "Vibration-based Damage Detection of Bridges under Varying Temperature Effects Using Time-series Analysis and Artificial Neural Networks," *J. Bridg. Eng.*, vol. 22, no. 10, p. 04017065, 2017.

[82]   H. Zhang, M. Gül, and B. Kostić, "Eliminating Temperature Effects in Damage Detection for Civil Infrastructure Using Time Series Analysis and Autoassociative Neural Networks," *J. Aerosp. Eng.*, vol. 32, no. 2, p. 04019001, 2019.

[83]   J. Gu, M. Gul, and X. Wu, "Damage Detection Under Varying Temperature Using Artificial Neural Networks," *Struct. Control Heal. Monit.*, vol. 24, no. 11, 2017.

[84]   S. Staacks, S. Hütz, H. Heinke, and C. Stampfer, "Advanced Tools for Smartphone-based Experiments: Phyphox," *Phys. Educ.*, vol. 53, no. 4, p. 045009, 2018.

[85]   D. G. Childers, D. P. Skinner, and R. C. Kemerait, "The Cepstrum: A Guide to Processing," *Proc. IEEE*, vol. 65, no. 10, pp. 1428–1443, 1977.

[86]   K. Tokuda, T. Kobayashi, and S. Imai, "Adaptive Cepstral Analysis of Speech," *IEEE Trans. Speech Audio Process.*, vol. 3, no. 6, pp. 481–489, 1995.

[87]   P. Alexandre and P. Lockwood, "Root Cepstral Analysis: A Unified View. Application to Speech Processing in Car Noise Environments," *Speech Commun.*, vol. 12, no. 3, pp. 277–288, 1993.

[88]   S. Furui, "Cepstral Analysis Technique for Automatic Speaker Verification," *IEEE Trans. Acoust.*, vol. 29, no. 2, pp. 254–272, 1981.

[89]   C. K. On, P. M. Pandiyan, S. Yaacob, and A. Saudi, "Mel-frequency Cepstral Coefficient Analysis in Speech Recognition," *Int. Conf. Comp. & Inf.*, 1–5, 2006.

[90]   R. Vergin, D. O'Shaughnessy, and A. Farhat, "Generalized Mel-frequency Cepstral Coefficients for Large-vocabulary Speaker-independent Continuous-speech Recognition," *IEEE Trans. Speech Audio Process.*, vol. 7, no. 5, pp. 525–532, 1999.

[91]   F. Zheng, G. Zhang, and Z. Song, "Comparison of Different Implementations of MFCC," *J. Comput. Sci. Technol.*, vol. 16, no. 6, pp. 582–589, 2001.

[92]   G. Zhang, R. S. Harichandran, and P. Ramuhalli, "Application of Noise Cancelling and Damage Detection Algorithms in NDE of Concrete Bridge Decks Using Impact Signals," *J. Nondestruct. Eval.*, vol. 30, no. 4, pp. 259–272, 2011.

[93]   L. Balsamo, R. Betti, and H. Beigi, "A Structural Health Monitoring Strategy Using Cepstral Features," *J. Sound Vib.*, vol. 333, no. 19, pp. 4526–4542, Sep. 2014.

[94]   S. A. Gelfand, *Essentials of Audiology*, New York: Thieme, 1997.